AD NUMBER
ADB372258
LIMITATION CHANGES
TO: **Approved for public release; distribution is unlimited.**
FROM: **Distribution: Further dissemination only as directed by President, Naval Postgraduate School, Attn: Code 261, Monterey, CA 93943-5000, JUN 2011, or higher DoD authority.**
AUTHORITY
NPS ltr dtd 14 May 2014

NAVAL POSTGRADUATE SCHOOL

MONTEREY, CALIFORNIA

THESIS

PERFORMANCE OF COMPLEX SPREADING MIMO SYSTEMS WITH INTERFERENCE

by

Efstathios Mintzias

June 2011

Thesis Co-Advisors: Tri Ha
Ric Romero

~~**Further dissemination only as directed by (Naval Postgraduate School) (June 2011) or higher DoD authority**~~

Approved for public release; distribution is unlimited

THIS PAGE INTENTIONALLY LEFT BLANK

May 13, 2014

SUBJECT: Change in distribution statement for *Performance of Complex Spreading MIMO Systems with Interference* – June 2011.

1. Reference: Mintzias, Efstathios. *Performance of Complex Spreading MIMO Systems with Interference*. Monterey, CA: Naval Postgraduate School, Department of Electrical and Computer Engineering, June 2011. UNCLASSIFIED [Further dissemination only as directed by Naval Postgraduate School June 2011 or higher DoD authority].

2. Upon consultation with NPS faculty, the School has determined that this thesis may be released to the public, its distribution is unlimited, effective May 13, 2014.

University Librarian
Naval Postgraduate School

THIS PAGE INTENTIONALLY LEFT BLANK

REPORT DOCUMENTATION PAGE			Form Approved OMB No. 0704-0188
Public reporting burden for this collection of information is estimated to average 1 hour per response, including the time for reviewing instruction, searching existing data sources, gathering and maintaining the data needed, and completing and reviewing the collection of information. Send comments regarding this burden estimate or any other aspect of this collection of information, including suggestions for reducing this burden, to Washington headquarters Services, Directorate for Information Operations and Reports, 1215 Jefferson Davis Highway, Suite 1204, Arlington, VA 22202-4302, and to the Office of Management and Budget, Paperwork Reduction Project (0704-0188) Washington DC 20503.			
1. AGENCY USE ONLY ***(Leave blank)***	**2. REPORT DATE** June 2011	**3. REPORT TYPE AND DATES COVERED** Master's Thesis	
4. TITLE AND SUBTITLE Performance of Complex Spreading MIMO Systems With Interference		**5. FUNDING NUMBERS**	
6. AUTHOR(S) Efstathios Mintzias			
7. PERFORMING ORGANIZATION NAME(S) AND ADDRESS(ES) Naval Postgraduate School Monterey, CA 93943-5000		**8. PERFORMING ORGANIZATION REPORT NUMBER**	
9. SPONSORING /MONITORING AGENCY NAME(S) AND ADDRESS(ES) N/A		**10. SPONSORING/MONITORING AGENCY REPORT NUMBER**	
11. SUPPLEMENTARY NOTES The views expressed in this thesis are those of the author and do not reflect the official policy or position of the Department of Defense or the U.S. Government. IRB Protocol number _____N/A_____.			
12a. DISTRIBUTION / AVAILABILITY STATEMENT ~~Further dissemination only as directed by (Naval Postgraduate School) (June 2011) or higher DoD authority~~ Approved for public release; distribution is unlimited		**12b. DISTRIBUTION CODE** A	

13. ABSTRACT (maximum 200 words)

The objective of this thesis is to investigate the performances of digital communication systems that employ complex spreading modulation schemes in a Rayleigh fading channel. First, we examine binary modulation systems with multiple-input, single-output (MISO) configurations. Later, we study MISO systems for complex spreading modulation systems in general. We demonstrate the performances of specific and widely used modulation schemes such as quadrature phase-shift keying (QPSK), 16-quadrature amplitude modulation (16-QAM) and 64-quadrature amplitude modulation (64-QAM).

We also investigate the performances of the previous systems for multiple-input, multiple-output (MIMO) configurations for various combinations of transmit and receive antennas. In all systems, we apply maximal ratio combining (MRC) in order to obtain the maximum signal-to-noise ratio for MIMO systems.

Finally, for all the different systems and configurations, we evaluate their performances for a Rayleigh fading channel and in the presence of different types of jamming (barrage noise jamming, pulsed-jamming and tone jamming).

14. SUBJECT TERMS Complex Spreading, MISO, MIMO, Rayleigh Fading, Interference, Barrage Noise Jamming, Pulsed Jamming, Tone Jamming, Maximum Ratio Combining, MRC.			**15. NUMBER OF PAGES** 143
			16. PRICE CODE
17. SECURITY CLASSIFICATION OF REPORT Unclassified	**18. SECURITY CLASSIFICATION OF THIS PAGE** Unclassified	**19. SECURITY CLASSIFICATION OF ABSTRACT** Unclassified	**20. LIMITATION OF ABSTRACT** UU

NSN 7540-01-280-5500 Standard Form 298 (Rev. 2-89)
Prescribed by ANSI Std. 239-18

THIS PAGE INTENTIONALLY LEFT BLANK

~~**Further dissemination only as directed by (Naval Postgraduate School) (June 2011) or higher DoD authority**~~
Approved for public release; distribution is unlimited

PERFORMANCE OF COMPLEX SPREADING MIMO SYSTEMS WITH INTERFERENCE

Efstathios Mintzias
Lieutenant Junior Grade, Hellenic Navy
B.S., Hellenic Naval Academy, 2004

Submitted in partial fulfillment of the
requirements for the degrees of

ELECTRICAL ENGINEER
and
MASTER OF SCIENCE IN ELECTRICAL ENGINEERING

from the

NAVAL POSTGRADUATE SCHOOL
June 2011

Author: Efstathios Mintzias

Approved by: Tri Ha
Thesis Co-Advisor

Ric Romero
Thesis Co-Advisor

Ralph C. Robertson
Chair, Department of Electrical and Computer Engineering

THIS PAGE INTENTIONALLY LEFT BLANK

ABSTRACT

The objective of this thesis is to investigate the performances of digital communication systems that employ complex spreading modulation schemes in a Rayleigh fading channel. First, we examine binary modulation systems with multiple-input, single-output (MISO) configurations. Later, we study MISO systems for complex spreading modulation systems in general. We demonstrate the performances of specific and widely used modulation schemes such as quadrature phase-shift keying (QPSK), 16-quadrature amplitude modulation (16-QAM) and 64-quadrature amplitude modulation (64-QAM).

We also investigate the performances of the previous systems for multiple-input, multiple-output (MIMO) configurations for various combinations of transmit and receive antennas. In all systems, we apply maximal ratio combining (MRC) in order to obtain the maximum signal-to-noise ratio for MIMO systems.

Finally, for all the different systems and configurations, we evaluate their performances for a Rayleigh fading channel and in the presence of different types of jamming (barrage noise jamming, pulsed-jamming and tone jamming).

THIS PAGE INTENTIONALLY LEFT BLANK

TABLE OF CONTENTS

THIS PAGE INTENTIONALLY LEFT BLANK

LIST OF FIGURES

LIST OF ACRONYMS AND ABBREVIATIONS

AWGN	Additive White Gaussian Noise
BER	Bit Error Rate
DS	Direct Sequence
DSSS	Direct Sequence Spread Spectrum
FEC	Forward Error Correction
FHSS	Frequency Hopping Spread Spectrum
GPS	Global Positioning System
I-Q	In-Phase/Quadrature
LFSR	Linear Feedback Shift Register
MIMO	Multiple Input Multiple Output
MISO	Multiple Input Single Output
MQAM	*M*-ary Quadrature Amplitude Modulation
MRC	Maximal Ratio Combining
OSTBC	Orthogonal Space Time Block Code
PN	Pseudo Noise
PSD	Power Spectral Density
PSK	Phase Shift Keying
QPSK	Quadrature Phase Shift Keying
SISO	Single Input Single Output
SIMO	Single Input Multiple Output
SNR	Signal to Noise Ratio
SJR	Signal to Jamming Ratio
SJNR	Signal to Jamming plus Noise Ratio

SS	Spread Spectrum
TCM	Trellis Coded Modulation
W-CDMA	Wideband Code Division Multiple Access

EXECUTIVE SUMMARY

Usually, when we refer to a typical communication system, we think of a system with one transmit antenna and one receive antenna. Recently, a very important emerging technology for communications systems is the use of antenna diversity. This terminology is used for systems with multiple transmit and receive antennas, also referred to as multiple input, multiple output (MIMO) systems. MIMO systems appear quite often in modern wireless communications applications. This technology is used to improve the overall performance of a communication system. One very important characteristic of MIMO systems is that they provide better performance in fading environments. The use of MIMO systems in fading channels is now ubiquitous.

Another widespread technology that originated from military applications is spread spectrum (SS) communications. By using periodic pseudo-noise (PN) sequences, we spread the spectrum of a narrowband signal to achieve better performance in the presence of interference signals.

In our research, we analyze and evaluate a variety of communication systems. All the systems that we evaluate use a specific type of SS, namely, direct sequence spread spectrum (DSSS). We consider Rayleigh fading channel and three different types of interference: broadband (barrage) noise, pulsed-noise and tone. In addition, we use maximal ratio combining (MRC), which is a combining technique that ensures maximum signal–to-noise ratio (SNR) when only additive white Gaussian noise (AWGN) is present.

Another important characteristic that we examine is the number of transmit and receive antennas. Firstly, we examine multiple input, single output (MISO) systems, and then we evaluate MIMO systems. The analysis applies to in-phase/quadrature (*I*-*Q*) complex spreading modulation, but we first focus on DSSS phase-shift keying (DS-PSK), which is a binary modulation scheme. Then, we study DSSS quadrature phase-shift

keying (DS-QPSK), DSSS 16-quadrature amplitude modulation (DS-16QAM) and DSSS 64-quadrature amplitude modulation (DS-64QAM), which are some of the widespread *I-Q* modulation schemes.

We analyze the preceding systems in order to determine the most effective system combination of different diversities for the three types of jamming. The comparison assumes fixed signal bandwidth and fixed transmit power.

We indicate the robustness of a specific configuration in tone jamming, and we see that for most cases broadband jamming is more effective than tone jamming. We also evaluate the worst-case ρ in order to perform effective pulsed jamming.

Another aspect that we analyze is the orthogonal space-time block codes (OSTBC), which we use for different diversities. We demonstrate the improved performance that we obtain via an Alamouti OSTBC.

Finally, we analyze MIMO systems for different transmit and receive diversities. We point out the MIMO configuration with increased receive diversity that achieves the best performance to improve overall performance without imposing any power penalty on the system.

ACKNOWLEDGMENTS

I dedicate this work to my wife, Kalliopi, for her continuous loving support and patience, and to my daughter, Athanasia, for the happiness that she brings in my life.

I would like to deeply thank my advisor, Professor Tri Ha, for the invaluable guidance and support that he provided me during the research and for his unique patience.

I would also like to express my appreciation to Professor Ric Romero for evaluating this work and giving me an additional insight.

THIS PAGE INTENTIONALLY LEFT BLANK

I. INTRODUCTION

A. OVERVIEW

The use of spread spectrum (SS) communications in many applications is widespread. This technique originated from military applications and is now commonly used in a variety of civilian applications such as cellular systems, global positioning systems (GPS) and more.

One of the main advantages of this technique is the improvement of performance in the presence of interference signals [1], [2], [3]. This is a vital element for military applications, where the presence of hostile jamming signals is likely and can severely degrade the performance of communication systems. For civilian applications, the great advantage SS offers is the elimination of co-channel interference [1], which does not originate from hostile signals but from other users in the system. This is very common in cellular systems like IS-95, wideband code-division multiple access (W-CDMA) and CDMA 2000, where the signal of each user is interference to other users in the network. The application of spread spectrum helps in reducing the effect of interference and also provides the users a higher level of privacy [1], [2], [3].

Another emerging technology is the use of antenna diversity. Systems with multiple transmit and receive antennas, called multiple input-multiple output (MIMO), have become popular in wireless communications. The advantages of this technology are numerous. The effective range of the communication link and the data throughput are significantly increased without additional transmit power or bandwidth and the performance in fading channels is improved [4], [5]. These important characteristics of MIMO make it the choice for modern wireless communication standards such as IEEE 802.11, 4G and WiMAX [4], [6], [7].

B. LITERATURE REVIEW

In 3G standards WCDMA and CDMA2000, the complex spreading modulation technology is employed. In [8], Richardson presents the use of complex spreading in WCDMA downlink for channelization for single user. He also introduces complex spreading for multiple users and presents the equivalent constellation diagrams.

In [9], a study of adaptive quadrature amplitude modulation (QAM) with complex spreading for high-speed mobile multimedia communications with non-coherent detection is presented. The study reports an evaluation analysis and simulation for both flat fading and frequency-selective fading channels and a comparison between complex spreading and an oversampling technique. The result is that complex spreading of adaptive QAM does not perform efficiently for frequency-selective fading. In [10], a study of complex spreading for WCDMA uplink is presented, where the analysis is focused on the elimination of the nonlinear orthogonal interference in power amplifiers by introducing a scheme of complex scrambling with phase estimation. An analysis of a complex spreading in-phase/quadrature (*I-Q*) orthogonal covering system is presented in [11]. The system refers to multiple channels and applies pilot tone-aided demodulation and Doppler tracking in fading environment without the presence of interference for single transmit-single receive antenna systems.

C. THESIS OBJECTIVE

In our research, we evaluate complex spreading *I-Q* modulation systems for a fading environment and in the presence of various interferences. Moreover, we apply transmit and receive diversity to the above systems, which is a contribution of this work.

We analyze various spread spectrum communication systems. In this work, the systems that we evaluate employ direct sequence spread spectrum (DSSS). We study phase-shift keying (PSK), which is a binary modulation scheme, quadrature phase-shift keying (QPSK), 16-quadrature amplitude modulation (16QAM), and 64-quadrature amplitude modulation (64QAM), which are *I-Q* modulation systems.

The analysis is performed assuming a Rayleigh fading channel and various interference environments, namely, broadband noise, pulsed-noise and tone jamming. These different types of interference are presented in [12].

We also examine multiple input, single output (MISO) systems and MIMO systems. The performances of the various systems are analyzed for different modulation schemes and different types of jamming and for both MISO and MIMO systems.

By evaluating the results of the research, we can determine the most effective combination of different diversities with the three types of jamming. The comparison is based on fixed signal bandwidth and fixed transmit power.

D. THESIS OUTLINE

The thesis is organized as follows. Chapter I is the introduction that outlines the importance of the research. In Chapter II, the necessary background is developed in order to understand the analysis in the subsequent chapters. In Chapter III, we introduce and evaluate MISO-PSK systems. In Chapter IV, we evaluate MISO-*IQ* systems, and in Chapter V, we evaluate MIMO-*IQ* systems. Finally, based on the results of the analyses of the previous chapters, we present our conclusions in Chapter VI.

THIS PAGE INTENTIONALLY LEFT BLANK

II. BACKGROUND

The intention of this chapter is to provide basic background knowledge and concepts to the reader in order to understand the analyses presented in the succeeding chapters.

A. DIRECT SEQUENCE SPREAD SPECTRUM MODULATION

A spread spectrum modulated signal is a signal that has a much larger bandwidth than its narrowband counterpart. This type of modulation originated from military applications but nowadays is widely used in many civilian applications. One reason that makes spread spectrum popular is its ability to reduce the effectiveness of a jamming signal. The effectiveness of jamming is reduced since the jamming signal must spread its power over the larger bandwidth of the spread spectrum signal. This results in a reduction of the magnitude of the power spectral density (PSD) of the jamming signal. Thus, the effectiveness of jamming is reduced. There are two types of SS modulation techniques, DSSS and the frequency-hopping spread spectrum (FHSS). In our research, we study only DSSS systems.

We assume a data sequence (0s and 1s) with a bit rate of $R_b = 1/T_b$, where T_b is the bit time. We also assume a periodic pseudo-noise (PN) sequence of *N* chips (0s and 1s) with a chip rate of $R_c = 1/T_c = NR_b$, where the sequence period is the same as the bit time. Assuming that the data and PN sequences are synchronized, we can combine the two sequences; if we repeat each data bit *N* times and modulo-2 add it to the *N* chips of the *PN* sequence, then we generate the DSSS signal that is used to modulate the carrier signal. Because the chip rate R_c is *N* times the bit rate, the DSSS signal bandwidth is *N* times the bandwidth of the narrowband signal. The PN sequence period may also be selected to be an integer multiple of the bit duration. The number $N = T_b / T_c$ is defined as the spread factor of the DSSS signal. The effect of spreading the signal bandwidth is seen in Figure 1. The chipping (PN) and data waveforms are seen in Figure 2.

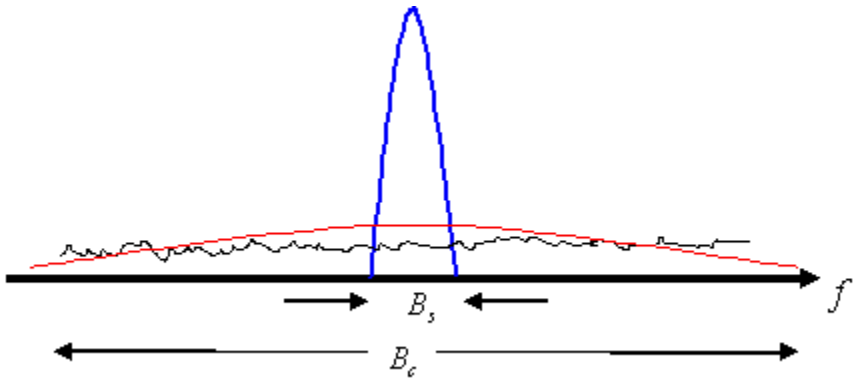

Figure 1. Bandwidths of the narrowband (blue) and the spread (red) signal. The black curve represents the noise level. (From [13])

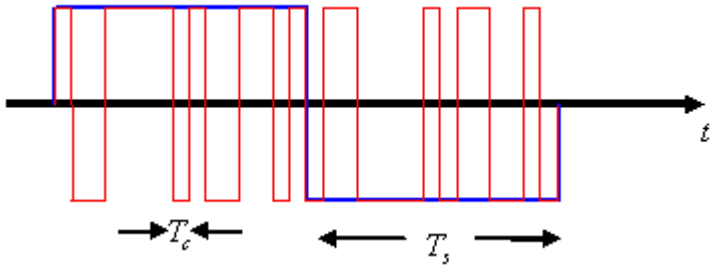

Figure 2. The data waveform (blue) and the PN, or chipping, waveform (red). (From [13])

A very important element of DSSS is the PN sequence. The most important and commonly used type of PN sequence is the maximal length sequence (m-sequence), which can be generated by linear feedback shift registers (LFSR). If the number of shift registers is *n*, then the PN sequence has a period of $N = 2^n - 1$ chips. An *m*-sequence can be generated by a primitive polynomial *h(x)*:

$$h(x) = 1 + h_1 x + h_2 x^2 + \ldots + h_{n-1} x^{n-1} + x^n \tag{2.1}$$

where $h_i \in \{0,1\}$. We show the configuration of an LFSR in Figure 3. A very important point to notice is that an *m*-sequence has 2^{n-1} ones and $2^{n-1} - 1$ zeros. We observe in Figure 4 the autocorrelation function of a periodic *m*-sequence when a unit amplitude square wave of duration T_c is employed as the pulse shape of a chip. For our research, we consider only *m*-sequences.

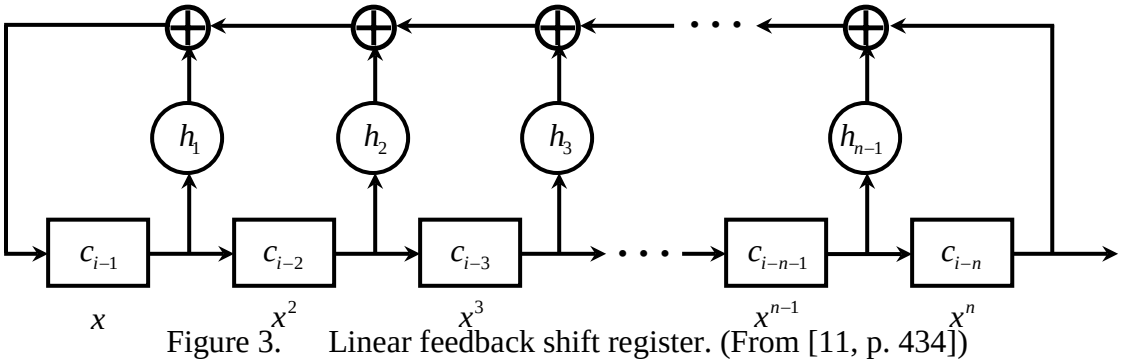

Figure 3. Linear feedback shift register. (From [11, p. 434])

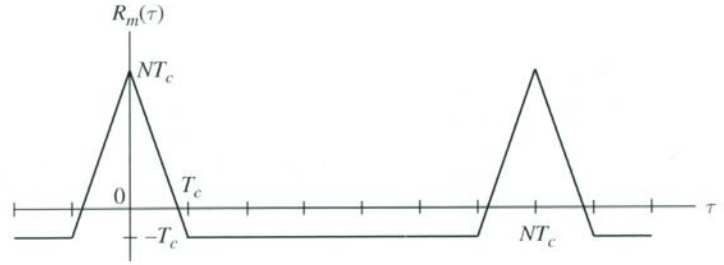

Figure 4. Autocorrelation function of an *m*-sequence, $N = 2^n - 1$. (From [11, p. 435])

B. FADING CHANNELS

A very effective channel model that simulates a realistic channel is the multipath fading channel. This type of channel is encountered in most mobile wireless communications applications.

In a multipath fading channel, the transmitted signal arrives at the receiver via multiple paths. These multipaths arise via signal reflections from ground, buildings, and various structures in general. They also arise from signal diffraction via bending around building corners or other edged points and signal scattering from a variety of objects such as vehicles, trees, etc. Each signal path results in a randomly delayed, attenuated, and phase-shifted copy of the transmitted signal. These multipath copies combine at the receiver to give rise to a received signal whose attenuation can be modeled as a Rayleigh fading process (for no line-of-sight path), a Rician fading process (for one line-of-sight path), or a Nakagami fading process. In addition, because the arrival times of the

multipath copies are random, especially in a mobile environment, the multipath copies in some cases overlap the next bit or symbol and cause inter-symbol interference.

For the time-invariant channel, the complex envelope and the frequency response of the channel are obtained as [11, pp. 526-529]:

$$h(\tau) = \sum_i h_i \delta(\tau - \tau_i), \tag{2.2}$$

$$H(f) = \sum_i h_i e^{-j2\pi f \tau_i}, \tag{2.3}$$

respectively. The multipath delay spread of a fading channel is defined as the maximum of the difference in propagation times between the first path with power P_1 and the last significant path of power P_l such that the ratio P_1 / P_l is over a given threshold γ [11, pp. 526-529]. A typical multipath intensity profile of a fading channel is shown in Figure 5. A channel is defined as flat fading when the multipath delay spread is less than the symbol time [11, pp. 526-529]. Therefore, for a flat fading channel, we obtain the complex channel tap as $h = |h| e^{j\theta}$, where $|h|$ is the attenuation coefficient of the signal and θ is the phase shift that the fading channel introduces. In this research, we assume that the complex channel tap is available via perfect channel estimation.

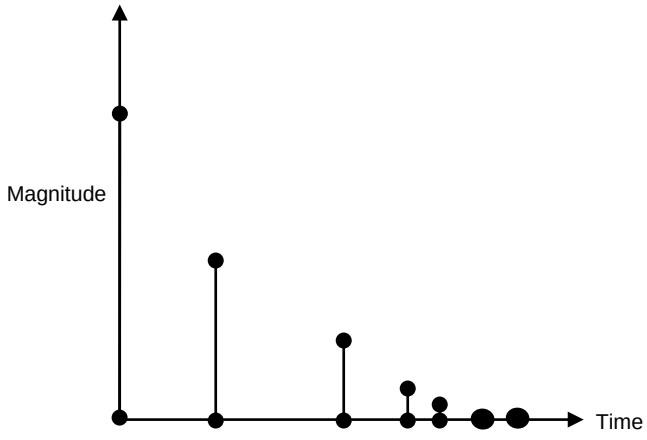

Figure 5. Multipath intensity profile of a fading channel. (From [11, pp. 526-529])

C. MULTIPLE INPUT-MULTIPLE OUTPUT SYSTEMS

The simplest system that we examine is a system with one transmit and one receive antenna, also called single input-single output (SISO). In order to achieve better performance, especially in fading channels, one method is to implement antenna diversity. This can be done by using multiple transmit antennas, referred to as MISO, or multiple receive antennas, referred to as single input multiple output, referred to as SIMO, or by using multiple transmit and receive antennas, referred to as MIMO. In this work, we study and compare MISO and MIMO configurations.

The system configuration of a MISO system is shown in Figure 6. Transmit antenna diversity provides spatial repetition of a transmitted symbol via different antennas. The idea is similar to time diversity, where a transmitted symbol is repeated multiple times. Time diversity is a type of repetition code in which the symbol is transmitted multiple times. These channel-tap weighted copies are available at the input of the combiner. Spatial repetition via different transmit antennas alone cannot provide separate copies of the symbol at the receiver because the single-antenna receiver receives the sum of these copies without the ability to separate them for combining. A combination of transmit antenna diversity and time diversity should provide the receiver sufficient statistics to separate the copies in order to combine them. We can achieve this by applying orthogonal space-time block codes (OSTBC). Finally, we assume that the transmit antennas have sufficient inter-element spacing in order to have uncorrelated paths.

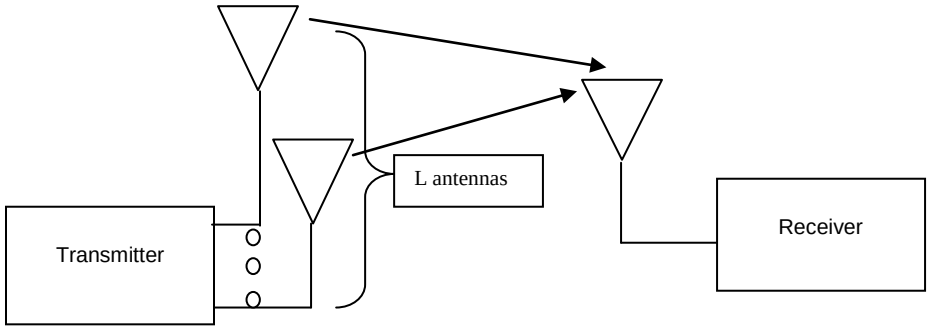

Figure 6. Configuration of a MISO system. (After [11, p. 600])

If we use a MIMO system, we can achieve full diversity benefit. We represent transmit diversity by using space-time coding with a complex $L_s \times L_t$ code matrix $\boldsymbol{G}$, where we obtain L_t-fold diversity via L_t transmit antennas for m complex symbols transmitting over L_s symbol times and a code rate $R = m / L_s$. On the receive side, we obtain diversity with L_r receive antennas. With the proper use of maximal ratio combining (MRC), we can achieve diversity of order $L = L_t L_r$ [11, pp. 578-580], [11, pp. 605-608]. The MIMO configuration is shown in Figure 7.

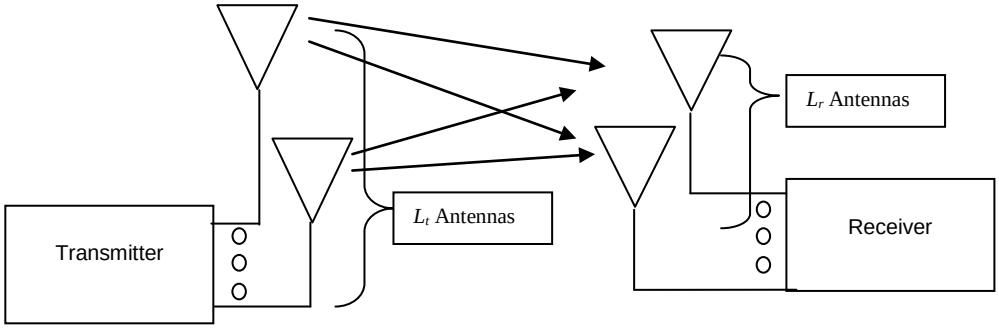

Figure 7. Configuration of a MIMO system.

D. MAXIMAL-RATIO COMBINING- RAYLEIGH FADING CHANNEL

1. Maximal Ratio Combining

The technique presented in this section is known as MRC. For an *L*-fold diversity system, we assume fixed throughput and fixed transmitted power in order to obtain a proper comparison. Thus, the energy of a transmitted copy is *1/L* of the symbol energy. Therefore, an optimum coherent combiner in the receiver must execute a combining operation in order to obtain a signal-to-noise ratio that is the sum of signal-to-noise ratios of the *L* received copies. More specifically, this means that the combiner must rotate the phases of the decision sample of *L* copies to align their phases (co-phasing) and weight each copy with their respective sub-channel tap before summing (weighting). Therefore, strong sub-channels are taken into account more than weak sub-channels. Consider the

pre-combining samples of L copies of an arbitrary transmitted symbol s_i at the output of the matched filter. Each copy has a corresponding complex sub-channel tap h_l. We have

$$Y_l = h_l s_i + N_l,\ l = 1, 2, ..., L, \tag{2.4}$$

where Y_l is the received complex signal from l-th sub channel and N_l is the complex additive white Gaussian noise (AWGN) of l-th sub channel. The complex Gaussian random variable N_l has a variance $2\sigma^2$ [11, pp. 578-580]. We can express (2.4) in vectors such that

$$\boldsymbol{Y} = \boldsymbol{h} s_i + \boldsymbol{N}, \tag{2.5}$$

where $\boldsymbol{Y} = [Y_1\ Y_2 ... Y_L]^t$, $\boldsymbol{h} = [h_1\ h_2 ... h_L]^t$ and $\boldsymbol{N} = [N_1\ N_2 ... N_L]^t$.

We assume perfect channel estimation. Thus, the sufficient statistic for coherent demodulation is $\left(\boldsymbol{h}^* / \|\boldsymbol{h}\|\right)\boldsymbol{Y}$, where $\boldsymbol{h}^*$ is the conjugate transpose of vector $\boldsymbol{h}$ and $\|\boldsymbol{h}\|$ is the norm of vector $\boldsymbol{h}$. We have the following MRC decision variable

$$X = \frac{\boldsymbol{h}^*}{\|\boldsymbol{h}\|}(\boldsymbol{h} s_i + \boldsymbol{N}) = \|\boldsymbol{h}\| s_i + \frac{\boldsymbol{h}^*}{\|\boldsymbol{h}\|}\boldsymbol{N}. \tag{2.6}$$

The complex Gaussian noise $\left(\boldsymbol{h}^* / \|\boldsymbol{h}\|\right)\boldsymbol{N}$ has variance $2\sigma^2$. The instantaneous MRC output signal-to-noise ratio $\boldsymbol{SNR}_{0,i}$ given a symbol s_i is

$$\boldsymbol{SNR}_{0,i} = \|\boldsymbol{h}\|^2 |s_i|^2 / 2\sigma^2 = \sum_l |h_l|^2 |s_i|^2 / 2\sigma^2 = \sum_l \boldsymbol{SNR}_{l,i}, \tag{2.7}$$

where $\boldsymbol{SNR}_{l,i} = |h_l|^2 |s_i|^2 / 2\sigma^2$ [11, pp. 578-580] is the instantaneous signal-to-noise ratio of the pre-combining l^{th} copy of symbol s_i. Thus, MRC achieves the maximum output signal-to-noise ratio, which is the sum of L input SNR of the multiple copies of the received signal.

Assuming perfect channel estimation and using the mapping $s_i \rightarrow \boldsymbol{s}_i$ for complex variable to two-dimensional vector for *I-Q* modulation signals, we get the conditional pair-wise error probability between two vectors $\|\boldsymbol{h}\|\boldsymbol{s}_i$ and $\|\boldsymbol{h}\|\boldsymbol{s}_j$ as [11, pp. 578-580]

$$\Pr\left(\|\boldsymbol{h}\|\boldsymbol{s}_i \to \|\boldsymbol{h}\|\boldsymbol{s}_j\right) = Q\left(\frac{\|\boldsymbol{h}\|\|\boldsymbol{s}_i - \boldsymbol{s}_j\|}{2\sigma}\right). \tag{2.8}$$

The conditional bit error probability for the Gray-coded signal set is given by the following approximation [11, pp. 578-580]

$$P_b\left(\|\boldsymbol{h}\|\right) \approx \frac{N_n}{\log_2 M} Q\left(\frac{\|\boldsymbol{h}\| d_{\min}}{2\sigma_T}\right), \tag{2.9}$$

where the minimum Euclidean distance is $d_{\min} = \min_{i,j} \| \boldsymbol{s}_i - \boldsymbol{s}_j \|$, $\sigma^2 = N_0 / 2$ is the noise variance, M is the total number of symbols of the modulation scheme, and N_n is average number of symbols at the minimum Euclidean distance $d_{\min}$ or the average number of nearest neighbors. Since we know the statistics of the Rayleigh fading channel, we can calculate the bit error probability as

$$P_b = \mathbf{E}\left[P_b\left(\|\boldsymbol{h}\|\right)\right] \approx \mathbf{E}\left[\frac{N_n}{\log_2 M} Q\left(\frac{\|\boldsymbol{h}\| d_{\min}}{2\sigma}\right)\right]. \tag{2.10}$$

We also define the modulation-dependent factor [11, pp. 578-580] as

$$\alpha \boldsymbol{SNR} = \frac{1}{2}\left(\frac{d_{\min}}{2\sigma}\right)^2. \tag{2.11}$$

The diversity symbol energy $\boldsymbol{\mathcal{E}}_s$ is given by $\boldsymbol{\mathcal{E}}_s = E_s / L$, where E_S is the symbol energy.

2. Rayleigh Fading Channel

When the sub-channel tap magnitudes $|h_l|$ are Rayleigh distributed with normalized mean square value $\mathbf{E}\left(|h_l|^2\right) = 1$, the combining channel tap magnitude $\|\boldsymbol{h}\|^2 = \sum_{l=1}^{L} |h_l|^2$ has a chi-square density function with $2L$ degrees of freedom: [11, pp. 578-580]

$$f_{\|\boldsymbol{h}\|^2}(y) = \frac{y^{L-1} e^{-y}}{(L-1)!}. \tag{2.12}$$

The corresponding bit error probability is given by [11, pp. 578-580]

$$P_b \approx \frac{N_n}{\log_2 M}\left(\frac{1-\mu}{2}\right)^L \sum_{l=0}^{L-1}\binom{L-1+l}{l}\left(\frac{1+\mu}{2}\right)^l, \tag{2.13}$$

where [11, pp. 578-580]

$$\mu = \sqrt{\frac{\alpha\, \boldsymbol{SNR}}{1+\alpha\, \boldsymbol{SNR}}}. \tag{2.14}$$

We obtain the following bit error probability expressions by changing the various parameters for the modulation schemes of interest.

a. PSK

The minimum Euclidean distance is $d_{\min} = 2\sqrt{\mathcal{E}_b}$, where $\mathcal{E}_b$ is the diversity bit energy [11, pp. 578-580]. We also know that $N_n = 1$ and $M = 2$. Thus, the bit error probability for PSK is

$$P_b = \left(\frac{1-\mu}{2}\right)^L \sum_{l=0}^{L-1}\binom{L-1+l}{l}\left(\frac{1+\mu}{2}\right)^l. \tag{2.15}$$

b. QPSK

The minimum Euclidean distance is $d_{\min} = \sqrt{2\mathcal{E}_s}$, where $\mathcal{E}_s$ is the diversity symbol energy [11, pp. 578-580]. We also know that $N_n = 2$ and $M = 4$. Thus, the bit error probability for QPSK is the same as that of PSK:

$$P_b = \left(\frac{1-\mu}{2}\right)^L \sum_{l=0}^{L-1}\binom{L-1+l}{l}\left(\frac{1+\mu}{2}\right)^l. \tag{2.16}$$

c. MQAM

The minimum Euclidean distance is $d_{\min} = \sqrt{6\mathcal{E}_s/(M-1)}$ [11, pp. 578-580]. We also know that $N_n = 4 - 4/\sqrt{M}$. Thus, the bit error probability for *M*-ary quadrature amplitude modulation (MQAM) is given by

$$P_b = \frac{4-4/\sqrt{M}}{\log_2 M}\left(\frac{1-\mu}{2}\right)^L \sum_{l=0}^{L-1}\binom{L-1+l}{l}\left(\frac{1+\mu}{2}\right)^l. \tag{2.17}$$

E. PRESENCE OF JAMMING

In this thesis, all the systems that we consider are evaluated for a Rayleigh fading channel and three types of jamming: broadband noise, pulsed-noise and tone. We present these types of jamming in detail in the following chapters to evaluate system performance in a hostile environment. In addition, we evaluate the effectiveness of the MIMO diversity and DSSS modulation in these systems.

III. PERFORMANCE ANALYSIS OF DS-PSK MISO

A. SYSTEM DESCRIPTION

In this chapter, we analyze the performance of a DSSS PSK MISO system. We examine this specific system under three types of jamming: broadband jamming, pulsed jamming and tone jamming. The system is shown in Figure 6. It has *L* transmit antennas and one receive antenna. At the receiver, in order to obtain a combining decision variable whose SNR is the sum of SNR of the *L* received copies of the transmit signal, we use MRC, which is an optimum coherent combining technique as mentioned in the previous chapter. The system experiences Rayleigh fading. The receiver is shown in Figure 8.

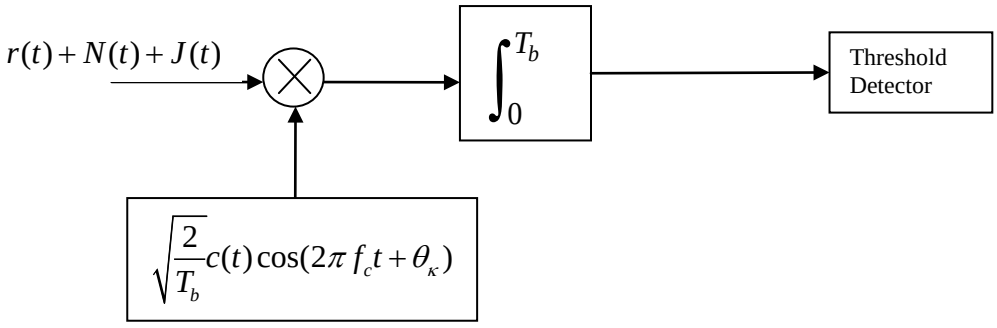

Figure 8. DSSS PSK Receiver

In Figure 8, we denote $r(t)$ as the total received signal (the sum of the signal from *L* transmit antennas), *J(t)* is the jamming signal and *N(t)* is the AWGN. The waveform *c(t)* is generated by the PN sequence, f_c is the carrier frequency of the signal, T_b is the bit time and θ_k is the arbitrary phase of the arriving signal. We assume perfect channel estimation. The power spectral density (PSD) of AWGN equals $N_0/2$.

B. BROADBAND JAMMING

In this section, we assume that broadband jamming is present. It is a signal similar to AWGN. The PSD of the jamming signal is $J_0'/2$. The received signal from *k*-th antenna is

$$r_k(t) = |h_k| A d_k c(t) \cos(2\pi f_c t + \theta_k) \tag{3.1}$$

for $iT_b < t < (i+1)T_b$, where h_k is the channel tap for *k*-th antenna, *A* is the amplitude of the signal, d_k is the information bit, and θ_k is the phase of the channel tap. Assuming perfect channel estimation means that we know h_k and θ_k. Thus, the total received signal, including noise and jamming signals, is

$$x_k(t) = |h_k| A d_k c(t) \cos(2\pi f_c t + \theta_k) + n(t) + j(t). \tag{3.2}$$

Therefore, the signal after the mixer becomes

$$\begin{aligned} x_k'(t) &= \sqrt{\frac{2}{T_b}} |h_k| A \cdot d_k c^2(t) \cos^2(2\pi f_c t + \theta_k) + \sqrt{\frac{2}{T_b}} c(t) \cdot n(t) \cos(2\pi f_c t + \theta_k) \\ &+ \sqrt{\frac{2}{T_b}} c(t) \cdot j(t) \cos(2\pi f_c t + \theta_k) \end{aligned} \tag{3.3}$$

$$\begin{aligned} \Rightarrow x_k'(t) &= \frac{|h_k| A \cdot d_k}{\sqrt{2T_b}} (1 + \cos(4\pi f_c t + 2\theta_k)) + \sqrt{\frac{2}{T_b}} c(t) \cdot n(t) \cos(2\pi f_c t + \theta_k) \\ &+ \sqrt{\frac{2}{T_b}} c(t) \cdot j(t) \cos(2\pi f_c t + \theta_k) \end{aligned} . \tag{3.4}$$

The high frequency terms are neglected in our analysis since they are rejected by the matched filter [11, p. 451]. After the integrator, the signal becomes

$$x_k''(t) = |h_k| A \cdot d_k \cdot \sqrt{\frac{T_b}{2}} + N_k + J_k, \tag{3.5}$$

where

$$N_k = \int_0^{T_b} \sqrt{\frac{2}{T_b}} c(t) \cdot n(t) \cos(2\pi f_c t + \theta_k) dt \tag{3.6}$$

and

$$J_k = \int_0^{T_b} \sqrt{\frac{2}{T_b}} c(t) \cdot j(t) \cos(2\pi f_c t + \theta_k) dt. \tag{3.7}$$

We calculate the variance of AWGN and jamming signals to be

$$\sigma_{N_k}^2 = \overline{N_k \cdot N_k^*} = E\left\{\left(\sqrt{\frac{2}{T_b}}\right)^2 \cdot \int_0^{T_b}\int_0^{T_b} (n(t)n(\tau)c(t)c(\tau)\cos(2\pi f_c t + \theta_\kappa)\cos(2\pi f_c \tau + \theta_\kappa))\, dt\, d\tau\right\} \quad (3.8)$$

and

$$\sigma_{N_k}^2 = \frac{2}{T_b}\int_0^{T_b}\int_0^{T_b}\left[E(n(t)n(\tau)) \cdot E(c(t)c(\tau)\cos(2\pi f_c t + \theta_\kappa)\cos(2\pi f_c \tau + \theta_\kappa))\right] dt\, d\tau\,. \quad (3.9)$$

We know that the auto covariance of noise is [11, p. 98]

$$E(n(t)n(\tau)) = \frac{N_0\delta(t-\tau)}{2}. \quad (3.10)$$

Thus, the variance of AWGN is

$$\sigma_{N_k}^2 = \frac{2}{T_b}\int_0^{T_b}\int_0^{T_b}\left[\frac{N_0\delta(t-\tau)}{2} \cdot E(c(t)c(\tau)\cos(2\pi f_c t + \theta_\kappa)\cos(2\pi f_c \tau + \theta_\kappa))\right] dt\, d\tau \quad (3.11)$$

$$\Rightarrow \sigma_{N_k}^2 = \frac{2}{T_b}\cdot\frac{N_0}{2}\int_0^{T_b} E(c^2(t)\cos^2(2\pi f_c t + \theta_k))\, dt \quad (3.12)$$

$$\Rightarrow \sigma_{N_k}^2 = \frac{N_0}{T_b}\int_0^{T_b} E(\frac{1}{2} + \frac{\cos(4\pi f_c t + 2\theta_k)}{2})\, dt \quad (3.13)$$

$$\Rightarrow \sigma_{N_k}^2 = \frac{N_0}{T_b}\cdot\frac{T_b}{2} = \frac{N_0}{2}. \quad (3.14)$$

Similarly, we have

$$\sigma_{J_k}^2 = \overline{J_k \cdot J_k^*} = E\left\{\left(\sqrt{\frac{2}{T_b}}\right)^2 \cdot \int_0^{T_b}\int_0^{T_b} (j(t)\, j(\tau)c(t)c(\tau)\cos(2\pi f_c t + \theta_\kappa)\cos(2\pi f_c \tau + \theta_\kappa))\, dt\, d\tau\right\} \quad (3.15)$$

$$\Rightarrow \sigma_{J_k}^2 = \frac{2}{T_b}\int_0^{T_b}\int_0^{T_b}\left[E(j(t)\, j(\tau)) \cdot E(c(t)c(\tau)\cos(2\pi f_c t + \theta_\kappa)\cos(2\pi f_c \tau + \theta_\kappa))\right] dt\, d\tau\,. \quad (3.16)$$

The jamming signal is a noise-like signal by definition and, therefore, we have

$$\sigma_{J_k}^2 = \frac{2}{T_b}\int_0^{T_b}\int_0^{T_b}\left[\frac{J_0'\delta(t-\tau)}{2} \cdot E(c(t)c(\tau)\cos(2\pi f_c t + \theta_\kappa)\cos(2\pi f_c \tau + \theta_\kappa))\right] dt\, d\tau \quad (3.17)$$

$$\Rightarrow \sigma_{J_k}^2 = \frac{2}{T_b}\cdot\frac{J_0'}{2}\int_0^{T_b} E(c^2(t)\cos^2(2\pi f_c t + \theta_k))\, dt = \frac{J_0'}{T_b}\int_0^{T_b} E(\frac{1}{2} + \frac{\cos(4\pi f_c t + 2\theta_k)}{2})\, dt \quad (3.18)$$

$$\Rightarrow \sigma_{J_k}^2 = \frac{J_0'}{T_b}\cdot\frac{T_b}{2} = \frac{J_0'}{2}. \quad (3.19)$$

In order to perform a proper comparison of the performances of a DS system and a non-DS system under barrage noise jamming, we assume that the overall jammer power is the same for both cases. We consider that the equivalent noise bandwidth of the conventional signal is $1/T_b$ and the equivalent noise bandwidth of the spread spectrum signal is $1/T_c$ [11, p. 449], where T_c is the chip time. We also denote, for the conventional system, the PSD of the jamming signal as J_0. For the spread spectrum system, we denote the PSD of the jamming signal as J_0'. Thus, the power of the jammer for the conventional system is $P_J = (J_0/2)(2/T_b)$ and for the SS system is $P_{J'} = (J_0'/2)(2/T_c)$. Then, we have $P_J = P_{J'} \Rightarrow J_0/T_b = J_0'/T_c$, and finally, we obtain

$$J_0' = \frac{J_0 T_c}{T_b} = \frac{J_0}{N} \tag{3.20}$$

where $N = T_b/T_c$ is the spread factor.

The total variance of noise and jamming signal is

$$\sigma_{T_k}^2 = \sigma_{N_k}^2 + \sigma_{J_k}^2 = \frac{N_0 + J_0'}{2}. \tag{3.21}$$

Since we utilize a Gray coded signal and MRC for a Rayleigh fading channel, we can use equation (2.13). Thus, the probability of error is given by

$$P_b = \frac{N_n}{\log_2 M}\left(\frac{1-\mu}{2}\right)^L \sum_{l=0}^{L-1}\binom{L-1+l}{l}\left(\frac{1+\mu}{2}\right)^l, \tag{3.22}$$

where for PSK modulation scheme, we have $N_n = 1$ and $log_2 M = 1$. We also define

$$\mu = \sqrt{\frac{aSJNR}{1+aSJNR}}, \tag{3.23}$$

and α-signal-to-jamming plus noise ratio $(aSJNR)$ is

$$aSJNR = \frac{1}{2}\left(\frac{d_{\min}}{2\sigma_T}\right)^2, \tag{3.24}$$

where $d_{\min} = 2\sqrt{\varepsilon_b}$, σ_T^2 is the total variance of jamming signal plus noise, and $\varepsilon_b = E_b/L$. Thus, for DS-PSK, by using (3.21) and (3.24) we obtain

$$aSJNR = \frac{1}{2}\left(\frac{d_{\min}}{2\sigma_T}\right)^2 = \frac{1}{2}\cdot\frac{4\cdot\varepsilon_b}{4\cdot\frac{(N_0+J_0')}{2}} = \frac{\varepsilon_b}{N_0+J_0'} \tag{3.25}$$

$$\Rightarrow aSJNR = \frac{E_b}{L(N_0+J_0')} = \frac{1}{L\left[\left(\frac{E_b}{N_0}\right)^{-1}+\left(\frac{E_b}{J_0'}\right)^{-1}\right]}. \tag{3.26}$$

Therefore, we obtain

$$\mu = \sqrt{\frac{1}{\frac{1}{aSJNR}+1}} = \sqrt{\frac{1}{L\left[\left(\frac{E_b}{N_0}\right)^{-1}+\left(\frac{E_b}{J_0'}\right)^{-1}\right]+1}}. \tag{3.27}$$

Finally, by using (3.20) and (3.27), we obtain the equation

$$\mu = \sqrt{\frac{1}{\frac{1}{aSJNR}+1}} = \sqrt{\frac{1}{L\left[\left(\frac{E_b}{N_0}\right)^{-1}+\frac{1}{N}\left(\frac{E_b}{J_0}\right)^{-1}\right]+1}}. \tag{3.28}$$

In Figures 9-12, we present the bit error rates (BER) versus E_b / N_0 for various diversities (L transmit antennas) and signal-to-jamming ratios $\left(SJR = E_b / J_0\right)$. We use equations (3.28) and (3.22) to calculate the BER. We also present the OSTBC codes that we use for each diversity order. All the plots are for a spread factor *N=64*.

1. Diversity *L*=1

In this case, we use one transmit antenna, thus we do not have an OSTBC.

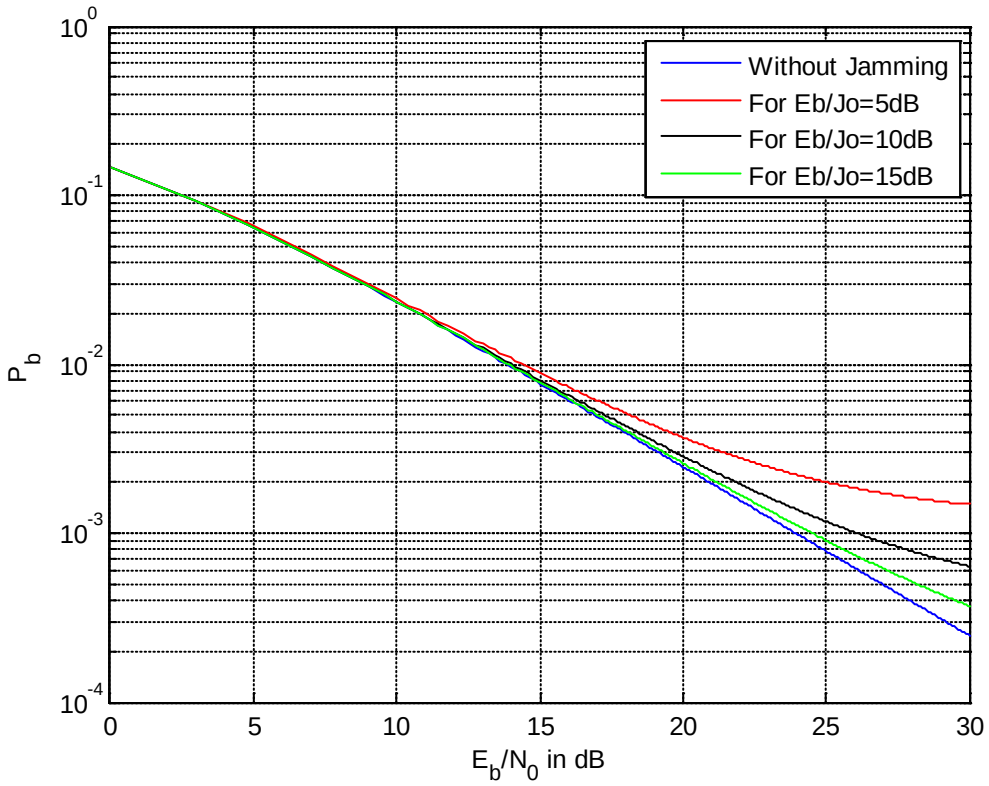

Figure 9. BER of DS PSK system for broadband jamming and diversity *L*=1.

2. Diversity *L*=2

In this case, we use an Alamouti OSTB code, which has a code rate of *R*=1, and its matrix *G* is given by [14, pp. 103-105]

$$G = \begin{bmatrix} s_1 & s_2 \\ -s_2^* & s_1^* \end{bmatrix}. \tag{3.29}$$

In order to do a proper comparison of the performances of the various systems examined, we consider fixed transmitted power. Because of the two transmit antennas, the symbol energy is divided by two. In addition, we have two symbols transmitted over two symbol times (code rate *R*=1). Thus, the symbol energy becomes $E_s^{'} = E_s / 2$. The BER plot is shown in Figure 10.

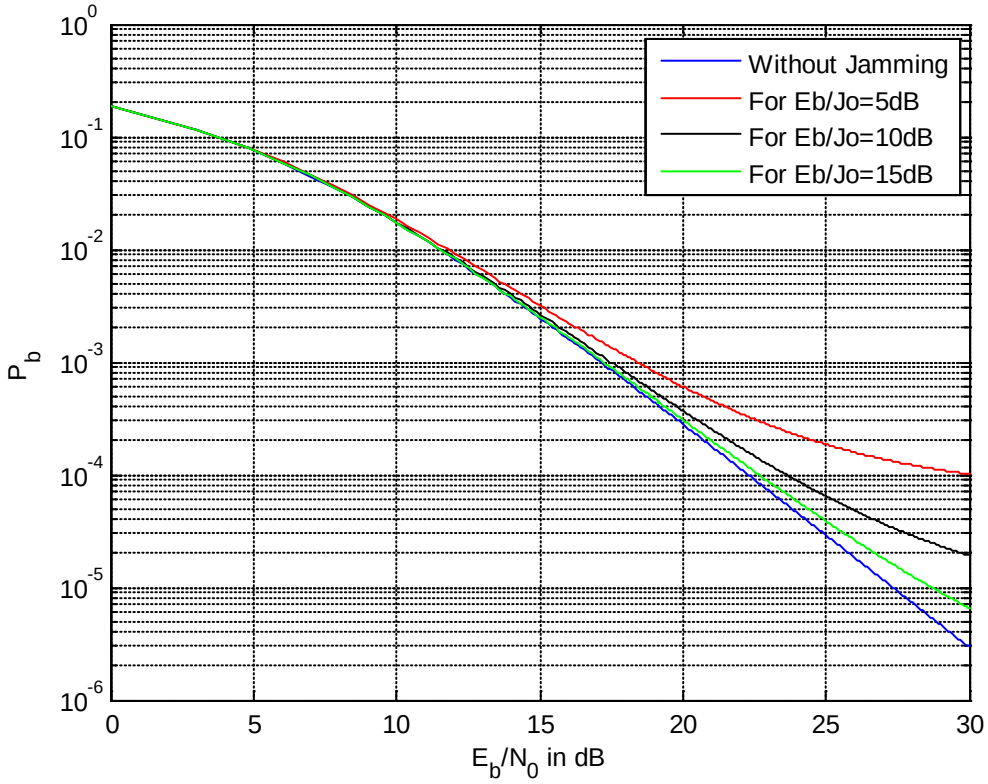

Figure 10. BER of DS PSK system for broadband jamming and diversity $L=2$.

3. Diversity L=3

In this case, we use an OSTBC code, three transmit antennas and rate $R = 3/4$. The matrix G of the code is [14, pp. 103-105]

$$G = \begin{vmatrix} s_1 & 0 & -s_2^* \\ 0 & s_1 & -s_3 \\ s_2 & s_3^* & s_1^* \\ -s_3 & s_2^* & 0 \end{vmatrix}. \tag{3.30}$$

We consider fixed transmitted power and because of the transmit antennas, the symbol energy is divided by three. In addition, we have three symbols transmitted over four symbol times (code rate R=3/4). Thus, the symbol energy becomes $E_s^{'} = E_s / 3$. Therefore, in order to maintain the same throughput, we have to increase the symbol rate by multiplying it by a factor of 4/3. Thus, the symbol energy is degraded by 3/4, and we obtain: $E_s^{''} = E_s^{'} = (E_s / 3)(3/4) = E_s / 4$. The BER plot is shown in Figure 11.

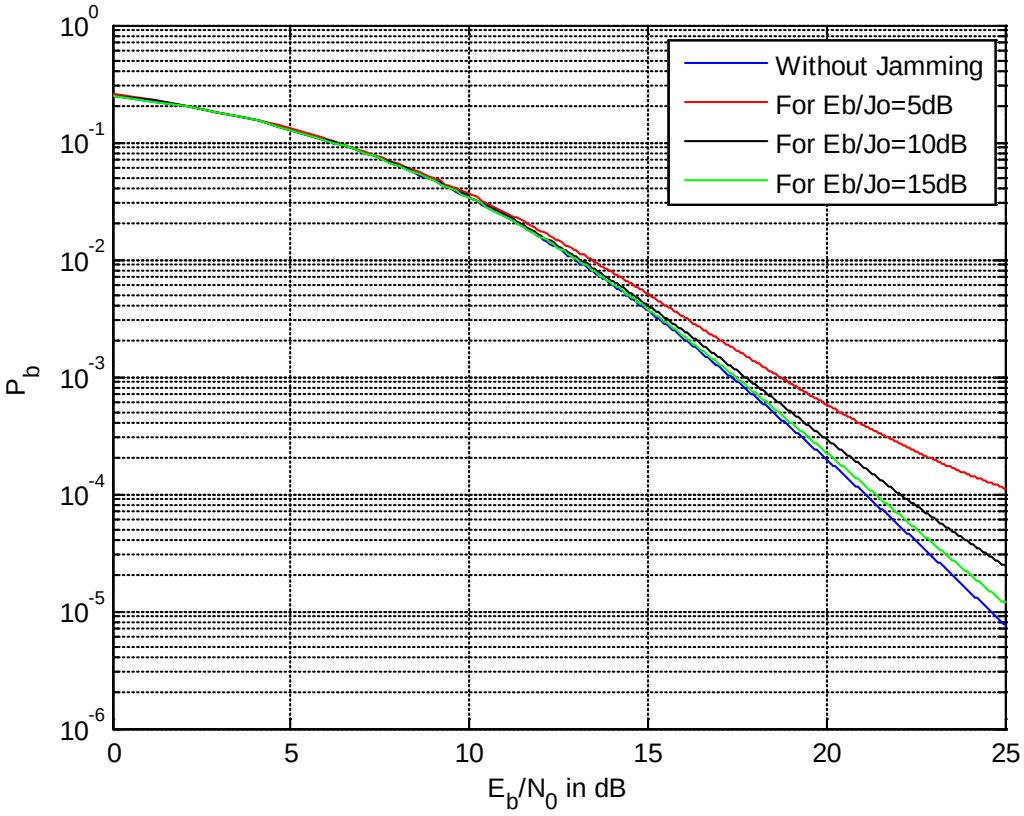

Figure 11. BER of DS PSK system for broadband jamming and diversity L=3.

4. Diversity L=4

In this case, we use an OSTBC code, four transmit antennas and rate R=3/4. The matrix G of the code is [14, pp. 103-105]

$$G = \begin{vmatrix} s_1 & 0 & -s_2^* & s_3^* \\ 0 & s_1 & -s_3 & -s_2 \\ s_2 & s_3^* & s_1^* & 0 \\ -s_3 & s_2^* & 0 & s_1^* \end{vmatrix}. \tag{3.31}$$

We consider fixed transmitted power, and because of the transmit antennas diversity, the symbol energy is divided by four. In addition, we have three symbols transmitted over four symbol times (code rate R=3/4). Thus, the symbol energy becomes $E_s^{'} = E_s / 4$. Therefore, in order to maintain the same throughput, we have to

increase the symbol rate by multiplying it by a factor of 4/3. Thus, the symbol energy is degraded by 3/4, and we obtain $E_s^{"} = E_s^{'} = (E_s / 4)(3/4) = (3/16)E_s$. The BER plot is shown in Figure 12.

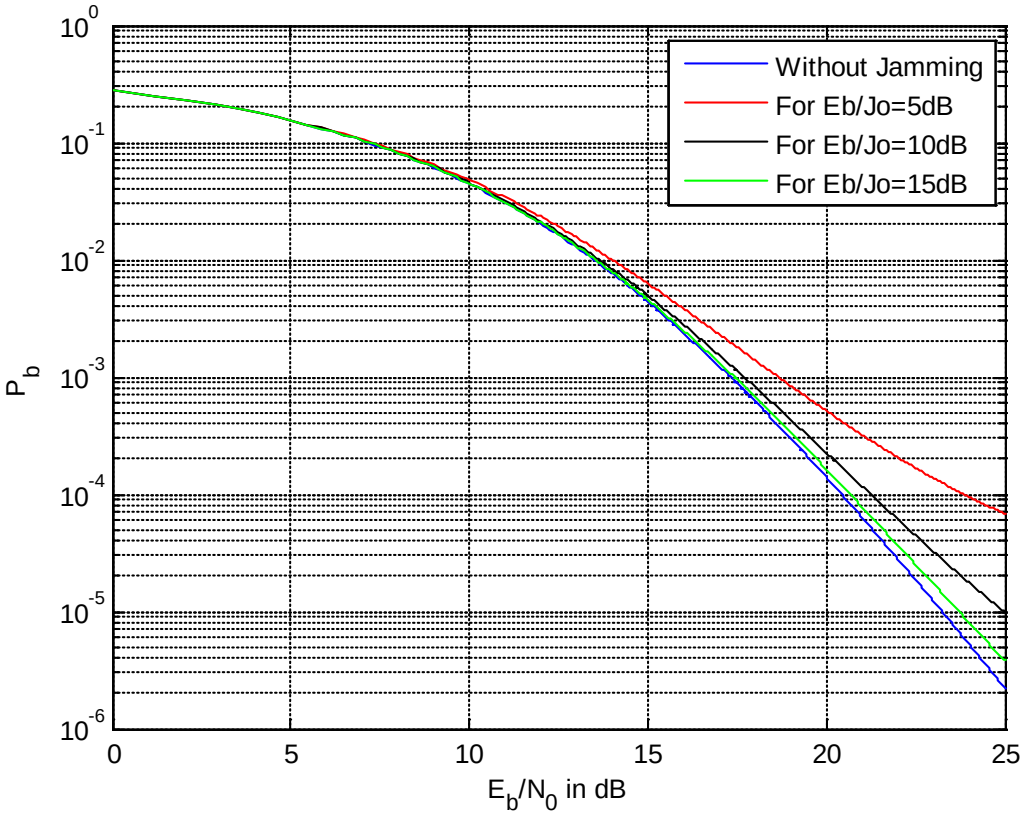

Figure 12. BER of DS PSK system for broadband jamming and diversity L=4.

C. PULSED JAMMING

In this section, the jamming signal is pulsed jamming. The jammer is on for ρ percent of the time. Therefore, ρ is defined to be the duty cycle of the jammer, and its values are between zero and one. Thus, when the jammer is off, the system performs with AWGN only and when the jammer is on, the system is affected by both AWGN and the jamming signal. From the total probability theorem, we obtain [11, p. 450]

$$P_b = \rho P_{b_{J+N}} + (1-\rho)P_{b_N}\ , \tag{3.32}$$

where $P_{b_{J+N}}$ is the BER with jamming and AWGN, and P_{b_N} is the BER with AWGN only. We consider the PSD of jamming signal as $J_0''/2$. The bit error probabilities are [11, pp. 578-580]

$$P_{b_{J+N}} = \left(\frac{1-\mu}{2}\right)^L \sum_{l=0}^{L-1} \binom{L-1+l}{l} \left(\frac{1+\mu}{2}\right)^l, \tag{3.33}$$

where

$$\mu = \sqrt{\frac{1}{\frac{1}{aSJNR}+1}} = \sqrt{\frac{1}{L\left[\left(\frac{E_b}{N_0}\right)^{-1} + \left(\frac{E_b}{J_0''}\right)^{-1}\right]+1}} \tag{3.34}$$

and

$$P_{b_N} = \left(\frac{1-\mu'}{2}\right)^L \sum_{l=0}^{L-1} \binom{L-1+l}{l} \left(\frac{1+\mu'}{2}\right)^l, \tag{3.35}$$

where

$$\mu' = \sqrt{\frac{1}{\frac{1}{aSNR}+1}} = \sqrt{\frac{1}{L\left(\frac{E_b}{N_0}\right)^{-1}+1}}. \tag{3.36}$$

If we consider

$$\left(\frac{E_b}{N_0}\right)^{-1} \ll \left(\frac{E_b}{J_0''}\right)^{-1}, \tag{3.37}$$

then the AWGN can be neglected, [11, p. 450], [15, p. 753]. We obtain

$$P_b \approx \rho P_{b_J}, \tag{3.38}$$

where P_{b_J} is the BER for jamming only. Therefore, we can use

$$P_{b_J} = \left(\frac{1-\mu''}{2}\right)^L \sum_{l=0}^{L-1} \binom{L-1-l}{l} \left(\frac{1+\mu''}{2}\right)^l, \tag{3.39}$$

where

$$\mu'' = \sqrt{\frac{1}{\frac{1}{aSJR}+1}} = \sqrt{\frac{1}{L\left(\frac{E_b}{J_0''}\right)^{-1}+1}}. \tag{3.40}$$

Similar to the case of barrage noise jamming, in order to perform a proper comparison of the performances of a DS system and a non-DS system under pulsed noise

jamming, we assume that the overall jammer power is the same for both cases. We note that the equivalent noise bandwidth of the conventional signal is $1/T_b$ and the equivalent noise bandwidth of the spread spectrum signal is $1/T_c$ [11, p. 449], where T_c is the chip time. We also denote, for the conventional system, the PSD of the jamming signal as J_0. For the spread spectrum system under pulsed noise, the PSD of the jamming signal as J_0" when the jammer is on. Thus, the power of the jammer for the conventional system is $P_J = (J_0/2)(2/T_b)$ and for the SS system is $P_{J'} = \rho(J_0"/2)(2/T_c)$. Then, we have $P_J = P_{J'} \Rightarrow J_0/(\rho T_b) = J_0"/T_c$, and

$$J_0" = \frac{J_0}{\rho N}. \tag{3.41}$$

By combining the (3.40) and (3.41), we obtain

$$\mu" = \sqrt{\frac{1}{\frac{1}{aSJR}+1}} = \sqrt{\frac{1}{\frac{L}{N\rho}\left(\frac{E_b}{J_0}\right)^{-1}+1}}. \tag{3.42}$$

By using equations (3.42) and (3.39), we present the BER performances versus E_b/J_0, for various diversities (L transmit antennas) and various values of duty cycle ρ in Figures 13-16. We use the same OSTBC that we described in the section on broadband jamming for the corresponding antenna diversities. All the plots are for spread factor N=64.

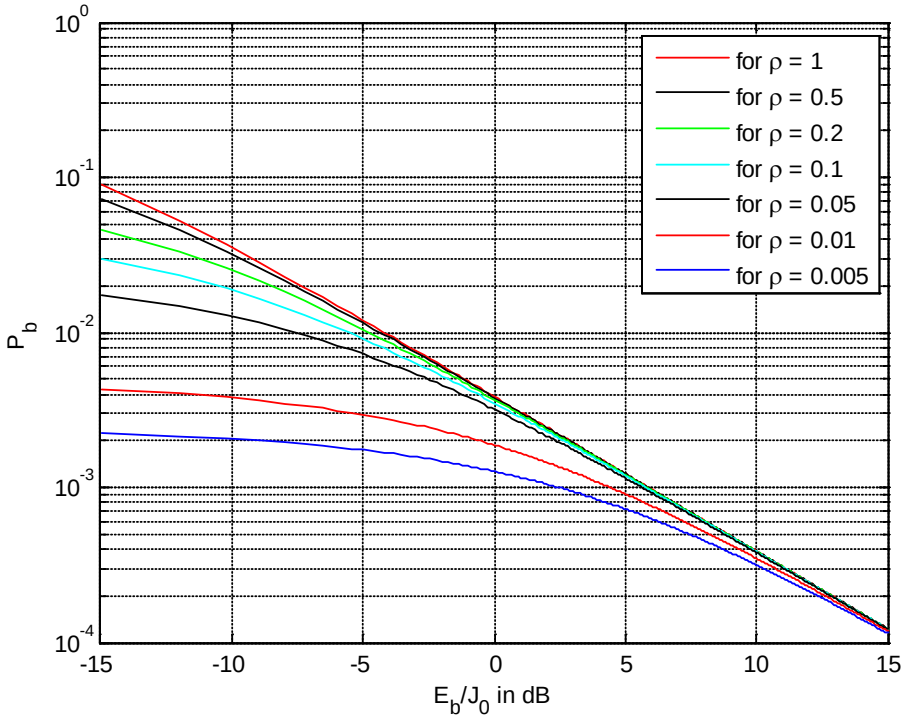

Figure 13. BER of DS PSK system for pulsed jamming and diversity L=1.

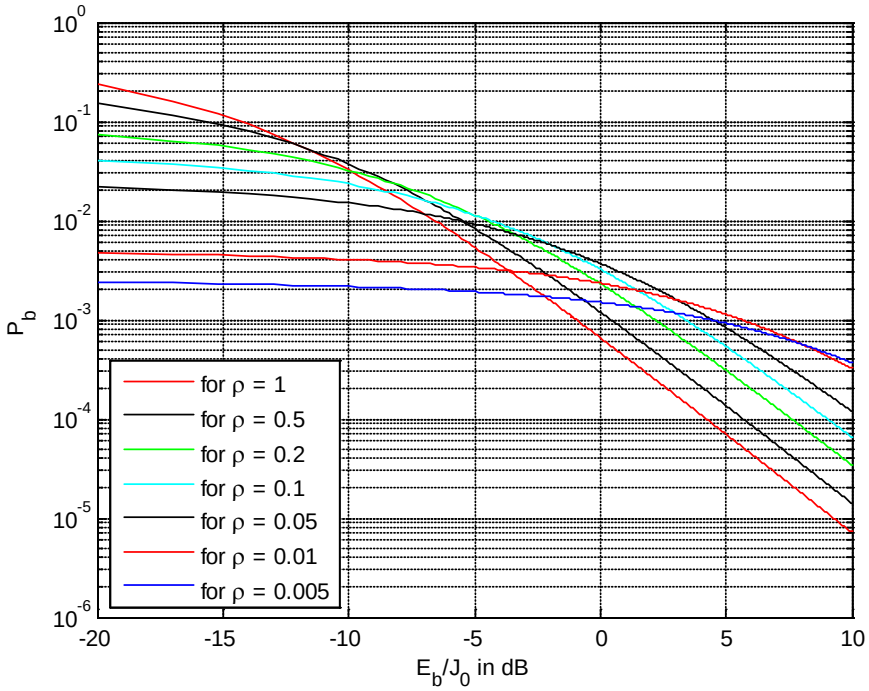

Figure 14. BER of DS PSK system for pulsed jamming and diversity L=2.

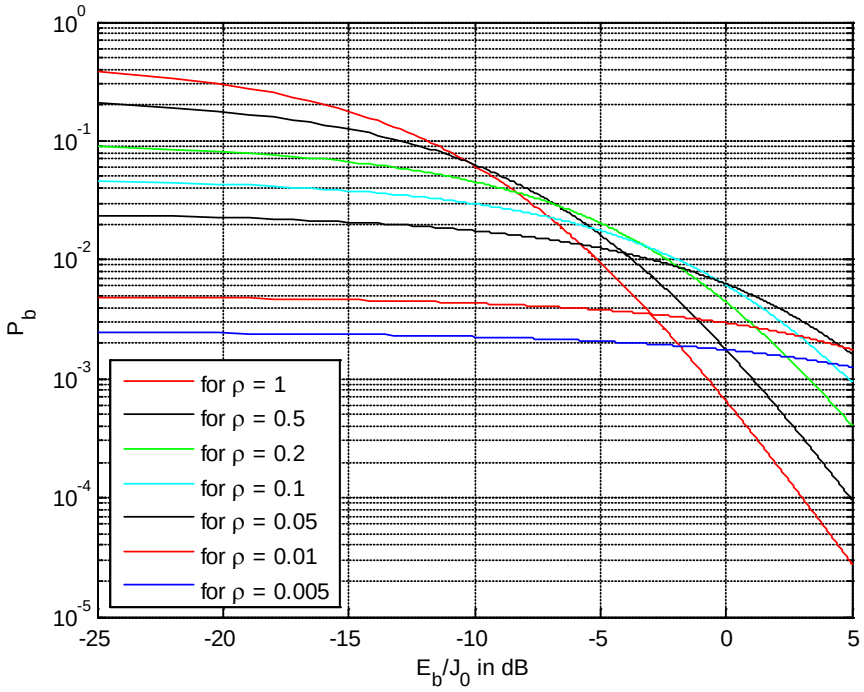

Figure 15. BER of DS PSK system for pulsed jamming and diversity *L*=3:

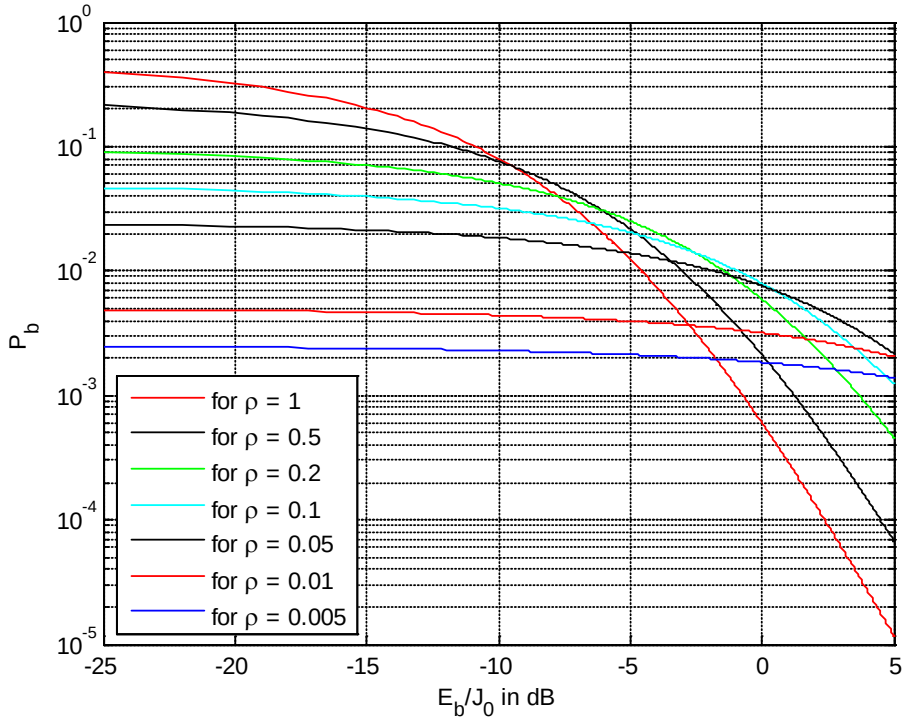

Figure 16. BER of DS PSK system for pulsed jamming and diversity *L*=4.

D. TONE JAMMING

In this section, the jamming signal is tone jamming. The system configuration is as shown in Figure 8, and the jamming signal is given by

$$j(t) = A_J \cos(2\pi f_c t + \theta_J), \tag{3.43}$$

where A_J is the amplitude and θ_J is the arbitrary phase of the jamming signal. Thus, the total received signal from *k*-th antenna is

$$x_k(t) = |h_k| A \cdot d_k c(t) \cos(2\pi f_c t + \theta_k) + n(t) + j(t). \tag{3.44}$$

After the mixer, we obtain

$$\begin{aligned} x_k'(t) &= \sqrt{\frac{2}{T_b}} |h_k| A \cdot d_k c^2(t) \cos^2(2\pi f_c t + \theta_k) + \sqrt{\frac{2}{T_b}} n(t) \cdot c(t) \cos(2\pi f_c t + \theta_k) \\ &+ \sqrt{\frac{2}{T_b}} \cdot c(t) \cos(2\pi f_c t + \theta_k) \cdot A_J \cos(2\pi f_c t + \theta_J) \end{aligned} \tag{3.45}$$

$$\begin{aligned} \Rightarrow x_k'(t) &= \frac{|h_k| A \cdot d_k}{\sqrt{2T_b}} \left[1 + \cos(4\pi f_c t + 2\theta_k)\right] + \sqrt{\frac{2}{T_b}} n(t) \cdot c(t) \cos(2\pi f_c t + \theta_k) \\ &+ \sqrt{\frac{2}{T_b}} \cdot A_J \cdot c(t) \cdot \frac{1}{2} \left[\cos(4\pi f_c t + \theta_k + \theta_J) + \cos(\theta_k - \theta_J)\right] \end{aligned} \tag{3.46}$$

$$\begin{aligned} \Rightarrow x'_k(t) &= \frac{|h_k| A \cdot d_k}{\sqrt{2T_b}} \left[1 + \cos(4\pi f_c t + 2\theta_k)\right] + \sqrt{\frac{2}{T_b}} n(t) \cdot c(t) \cos(2\pi f_c t + \theta_k) \\ &+ \frac{A_J \cdot c(t)}{\sqrt{2T_b}} \left[\cos(4\pi f_c t + \theta_k + \theta_J) + \cos(\theta_k - \theta_J)\right] \end{aligned} . \tag{3.47}$$

By neglecting the high frequency terms after the integrator [11, p. 451], we have

$$x_k''(t) = |h_k| A \cdot d_k \sqrt{\frac{T_b}{2}} + N + J, \tag{3.48}$$

where

$$N = \int_0^{T_b} \sqrt{\frac{2}{T_b}} n(t) \cdot c(t) \cos(2\pi f_c t + \theta_k)\, dt \tag{3.49}$$

and

$$J = \int_0^{T_b} \frac{A_J \cdot c(t)}{\sqrt{2T_b}} \cos(\theta_k - \theta_J)\, dt = \frac{A_J \cdot \cos(\theta_k - \theta_J)}{\sqrt{2T_b}} \int_0^{T_b} c(t)\, dt. \tag{3.50}$$

If we let *c(t)* be derived from a maximal sequence, we obtain

$$J = \frac{A_J \cdot \cos(\theta_k - \theta_J) \cdot T_c}{\sqrt{2T_b}}, \tag{3.51}$$

where $\theta_k - \theta_J = \theta$ and $(T_b / T_c) = N$ (spread factor). From (3.14), we know that $\sigma_{N_k}^2 = N_0 / 2$. We calculate the variance of the jamming signal to be

$$\sigma_J^2 = \overline{J \cdot J^*} = E\left[\frac{A_J^2 \cdot T_c^2}{2T_b} \cdot \cos^2\theta\right] = \frac{A_J^2 \cdot T_c^2}{2T_b} E\left[\cos^2\theta\right] \tag{3.52}$$

$$\Rightarrow \sigma_J^2 = \frac{A_J^2 \cdot T_c}{4N}. \tag{3.53}$$

Therefore,

$$\sigma_T^2 = \sigma_N^2 + \sigma_J^2 = \frac{N_0}{2} + \frac{A_J^2 \cdot T_c}{4N}. \tag{3.54}$$

Based on (2.15), we recall that

$$P_b = \left(\frac{1-\mu}{2}\right)^L \sum_{l=0}^{L-1} \binom{L-1+l}{l} \left(\frac{1+\mu}{2}\right)^l, \tag{3.55}$$

where

$$\mu = \sqrt{\frac{aSJNR}{1+aSJNR}} \tag{3.56}$$

and

$$aSJNR = \frac{1}{2}\left(\frac{d_{\min}}{2\sigma_T}\right)^2, \tag{3.57}$$

where $d_{\min} = 2\sqrt{\varepsilon_b}$ and $\varepsilon_b = E_b / L$. Thus, for DS-PSK, we obtain

$$aSJNR = \frac{1}{2}\left(\frac{d_{\min}}{2\sigma_T}\right)^2 = \frac{1}{2} \cdot \frac{4 \cdot \varepsilon_b}{4 \cdot \left(\frac{N_0}{2} + \frac{A_J^2 \cdot T_c}{4N}\right)} = \frac{\varepsilon_b}{N_0 + \frac{A_J^2 \cdot T_c}{2N}} \tag{3.58}$$

$$\Rightarrow aSJNR = \frac{E_b}{L\left(N_0 + \frac{A_J^2 \cdot T_c}{2N}\right)} = \frac{1}{L\left[\left(\frac{E_b}{N_0}\right)^{-1} + \frac{A_J^2 \cdot T_c}{2N \cdot E_b}\right]}. \tag{3.59}$$

We know that the bit energy is [11, p. 18]

$$E_b = \frac{1}{2} A^2 T_b , \tag{3.60}$$

where A is the amplitude of the information signal. By using (3.60) and by replacing the E_b at the second term of the denominator of (3.59), we obtain

$$aSJNR = \frac{1}{L\left[\left(\frac{E_b}{N_0}\right)^{-1} + \left(\frac{A^2}{A_J^2}\right)^{-1} \cdot \frac{1}{N^2}\right]} . \tag{3.61}$$

Thus, from (3.56) and (3.61) we have

$$\mu = \sqrt{\frac{1}{\frac{1}{aSJNR}+1}} = \sqrt{\frac{1}{L\left[\left(\frac{E_b}{N_0}\right)^{-1} + \left(\frac{A^2}{A_J^2}\right)^{-1} \cdot \frac{1}{N^2}\right]+1}} . \tag{3.62}$$

By using (3.62) and (3.55), we obtain the BER versus E_b / N_0 shown in Figures 17-20 for various diversities (L is the number of transmit antennas) and information signal-to-jamming signal amplitude ratio $\left(A_J / A\right)$. We also present the OSTBC codes used for each diversity. All the plots are for spread factor N=64.

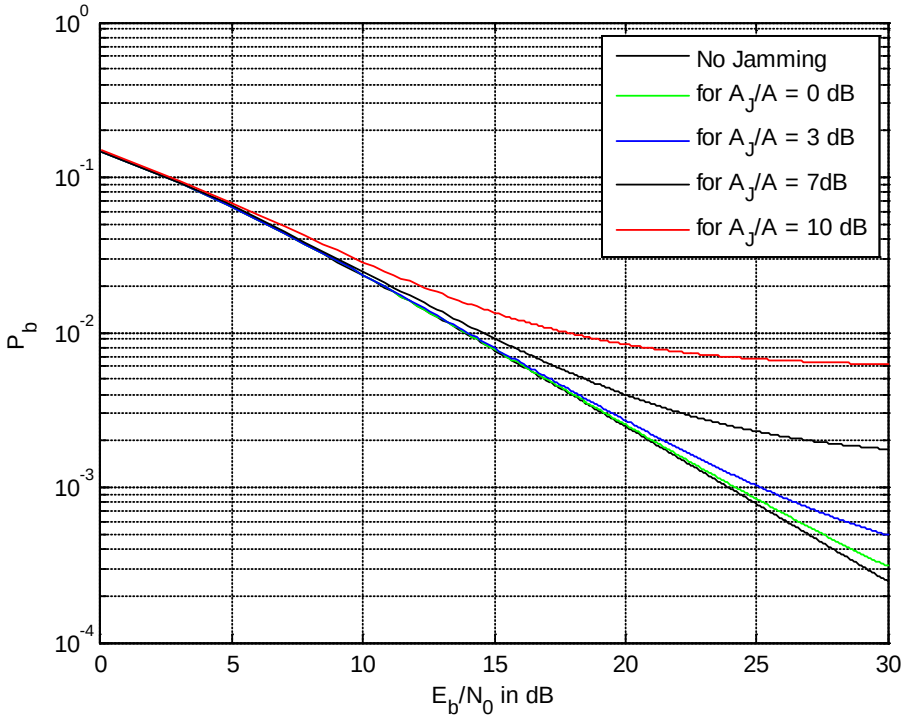

Figure 17. BER of DS PSK system for tone jamming and diversity L=1.

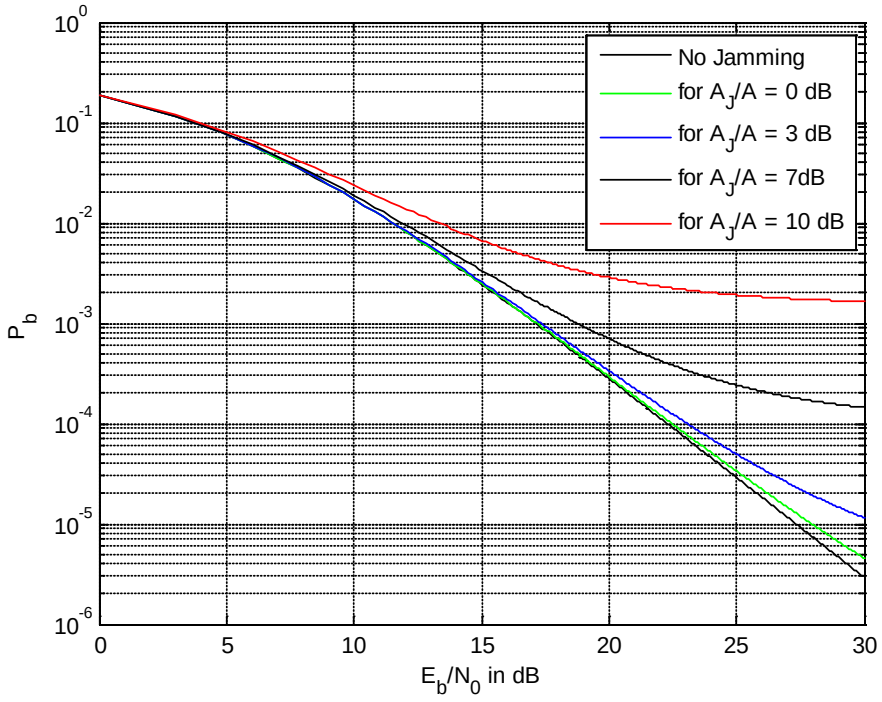

Figure 18. BER of DS PSK system for tone jamming and diversity L=2.

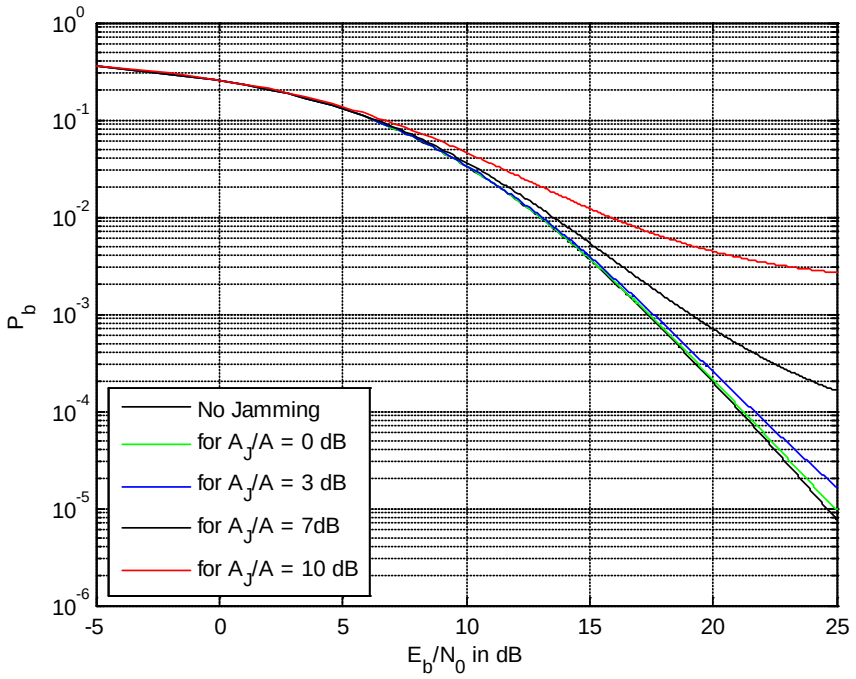

Figure 19. BER of DS PSK system for tone jamming and diversity L=3.

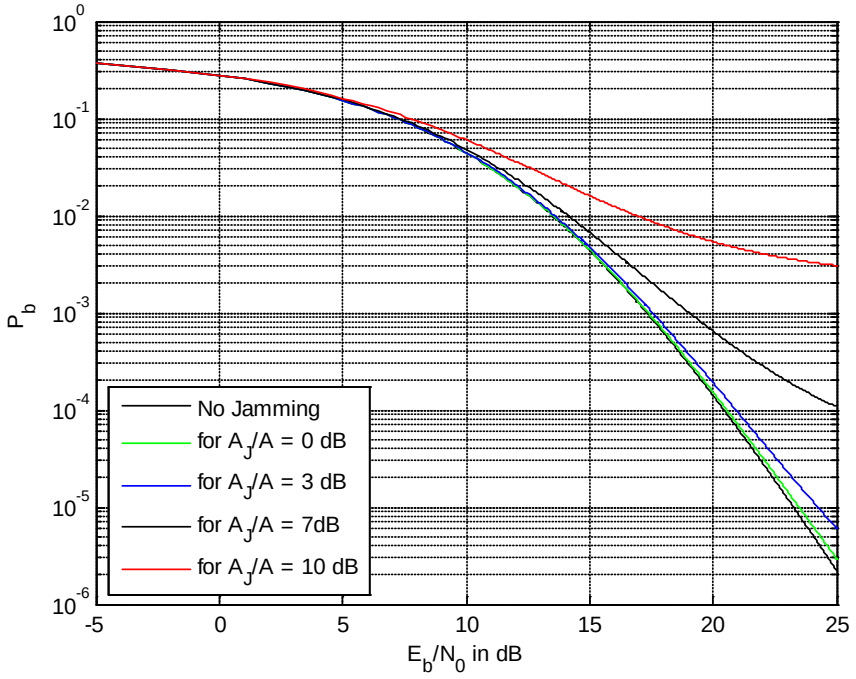

Figure 20. BER of DS PSK system for tone jamming and diversity L=4.

IV. PERFORMANCE ANALYSIS OF IQ COMPLEX SPREADING MISO SYSTEM

A. SYSTEM DESCRIPTION

In this chapter, we analyze the performance of a general *I-Q* complex spreading MISO system. We examine the system for various modulation schemes under three types of jamming: broadband, pulsed and tone. The system is shown in Figure 6. It has *L* transmit antennas and one receive antenna. We also use MRC. The system experiences Rayleigh fading. The receiver is shown in Figure 21.

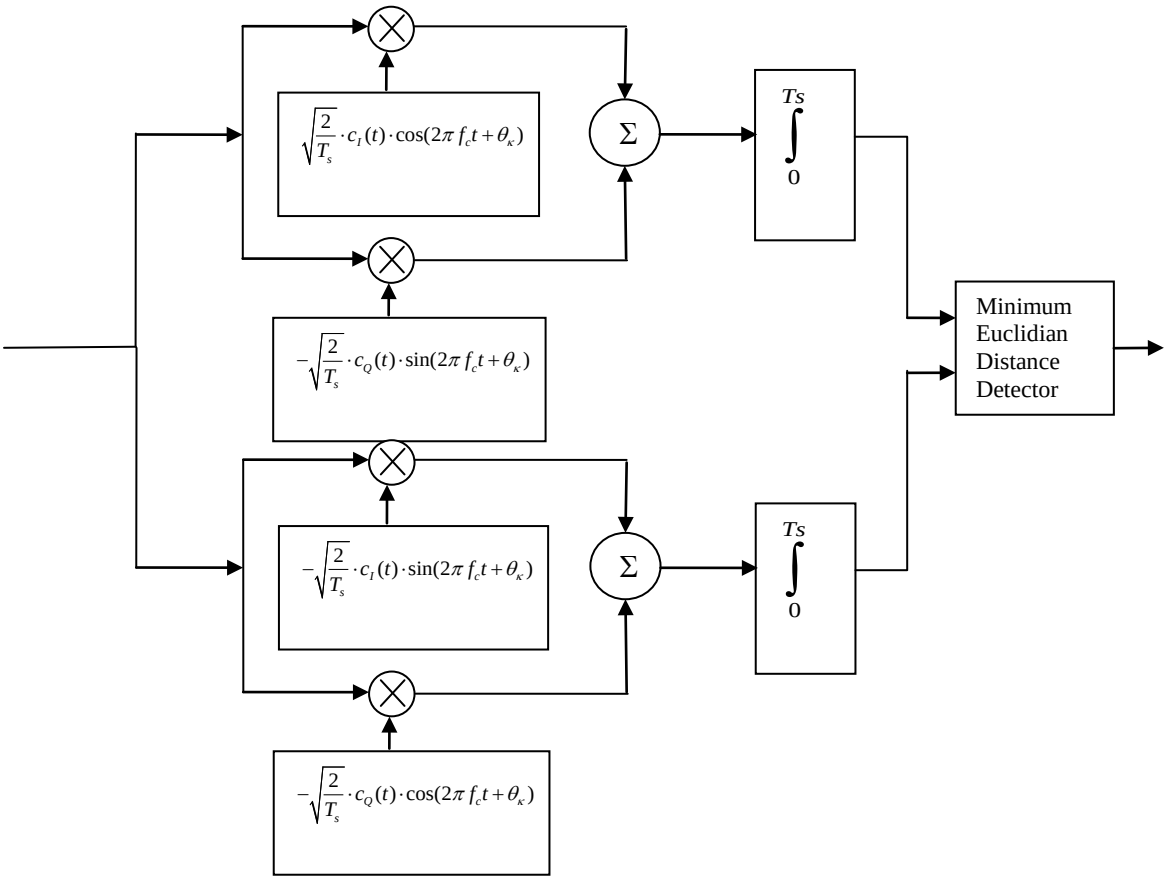

Figure 21. *IQ* complex spreading receiver.

In Figure 21, we denote $c_I(t)$ and $c_Q(t)$ the PN waveforms of the *I* and *Q* channels, respectively, and T_s as the symbol time. We assume perfect channel estimation, and the PSD of AWGN is equal to $N_0/2$.

B. BROADBAND JAMMING

In this section, the jamming signal is assumed to be broadband jamming. The PSD of the jamming signal is $J_0'/2$, and the symbol energy E_s is $E_s = (A^2 T_s)/2$, where *A* is the amplitude of the information signal.

In our system, we define the *I*-bit as *d* and the *Q*-bit as $\hat{d}$. The I-bit is spread by $c_I(t)$, and the *Q*-bit is spread by $c_Q(t)$. In addition, the *Q*-bit is spread by $c_I(t)$, and the *I*-bit is spread by $c_Q(t)$. Therefore, we obtain *I* and *Q* baseband signals as

$$s_{L,I}(t) = dc_I(t) - \hat{d}c_Q(t) \tag{4.1}$$

and

$$s_{L,Q}(t) = \hat{d}c_I(t) + dc_Q(t). \tag{4.2}$$

The complex baseband signal is

$$s_L(t) = s_{L,I}(t) + js_{L,Q}(t) = \mathbf{dc(t)}, \tag{4.3}$$

where $\mathbf{d} = d + j\hat{d}$ is the complex symbol and $\mathbf{c(t)} = c_I(t) + jc_Q(t)$ is the complex PN function. The received *I*-*Q* signal from *k*-th antenna is

$$r_k(t) = |h_k|\frac{A}{2}\left(dc_I(t) - \hat{d}c_Q(t)\right)\cos(2\pi f_c t + \theta) - |h_k|\frac{A}{2}\left(\hat{d}c_I(t) + dc_Q(t)\right)\sin(2\pi f_c t + \theta) + n(t) + j(t) \tag{4.4}$$

for $lT_S \le t \le (l+1)T_S$. We calculate the *I*-channel decision variable after the two mixers and the adder to get

$$r_{k_I}'(t) = r_k(t)\sqrt{\frac{2}{T_S}}\left[c_I(t)\cos(2\pi f_c t + \theta) - c_Q(t)\sin(2\pi f_c t + \theta)\right] \Rightarrow \tag{4.5}$$

$$r_{k_I}'(t) = \sqrt{\frac{2}{T_S}}|h_k|\frac{A}{4}\Big[dc_I(t)\cos(2\pi f_c t+\theta) - \hat{d}c_Q(t)\cos(2\pi f_c t+\theta) - \hat{d}c_I(t)\sin(2\pi f_c t+\theta) \tag{4.6}$$
$$-dc_Q(t)\sin(2\pi f_c t+\theta)\Big]\cdot\Big[c_I(t)\cos(2\pi f_c t+\theta) - c_Q(t)\sin(2\pi f_c t+\theta)\Big]$$

$$\Rightarrow r_{k_I}'(t) = \frac{|h_k|A}{2\sqrt{2T_S}}\Big[dc_I^2(t)\cos^2(2\pi f_c t+\theta) - dc_I(t)c_Q(t)\sin(2\pi f_c t+\theta)\cos(2\pi f_c t+\theta)$$
$$-\hat{d}c_I(t)c_Q(t)\cos^2(2\pi f_c t+\theta) + \hat{d}c_Q^2(t)\sin(2\pi f_c t+\theta)\cos(2\pi f_c t+\theta) \tag{4.7}$$
$$-\hat{d}c_I^2(t)\sin(2\pi f_c t+\theta)\cos(2\pi f_c t+\theta) + \hat{d}c_I(t)c_Q(t)\sin^2(2\pi f_c t+\theta)$$
$$-dc_I(t)c_Q(t)\sin(2\pi f_c t+\theta)\cos(2\pi f_c t+\theta) + dc_Q^2(t)\sin^2(2\pi f_c t+\theta)\Big] + N_I' + J_I'$$

$$\Rightarrow r_{k_I}'(t) = \frac{|h_k|A}{2\sqrt{2T_S}}\Big\{d\cos^2(2\pi f_c t+\theta) - 2dc_I(t)c_Q(t)\sin(2\pi f_c t+\theta)\cos(2\pi f_c t+\theta) \tag{4.8}$$
$$-\hat{d}c_I(t)c_Q(t)\Big[\cos^2(2\pi f_c t+\theta) - \sin^2(2\pi f_c t+\theta)\Big] + d\sin^2(2\pi f_c t+\theta)\Big\} + N_I' + J_I'$$

$$\Rightarrow r_{k_I}'(t) = \frac{|h_k|A}{2\sqrt{2T_S}}\Big\{d\Big[\cos^2(2\pi f_c t+\theta) + \sin^2(2\pi f_c t+\theta)\Big] - dc_I(t)c_Q(t)\sin(4\pi f_c t+2\theta) \tag{4.9}$$
$$-\hat{d}c_I(t)c_Q(t)\Big[2\cos^2(2\pi f_c t+\theta) - 1\Big]\Big\} + N_I' + J_I'$$

$$\Rightarrow r_{k_I}'(t) = \frac{|h_k|A}{2\sqrt{2T_S}}\Big[d - dc_I(t)c_Q(t)\sin(4\pi f_c t+2\theta) - \hat{d}c_I(t)c_Q(t)\cos(4\pi f_c t+2\theta)\Big] \tag{4.10}$$
$$+N_I' + J_I'$$

The high frequency terms are neglected since they are rejected by the matched filter [11, p. 98]; therefore, the *I*-channel decision variable reduces to

$$r_{k_I}'(t) = \frac{|h_k|A}{2\sqrt{2T_S}}d + N_I' + J_I'. \tag{4.11}$$

Similarly, we calculate the *Q*-channel decision variable after the two mixers and the adder to get

$$r_{k_Q}'(t) = -r_k(t)\sqrt{\frac{2}{T_S}}\Big[c_I(t)\sin(2\pi f_c t+\theta) + c_Q(t)\cos(2\pi f_c t+\theta)\Big] \Rightarrow \tag{4.12}$$

$$r_{k_Q}'(t) = -\sqrt{\frac{2}{T_S}}|h_k|\frac{A}{4}\Big[dc_I(t)\cos(2\pi f_c t+\theta) - \hat{d}c_Q(t)\cos(2\pi f_c t+\theta) - \hat{d}c_I(t)\sin(2\pi f_c t+\theta) \tag{4.13}$$
$$-dc_Q(t)\sin(2\pi f_c t+\theta)\Big]\cdot\Big[c_I(t)\sin(2\pi f_c t+\theta) + c_Q(t)\cos(2\pi f_c t+\theta)\Big] + N_Q' + J_Q'$$

$$\Rightarrow r_{k_Q}'(t) = -\frac{|h_k|A}{2\sqrt{2T_S}}\Big[dc_I^2(t)\sin(2\pi f_c t+\theta)\cos(2\pi f_c t+\theta) + dc_I(t)c_Q(t)\cos^2(2\pi f_c t+\theta)$$
$$-\hat{d}c_I(t)c_Q(t)\sin(2\pi f_c t+\theta)\cos(2\pi f_c t+\theta) - \hat{d}c_Q^2(t)\cos^2(2\pi f_c t+\theta) \quad (4.14)$$
$$-\hat{d}c_I^2(t)\sin^2(2\pi f_c t+\theta) - \hat{d}c_I(t)c_Q(t)\sin(2\pi f_c t+\theta)\cos(2\pi f_c t+\theta)$$
$$-dc_I(t)c_Q(t)\sin^2(2\pi f_c t+\theta) - dc_Q^2(t)\sin(2\pi f_c t+\theta)\cos(2\pi f_c t+\theta)\Big] + N_Q' + J_Q'$$

$$\Rightarrow r_{k_Q}'(t) = -\frac{|h_k|A}{2\sqrt{2T_S}}\Big\{ dc_I(t)c_Q(t)\Big[\cos^2(2\pi f_c t+\theta) - \sin^2(2\pi f_c t+\theta)\Big]$$
$$-2\hat{d}c_I(t)c_Q(t)\sin(2\pi f_c t+\theta)\cos(2\pi f_c t+\theta) - \hat{d}\Big[\cos^2(2\pi f_c t+\theta) + \sin^2(2\pi f_c t+\theta)\Big]\Big\} \quad (4.15)$$
$$+N_Q' + J_Q'$$

$$\Rightarrow r_{k_Q}'(t) = -\frac{|h_k|A}{2\sqrt{2T_S}}\Big\{ dc_I(t)c_Q(t)\Big[2\cos^2(2\pi f_c t+\theta) - 1\Big] - \hat{d}c_I(t)c_Q(t)\sin(4\pi f_c t+2\theta) - \hat{d}\Big\} \quad (4.16)$$
$$+N_Q' + J_Q'$$

$$\Rightarrow r_{k_Q}'(t) = \frac{|h_k|A}{2\sqrt{2T_S}}\Big[\hat{d} + \hat{d}c_I(t)c_Q(t)\sin(4\pi f_c t+2\theta) - dc_I(t)c_Q(t)\cos(4\pi f_c t+2\theta)\Big] \quad (4.17)$$
$$+N_Q' + J_Q'$$

The high frequency terms are neglected in our analysis since they are rejected by the matched filter [11, p. 451]; therefore, the *Q*-channel decision variable reduces to

$$r_{k_Q}'(t) = \frac{|h_k|A}{2\sqrt{2T_S}}\hat{d} + N_Q' + J_Q'. \quad (4.18)$$

After the integrators, we obtain the *I*-channel decision variable

$$r_{k_I}''(t) = \frac{\sqrt{T_S}|h_k|A}{2\sqrt{2}}d + N_I'' + J_I'' \quad (4.19)$$

and the *Q*-channel decision variable

$$r_{k_Q}''(t) = \frac{\sqrt{T_S}|h_k|A}{2\sqrt{2}}\hat{d} + N_Q'' + J_Q''. \quad (4.20)$$

Next, we calculate the variances of AWGN and the jamming signals. Firstly, we calculate the variance of N_I''. We know that N_I' equals

$$N_I' = \frac{n(t)}{\sqrt{2T_S}}\Big[c_I(t)\cos(2\pi f_c t+\theta) - c_Q(t)\sin(2\pi f_c t+\theta)\Big]. \quad (4.21)$$

Thus, after the integrator, we obtain

$$N_I^{"} = \int_0^{T_S} N_I^{'} dt = \frac{1}{\sqrt{2T_S}} \int_0^{T_S} \left\{ n(t) \left[c_I(t) \cos(2\pi f_c t + \theta) - c_Q(t) \sin(2\pi f_c t + \theta) \right] \right\} dt \,. \quad (4.22)$$

Then, the variance of $N_I^{"}$ is

$$\sigma^2_{N_I^{"}} = \mathrm{E}\left\{ N_I^{"2} \right\} = \mathrm{E}\left\{ \frac{1}{2T_S} \int_0^{T_S} \int_0^{T_S} \left\{ n(t) \left[c_I(t) \cos(2\pi f_c t + \theta) - c_Q(t) \sin(2\pi f_c t + \theta) \right] \cdot \right. \right. \quad (4.23)$$
$$\left. \left. n(\tau) \left[c_I(\tau) \cos(2\pi f_c \tau + \theta) - c_Q(\tau) \sin(2\pi f_c \tau + \theta) \right] \right\} dt d\tau \right\}$$

$$\Rightarrow \sigma^2_{N_I^{"}} = \frac{1}{2T_S} \int_0^{T_S} \int_0^{T_S} \left\{ E\left\{ n(t) n(\tau) \right\} \left[c_I(t) \cos(2\pi f_c t + \theta) - c_Q(t) \sin(2\pi f_c t + \theta) \right] \cdot \right. \quad (4.24)$$
$$\left. \left[c_I(\tau) \cos(2\pi f_c \tau + \theta) - c_Q(\tau) \sin(2\pi f_c \tau + \theta) \right] dt d\tau \right.$$

We know that the auto-covariance of noise is [11, p. 98]

$$E(n(t)n(\tau)) = \frac{N_0 \delta(t-\tau)}{2} \,. \quad (4.25)$$

Thus, we have

$$\sigma^2_{N_I^{"}} = \frac{1}{2T_S} \int_0^{T_S} \int_0^{T_S} \left\{ \frac{N_0}{2} \delta(t-\tau) \left[c_I(t) \cos(2\pi f_c t + \theta) - c_Q(t) \sin(2\pi f_c t + \theta) \right] \cdot \right. \quad (4.26)$$
$$\left. \left[c_I(\tau) \cos(2\pi f_c \tau + \theta) - c_Q(\tau) \sin(2\pi f_c \tau + \theta) \right] dt d\tau \right.$$

$$\Rightarrow \sigma^2_{N_I^{"}} = \frac{1}{2T_S} \frac{N_0}{2} \int_0^{T_S} \left[c_I(t) \cos(2\pi f_c t + \theta) - c_Q(t) \sin(2\pi f_c t + \theta) \right]^2 dt \quad (4.27)$$

$$\Rightarrow \sigma^2_{N_I^{"}} = \frac{N_0}{4T_S} \int_0^{T_S} \left[c_I^2(t) \cos^2(2\pi f_c t + \theta) - 2 c_I(t) c_Q(t) \sin(2\pi f_c t + \theta) \cos(2\pi f_c t + \theta) \right. \quad (4.28)$$
$$\left. + c_Q^2(t) \sin^2(2\pi f_c t + \theta) \right] dt$$

$$\Rightarrow \sigma^2_{N_I^{"}} = \frac{N_0}{4T_S} \int_0^{T_S} \left[1 - c_I(t) c_Q(t) \sin(4\pi f_c t + 2\theta) \right] dt \,. \quad (4.29)$$

The integral of the high frequency term is equal to zero. Therefore, we obtain

$$\sigma^2_{N_I^{"}} = \frac{N_0}{4} \,. \quad (4.30)$$

Now, we calculate the variance of $N_Q^{"}$. We know that $N_Q^{'}$ equals

$$N_Q^{'} = -\frac{n(t)}{\sqrt{2T_S}} \left[c_I(t) \sin(2\pi f_c t + \theta) + c_Q(t) \cos(2\pi f_c t + \theta) \right] . \quad (4.31)$$

Thus, after the integrator, we obtain

$$N_Q^{"} = \int_0^{T_S} N_Q^{'} dt = -\frac{1}{\sqrt{2T_S}} \int_0^{T_S} \left\{ n(t) \left[c_I(t) \sin(2\pi f_c t + \theta) + c_Q(t) \cos(2\pi f_c t + \theta) \right] \right\} dt \quad (4.32)$$

The variance of $N_Q^{"}$ is

$$\sigma^2_{N_Q^{"}} = \mathrm{E}\left\{ N_Q^{"\,2} \right\} = \mathrm{E}\left\{ \frac{1}{2T_S} \int_0^{T_S} \int_0^{T_S} \left\{ n(t) \left[c_I(t) \sin(2\pi f_c t + \theta) + c_Q(t) \cos(2\pi f_c t + \theta) \right] \cdot \right. \right. \quad (4.33)$$
$$\left. \left. n(\tau) \left[c_I(\tau) \sin(2\pi f_c \tau + \theta) + c_Q(\tau) \cos(2\pi f_c \tau + \theta) \right] \right\} dt d\tau \right\}$$

$$\Rightarrow \sigma^2_{N_Q^{"}} = \frac{1}{2T_S} \int_0^{T_S} \int_0^{T_S} \left\{ E\left\{ n(t) n(\tau) \right\} \left[c_I(t) \sin(2\pi f_c t + \theta) + c_Q(t) \cos(2\pi f_c t + \theta) \right] \right. \quad (4.34)$$
$$\left. \left[c_I(\tau) \sin(2\pi f_c \tau + \theta) + c_Q(\tau) \cos(2\pi f_c \tau + \theta) \right] dt d\tau \right.$$

$$\Rightarrow \sigma^2_{N_Q^{"}} = \frac{1}{2T_S} \int_0^{T_S} \int_0^{T_S} \left\{ \frac{N_0}{2} \delta(t-\tau) \left[c_I(t) \sin(2\pi f_c t + \theta) + c_Q(t) \cos(2\pi f_c t + \theta) \right] \cdot \right. \quad (4.35)$$
$$\left. \left[c_I(\tau) \sin(2\pi f_c \tau + \theta) + c_Q(\tau) \cos(2\pi f_c \tau + \theta) \right] dt d\tau \right.$$

$$\Rightarrow \sigma^2_{N_Q^{"}} = \frac{1}{2T_S} \frac{N_0}{2} \int_0^{T_S} \left[c_I(t) \sin(2\pi f_c t + \theta) + c_Q(t) \cos(2\pi f_c t + \theta) \right]^2 dt \quad (4.36)$$

$$\Rightarrow \sigma^2_{N_Q^{"}} = \frac{N_0}{4T_S} \int_0^{T_S} \left[c_I^2(t) \sin^2(2\pi f_c t + \theta) + 2 c_I(t) c_Q(t) \sin(2\pi f_c t + \theta) \cos(2\pi f_c t + \theta) \right. \quad (4.37)$$
$$\left. + c_Q^2(t) \cos^2(2\pi f_c t + \theta) \right] dt$$

$$\Rightarrow \sigma^2_{N_Q^{"}} = \frac{N_0}{4T_S} \int_0^{T_S} \left[1 + c_I(t) c_Q(t) \sin(4\pi f_c t + 2\theta) \right] dt \,. \quad (4.38)$$

The integral of the high frequency term is equal to zero. Therefore, we obtain

$$\sigma^2_{N_Q^{"}} = \frac{N_0}{4}. \quad (4.39)$$

Next we calculate the variances jamming signals. We know by definition that they are both noise-like signals. Firstly, we calculate the variance of $J_I^{"}$. We know that $J_I^{'}$ is given by

$$J_I^{'} = \frac{j(t)}{\sqrt{2T_S}} \left[c_I(t) \cos(2\pi f_c t + \theta) - c_Q(t) \sin(2\pi f_c t + \theta) \right]. \quad (4.40)$$

Thus, after the integrator, we obtain

$$J_I^{"} = \int_0^{T_S} J_I^{'} dt = \frac{1}{\sqrt{2T_S}} \int_0^{T_S} \left\{ j(t) \left[c_I(t) \cos(2\pi f_c t + \theta) - c_Q(t) \sin(2\pi f_c t + \theta) \right] \right\} dt \quad (4.41)$$

The variance of $J_I^{"}$ is

$$\sigma_{J_I^{"}}^2 = \mathrm{E}\left\{J_I^{"2}\right\} = \mathrm{E}\left\{\frac{1}{2T_S}\int_0^{T_S}\int_0^{T_S}\left\{j(t)\left[c_I(t)\cos(2\pi f_c t+\theta)-c_Q(t)\sin(2\pi f_c t+\theta)\right]\right.\right. \tag{4.42}$$
$$\left.\left. j(\tau)\left[c_I(\tau)\cos(2\pi f_c \tau+\theta)-c_Q(\tau)\sin(2\pi f_c \tau+\theta)\right]\right\} dtd\tau\right\}$$

$$\Rightarrow \sigma_{J_I^{"}}^2 = \frac{1}{2T_S}\int_0^{T_S}\int_0^{T_S}\left\{E\left\{j(t)\,j(\tau)\right\}\left[c_I(t)\cos(2\pi f_c t+\theta)-c_Q(t)\sin(2\pi f_c t+\theta)\right]\right. \tag{4.43}$$
$$\left.\left[c_I(\tau)\cos(2\pi f_c \tau+\theta)-c_Q(\tau)\sin(2\pi f_c \tau+\theta)\right] dtd\tau\right.$$

$$\Rightarrow \sigma_{J_I^{"}}^2 = \frac{1}{2T_S}\int_0^{T_S}\int_0^{T_S}\left\{\frac{J_0{}'}{2}\delta(t-\tau)\left[c_I(t)\cos(2\pi f_c t+\theta)-c_Q(t)\sin(2\pi f_c t+\theta)\right]\right. \tag{4.44}$$
$$\left.\left[c_I(\tau)\cos(2\pi f_c \tau+\theta)-c_Q(\tau)\sin(2\pi f_c \tau+\theta)\right] dtd\tau\right.$$

$$\Rightarrow \sigma_{J_I^{"}}^2 = \frac{1}{2T_S}\frac{J_0{}'}{2}\int_0^{T_S}\left[c_I(t)\cos(2\pi f_c t+\theta)-c_Q(t)\sin(2\pi f_c t+\theta)\right]^2 dt \tag{4.45}$$

$$\Rightarrow \sigma_{J_I^{"}}^2 = \frac{J_0{}'}{4T_S}\int_0^{T_S}\left[c_I^2(t)\cos^2(2\pi f_c t+\theta)-2c_I(t)c_Q(t)\sin(2\pi f_c t+\theta)\cos(2\pi f_c t+\theta)\right. \tag{4.46}$$
$$\left.+c_Q^2(t)\sin^2(2\pi f_c t+\theta)\right] dt$$

$$\Rightarrow \sigma_{J_I^{"}}^2 = \frac{J_0{}'}{4T_S}\int_0^{T_S}\left[1-c_I(t)c_Q(t)\sin(4\pi f_c t+2\theta)\right]dt\,. \tag{4.47}$$

The integral of the high frequency term is equal to zero. Therefore, we obtain

$$\sigma_{J_I^{"}}^2 = \frac{J_0{}'}{4}\,. \tag{4.48}$$

Now we calculate the variance of $J_Q^{"}$. We know that $J_Q{}'$ is given by

$$J_Q^{'} = -\frac{j(t)}{\sqrt{2T_S}}\left[c_I(t)\sin(2\pi f_c t+\theta)+c_Q(t)\cos(2\pi f_c t+\theta)\right]. \tag{4.49}$$

Thus, after the integrator, we obtain

$$J_Q^{"} = \int_0^{T_S} J_Q^{'}dt = -\frac{1}{\sqrt{2T_S}}\int_0^{T_S}\left\{j(t)\left[c_I(t)\sin(2\pi f_c t+\theta)+c_Q(t)\cos(2\pi f_c t+\theta)\right]\right\}dt\,. \tag{4.50}$$

The variance of $J_Q^{"}$ is

$$\sigma_{J_Q^{"}}^2 = \mathrm{E}\left\{J_Q^{"2}\right\} = \mathrm{E}\left\{\frac{1}{2T_S}\int_0^{T_S}\int_0^{T_S}\left\{j(t)\left[c_I(t)\sin(2\pi f_c t+\theta)+c_Q(t)\cos(2\pi f_c t+\theta)\right]\right.\right. \tag{4.51}$$
$$\left.\left. j(\tau)\left[c_I(\tau)\sin(2\pi f_c \tau+\theta)+c_Q(\tau)\cos(2\pi f_c \tau+\theta)\right]\right\} dtd\tau\right\}$$

$$\Rightarrow \sigma_{J_Q^*}^2 = \frac{1}{2T_S}\int_0^{T_S}\int_0^{T_S}\left\{E\{j(t)\,j(\tau)\}\left[c_I(t)\sin(2\pi f_c t+\theta)+c_Q(t)\cos(2\pi f_c t+\theta)\right]\cdot\right. \tag{4.52}$$
$$\left.\left[c_I(\tau)\sin(2\pi f_c \tau+\theta)+c_Q(\tau)\cos(2\pi f_c \tau+\theta)\right]dt d\tau$$

$$\Rightarrow \sigma_{J_Q^*}^2 = \frac{1}{2T_S}\int_0^{T_S}\int_0^{T_S}\left\{\frac{J_0'}{2}\delta(t-\tau)\left[c_I(t)\sin(2\pi f_c t+\theta)+c_Q(t)\cos(2\pi f_c t+\theta)\right]\cdot\right. \tag{4.53}$$
$$\left.\left[c_I(\tau)\sin(2\pi f_c \tau+\theta)+c_Q(\tau)\cos(2\pi f_c \tau+\theta)\right]dt d\tau$$

$$\Rightarrow \sigma_{J_Q^*}^2 = \frac{1}{2T_S}\frac{J_0'}{2}\int_0^{T_S}\left[c_I(t)\sin(2\pi f_c t+\theta)+c_Q(t)\cos(2\pi f_c t+\theta)\right]^2 dt \tag{4.54}$$

$$\Rightarrow \sigma_{J_Q^*}^2 = \frac{J_0'}{4T_S}\int_0^{T_S}\left[c_I^2(t)\sin^2(2\pi f_c t+\theta)+2c_I(t)c_Q(t)\sin(2\pi f_c t+\theta)\cos(2\pi f_c t+\theta)\right. \tag{4.55}$$
$$\left.+c_Q^2(t)\cos^2(2\pi f_c t+\theta)\right]dt$$

$$\Rightarrow \sigma_{J_Q^*}^2 = \frac{J_0'}{4T_S}\int_0^{T_S}\left[1+c_I(t)c_Q(t)\sin(4\pi f_c t+2\theta)\right]dt\,. \tag{4.56}$$

The integral of the high frequency term is equal to zero. Therefore, we obtain

$$\sigma_{J_Q^*}^2 = \frac{J_0'}{4}\,. \tag{4.57}$$

Thus, the variances of *I*-channel and *Q*-channel variables are

$$\sigma_I^2 = \sigma_Q^2 = \frac{N_0 + J_0'}{4}\,. \tag{4.58}$$

Due to the summation of the variances of *I* and *Q* channels, the total variance in the detector is

$$\sigma_T^2 = \frac{N_0 + J_0'}{2}\,. \tag{4.59}$$

In order to perform proper comparison and evaluation between a non-DS and a DS system under broadband jamming, we assume that the overall jammer power is the same for both. If we denote the PSD of the non-DSSS system as $J_0/2$ and the PSD of a DSSS system as $J_0'/2$, then from (3.20) we obtain

$$J_0' = \frac{J_0}{N}\,. \tag{4.60}$$

Since we utilize a Gray coded signal in a Rayleigh fading channel and MRC, we use (2.10). Thus, the probability of error is given by (2.13):

$$P_b = \frac{N_n}{\log_2 M}\left(\frac{1-\mu}{2}\right)^L \sum_{l=0}^{L-1}\binom{L-1+l}{l}\left(\frac{1+\mu}{2}\right)^l . \tag{4.61}$$

From (2.11) we have

$$aSJNR = \frac{1}{2}\left(\frac{d_{\min}}{2\sigma_T}\right)^2 . \tag{4.62}$$

In the following sub-sections, we evaluate the performances of the system for three different *I-Q* modulation schemes. We apply QPSK, 16-QAM and 64-QAM. We calculate the BER versus the E_b / N_0 for various diversities (*L* transmit antennas) and signal-to-jamming ratios $\left(SJR = E_b / J_0\right)$. We use the OSTBCs that we presented in Chapter III, Section B for the corresponding diversities. All the plots are for spread factor *N=64*.

1. QPSK

For QPSK, we have $N_n = 2$, $log_2 M = 2$, $d_{\min} = \sqrt{2\varepsilon_S}$ and $\varepsilon_S = E_S / L$ [11, pp. 578-580], where ε_S is the diversity symbol energy. From (4.59) and (4.62), we obtain

$$aSJNR = \frac{1}{2}\left(\frac{d_{\min}}{2\sigma_T}\right)^2 = \frac{1}{2}\cdot\frac{2\cdot\varepsilon_s}{4\cdot\frac{(N_0 + J_0')}{2}} = \frac{\varepsilon_s}{2(N_0 + J_0')} \tag{4.63}$$

$$\Rightarrow aSJNR = \frac{E_S}{2L(N_0 + J_0')} = \frac{E_b}{L(N_0 + J_0')} = \frac{1}{L\left[\left(\frac{E_b}{N_0}\right)^{-1} + \left(\frac{E_b}{J_0'}\right)^{-1}\right]} . \tag{4.64}$$

Therefore, we obtain

$$\mu = \sqrt{\frac{1}{\frac{1}{aSJNR}+1}} = \sqrt{\frac{1}{L\left[\left(\frac{E_b}{N_0}\right)^{-1} + \left(\frac{E_b}{J_0'}\right)^{-1}\right]+1}} . \tag{4.65}$$

Finally, we use (4.60) to obtain

$$\mu = \sqrt{\frac{1}{\frac{1}{aSJNR}+1}} = \sqrt{\frac{1}{L\left[\left(\frac{E_b}{N_0}\right)^{-1} + \frac{1}{N}\left(\frac{E_b}{J_0}\right)^{-1}\right]+1}} . \tag{4.66}$$

Thus, as expected, we observe that the QPSK performance is identical to PSK. We obtain Figures 22-25 for the different diversities and use the same OSTBCs that we used for the corresponding diversities for PSK.

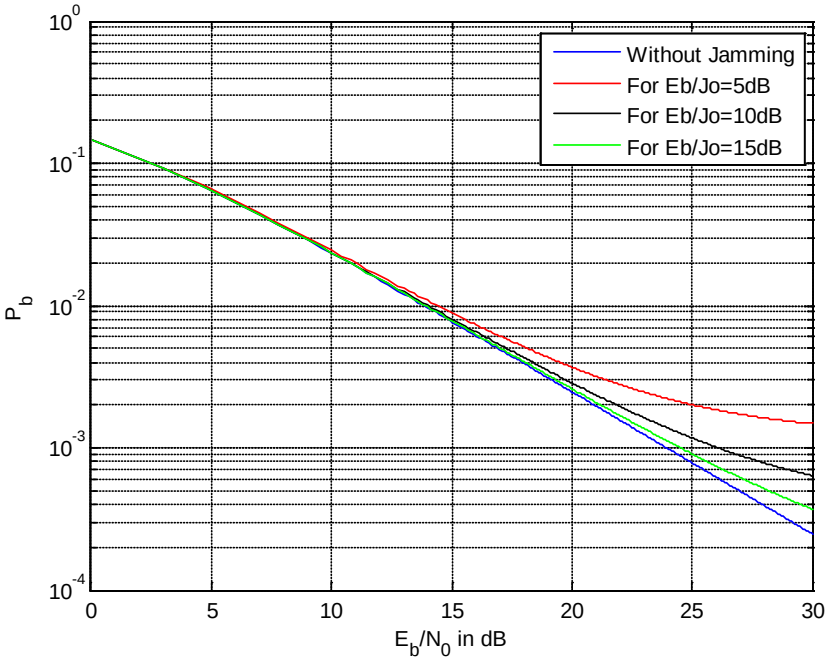

Figure 22. BER of DS QPSK system for broadband jamming and diversity L=1.

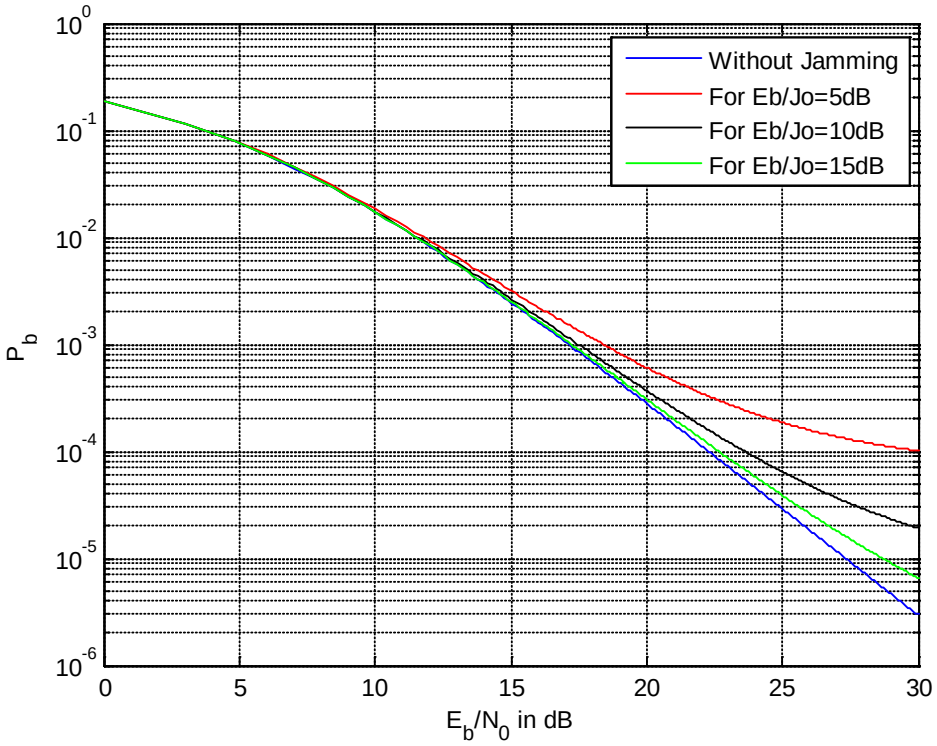

Figure 23. BER of DS QPSK system for broadband jamming and diversity *L*=2.

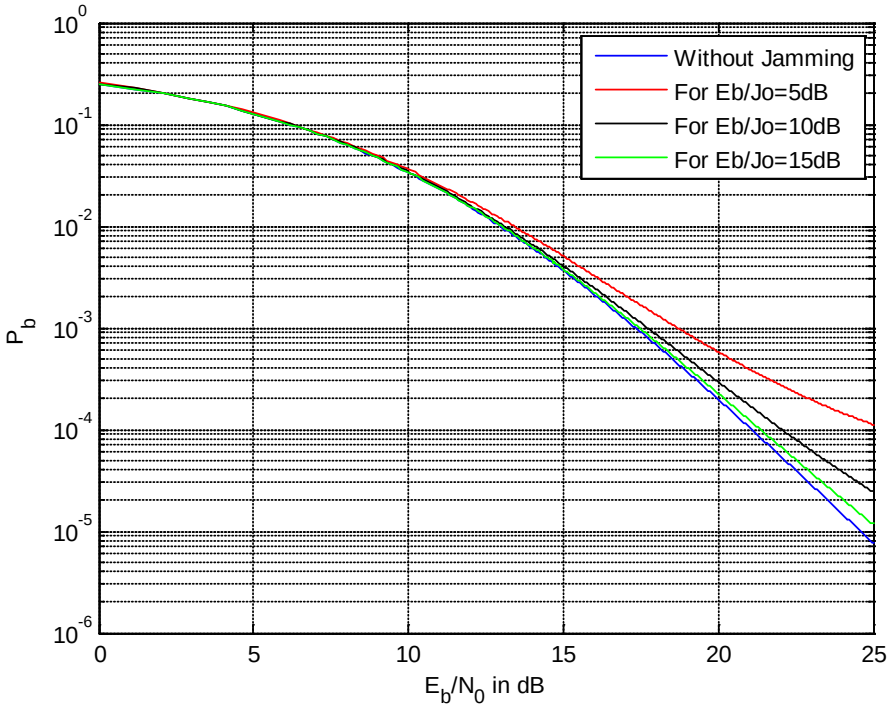

Figure 24. BER of DS QPSK system for broadband jamming and diversity *L*=3.

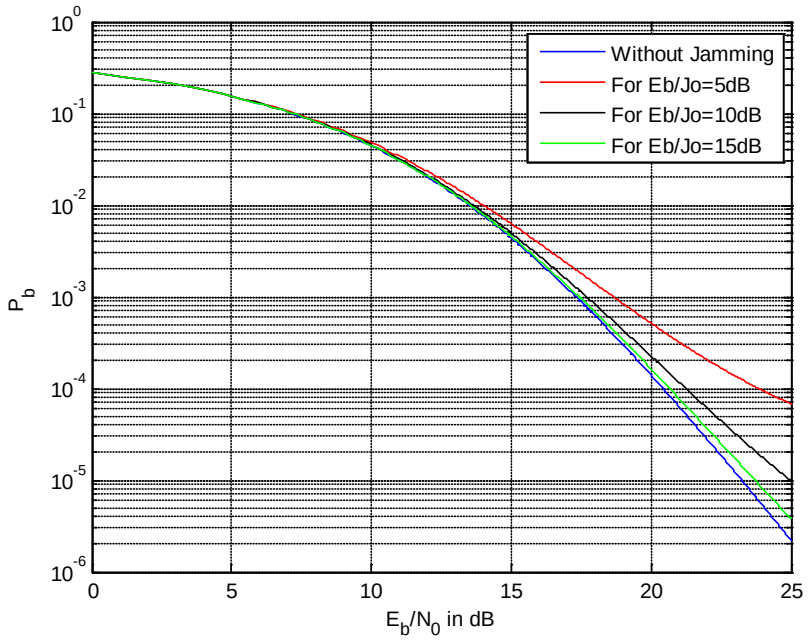

Figure 25. BER of DS QPSK system for broadband jamming and diversity L=4.

2. 16-QAM

For 16-QAM, the BER is given by (2.17) and M=16, N_n=3, log_2M=4. $d_{\min} = \sqrt{6\varepsilon_S / 15}$ and $\varepsilon_S = E_S / L$ [11, pp. 578-580]. We obtain from (4.62) and (4.59)

$$aSJNR = \frac{1}{2}\left(\frac{d_{\min}}{2\sigma_T}\right)^2 = \frac{1}{2}\cdot\frac{6\cdot\varepsilon_s}{15\cdot 4\cdot\frac{(N_0 + J_0')}{2}} = \frac{\varepsilon_s}{10(N_0 + J_0')} \tag{4.67}$$

$$\Rightarrow aSJNR = \frac{E_S}{10L(N_0 + J_0)} = \frac{2E_b}{5L(N_0 + J_0)} = \frac{2}{5L\left[\left(\frac{E_b}{N_0}\right)^{-1} + \left(\frac{E_b}{J_0}\right)^{-1}\right]}. \tag{4.68}$$

From (4.60), we obtain

$$\mu = \sqrt{\frac{1}{\frac{1}{aSJNR}+1}} = \sqrt{\frac{1}{\frac{5}{2}L\left[\left(\frac{E_b}{N_0}\right)^{-1} + \frac{1}{N}\left(\frac{E_b}{J_0}\right)^{-1}\right]+1}}. \tag{4.69}$$

We use the same OSTBCs for the corresponding diversities as PSK. The BER plots for the different diversities are shown in Figures 26–29.

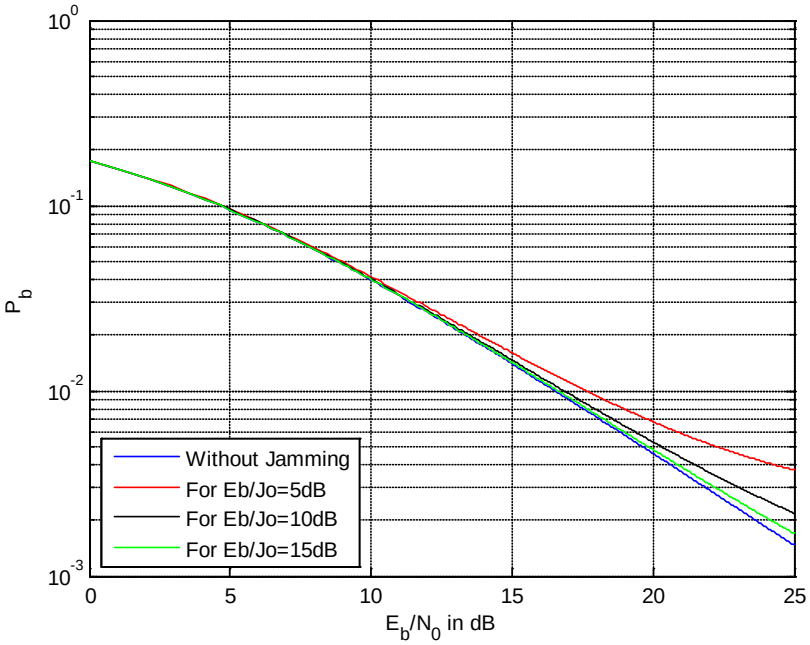

Figure 26. BER of DS 16-QAM system for broadband jamming and diversity *L*=1.

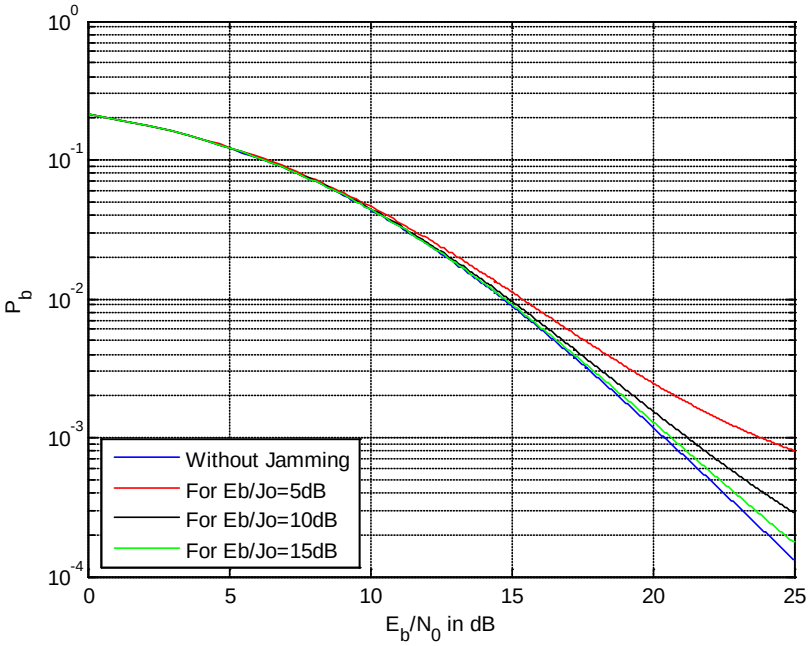

Figure 27. BER of DS 16-QAM system for broadband jamming and diversity *L*=2..

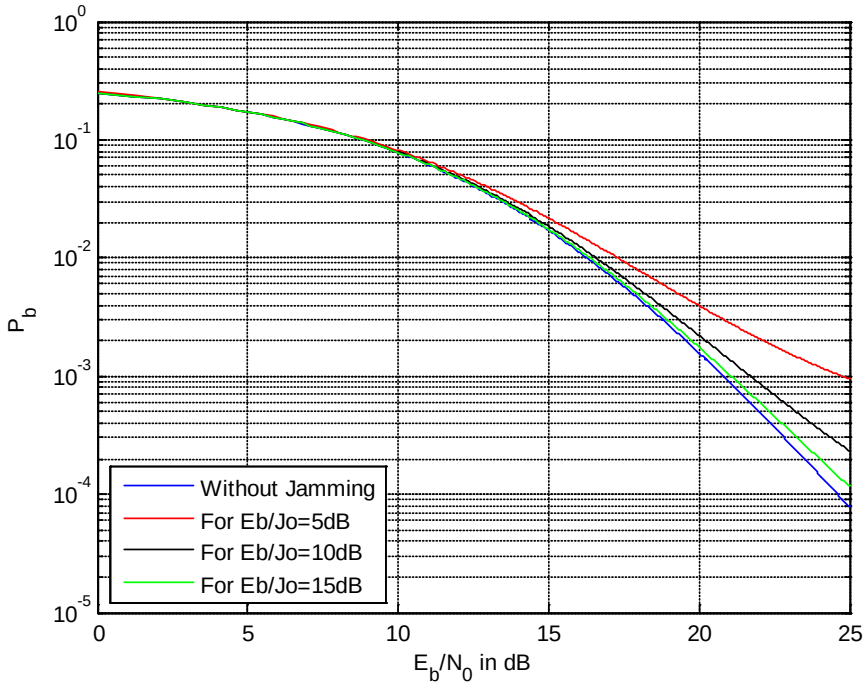

Figure 28. BER of DS 16-QAM system for broadband jamming and diversity *L*=3.

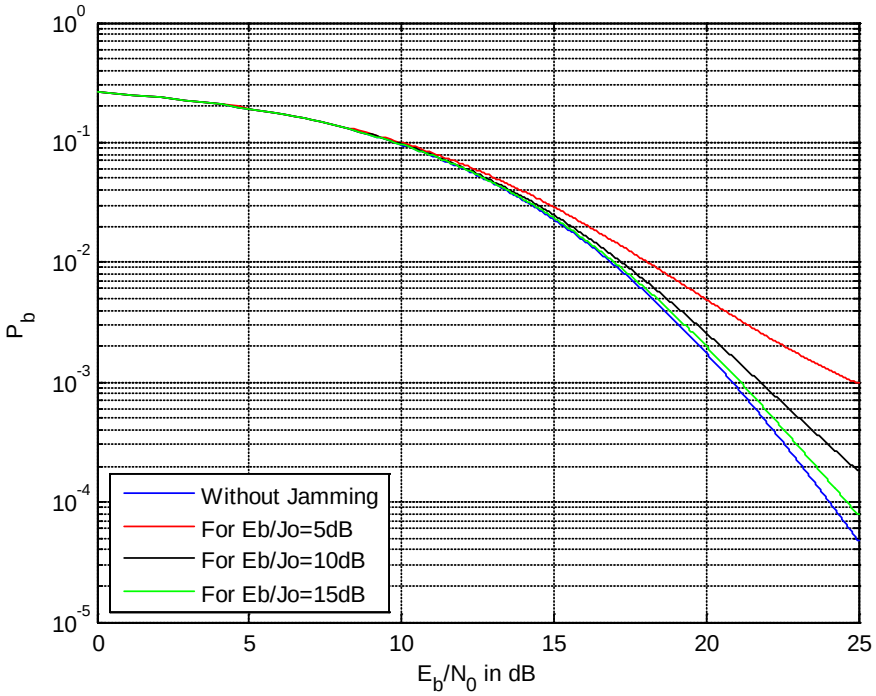

Figure 29. BER of DS 16-QAM system for broadband jamming and diversity *L*=4.

3. 64-QAM

For 64-QAM, the BER is given from (2.17) and M=64, $N_n = 7/2$, $log_2 M = 6$, $d_{\min} = \sqrt{6\varepsilon_S / 63}$ and $\varepsilon_S = E_S / L$ [11, pp. 578-580]. From (4.62) and (4.59), we get

$$aSJNR = \frac{1}{2}\left(\frac{d_{\min}}{2\sigma_T}\right)^2 = \frac{1}{2}\cdot\frac{6\cdot\varepsilon_s}{63\cdot 4\cdot\frac{(N_0 + J_0')}{2}} = \frac{\varepsilon_s}{42(N_0 + J_0')} \tag{4.70}$$

$$\Rightarrow aSJNR = \frac{E_S}{42L(N_0 + J_0')} = \frac{E_b}{7L(N_0 + J_0')} = \frac{1}{7L\left[\left(\frac{E_b}{N_0}\right)^{-1} + \left(\frac{E_b}{J_0'}\right)^{-1}\right]}. \tag{4.71}$$

Therefore, using (4.60), we obtain

$$\mu = \sqrt{\frac{1}{\frac{1}{aSJNR}+1}} = \sqrt{\frac{1}{7L\left[\left(\frac{E_b}{N_0}\right)^{-1} + \frac{1}{N}\left(\frac{E_b}{J_0}\right)^{-1}\right]+1}}. \tag{4.72}$$

We use the same OSTBCs for the corresponding diversities as were used for PSK. The BER plots for the different diversities are shown in Figures 30-33.

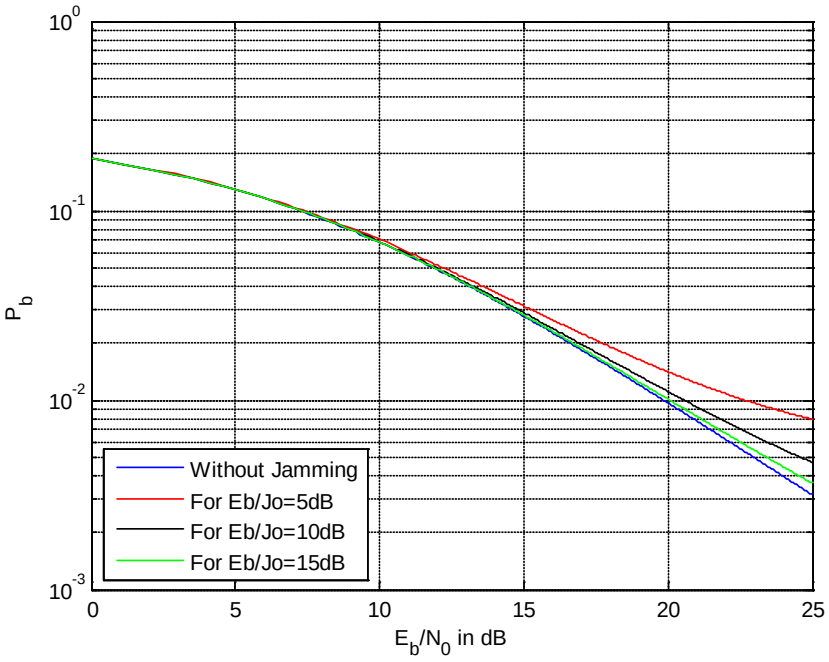

Figure 30. BER of DS 64-QAM system for broadband jamming and diversity *L*=1.

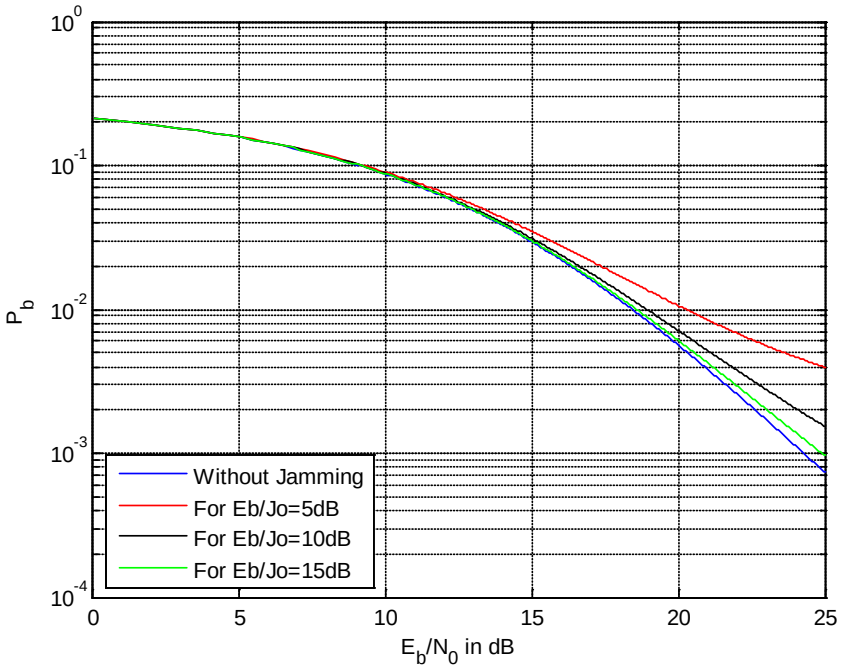

Figure 31. BER of DS 64-QAM system for broadband jamming and diversity *L*=2.

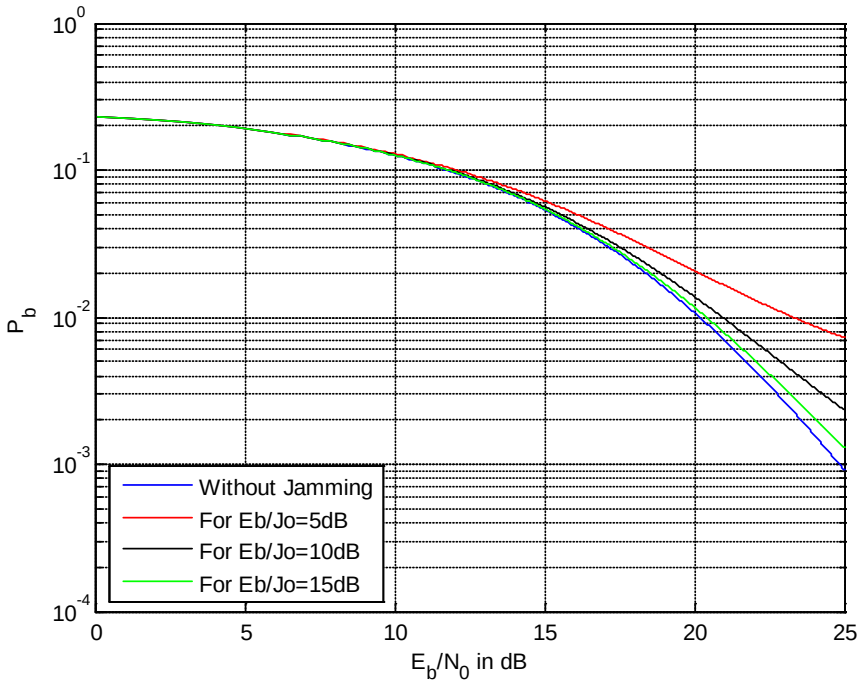

Figure 32. BER of DS 64-QAM system for broadband jamming and diversity *L*=3.

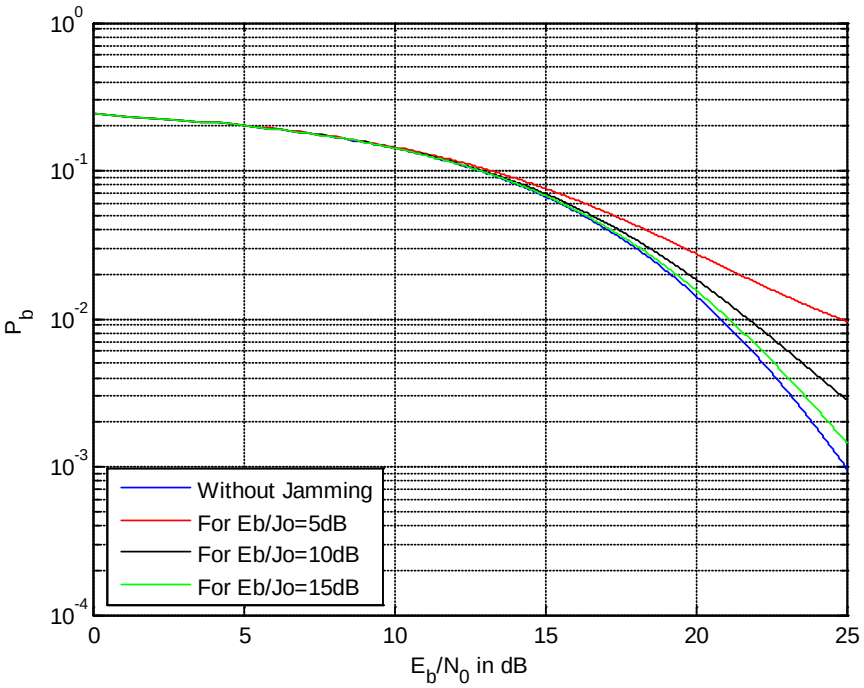

Figure 33. BER of DS 64-QAM system for broadband jamming and diversity *L*=4.

C. PULSED JAMMING

In this section, the jamming signal is pulsed jamming. The jammer is on for ρ percent of the time. Using the total probability theorem [11, p. 450], we obtain

$$P_b = \rho P_{b_{J+N}} + (1-\rho)P_{b_N}\,, \tag{4.73}$$

where $P_{b_{J+N}}$ is the BER with jamming and AWGN, and P_{b_N} is the BER with AWGN only. Based on results of Section III-C and using (3.41), we define the PSD of the jamming signal as $J_0"/2$, where

$$J_0" = J_0/(\rho N)\,. \tag{4.74}$$

We define J_0 as the PSD of the jamming signal in the case of broadband jamming for the non-spread spectrum equivalent system, noting that the jammer is assumed to have the same power in both cases in order to have a proper comparison.

For QPSK, we have

$$P_{b_{J+N}} = \left(\frac{1-\mu}{2}\right)^L \sum_{l=0}^{L-1}\binom{L-1+l}{l}\left(\frac{1+\mu}{2}\right)^l\,, \tag{4.75}$$

where

$$\mu = \sqrt{\frac{1}{\frac{1}{aSJNR}+1}} = \sqrt{\frac{1}{L\left[\left(\frac{E_b}{N_0}\right)^{-1}+\left(\frac{E_b}{J_0"}\right)^{-1}\right]+1}}\,, \tag{4.76}$$

and

$$P_{b_N} = \left(\frac{1-\mu'}{2}\right)^L \sum_{l=0}^{L-1}\binom{L-1+l}{l}\left(\frac{1+\mu'}{2}\right)^l\,, \tag{4.77}$$

where

$$\mu' = \sqrt{\frac{1}{\frac{1}{aSNR}+1}} = \sqrt{\frac{1}{L\left(\frac{E_b}{N_0}\right)^{-1}+1}}\,. \tag{4.78}$$

For MQAM, we have

$$P_{b_{J+N}} = \frac{4-4/\sqrt{M}}{\log_2 M}\left(\frac{1-\mu}{2}\right)^L \sum_{l=0}^{L-1}\binom{L-1+l}{l}\left(\frac{1+\mu}{2}\right)^l\,, \tag{4.79}$$

where

$$\mu = \sqrt{\frac{1}{\frac{1}{aSJNR}+1}} = \sqrt{\frac{1}{\frac{2(M-1)}{3\log_2 M} L\left[\left(\frac{E_b}{N_0}\right)^{-1} + \left(\frac{E_b}{J_0"}\right)^{-1}\right]+1}}. \tag{4.80}$$

If we consider

$$\left(\frac{E_b}{N_0}\right)^{-1} \ll \left(\frac{E_b}{J_0^"}\right)^{-1}, \tag{4.81}$$

then the AWGN can be neglected [11, p. 450], [15, p. 753], and we obtain

$$P_b \approx \rho P_{b_j}, \tag{4.82}$$

where P_{b_j} is the BER for jamming only.

For QPSK,

$$P_{b_j} = \left(\frac{1-\mu"}{2}\right)^L \sum_{l=0}^{L-1} \binom{L-1-l}{l} \left(\frac{1+\mu"}{2}\right)^l, \tag{4.83}$$

where

$$\mu" = \sqrt{\frac{1}{\frac{1}{aSJR}+1}} = \sqrt{\frac{1}{L\left(\frac{E_b}{J_0"}\right)^{-1}+1}}. \tag{4.84}$$

Then, using (4.74), we obtain

$$\mu" = \sqrt{\frac{1}{\frac{1}{aSJR}+1}} = \sqrt{\frac{1}{\frac{L}{N\rho}\left(\frac{E_b}{J_0}\right)^{-1}+1}}. \tag{4.85}$$

For MQAM,

$$P_{b_{J+N}} = \frac{4-4/\sqrt{M}}{\log_2 M}\left(\frac{1-\mu"}{2}\right)^L \sum_{l=0}^{L-1} \binom{L-1+l}{l} \left(\frac{1+\mu"}{2}\right)^l, \tag{4.86}$$

where

$$\mu" = \sqrt{\frac{1}{\frac{1}{aSJR}+1}} = \sqrt{\frac{1}{\frac{2(M-1)}{3\log_2 M} L\left(\frac{E_b}{J_0"}\right)^{-1}+1}}. \tag{4.87}$$

Again using the relationship (4.74), we obtain

$$\mu'' = \sqrt{\frac{1}{\frac{1}{aSJR}+1}} = \sqrt{\frac{1}{\frac{2(M-1)}{3\log_2 M}\frac{L}{N\rho}\left(\frac{E_b}{J_0}\right)^{-1}+1}}. \tag{4.88}$$

We demonstrate the performance of the system for three different *I*-*Q* modulation schemes. We use (4.88), (4.86) and (4.82) for MQAM and (4.83), (4.85) and (4.82) for QPSK. We utilize QPSK, 16-QAM and 64-QAM. We calculate the BER versus E_b / J_0 for various diversities (*L* transmit antennas) and various values of duty cycle ρ and obtain Figures 34–45. We use the same OSTBCs that were used in Chapter III, Section B. All the plots are for a spread factor *N*=64.

1. QPSK

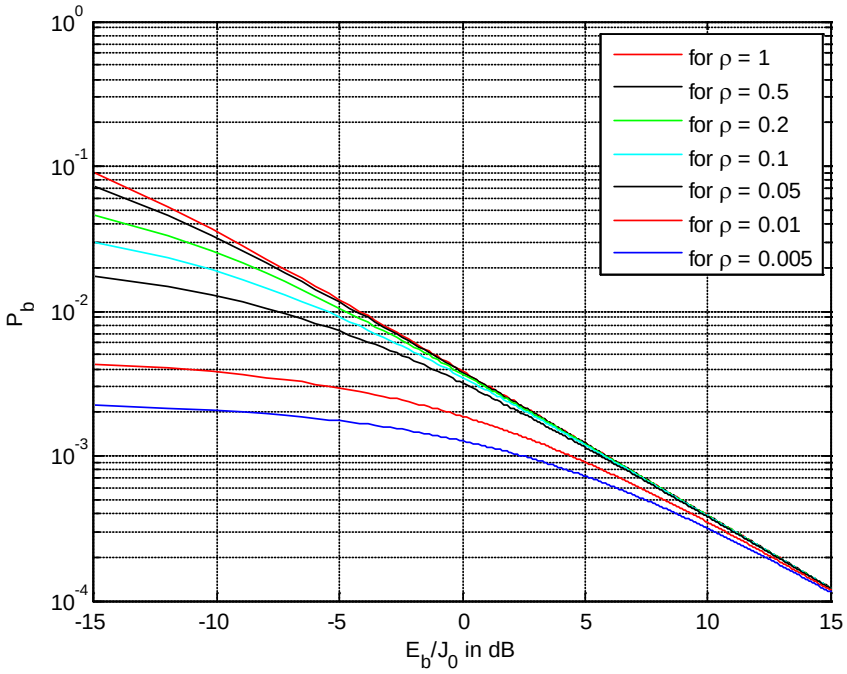

Figure 34. BER of DS QPSK system for pulsed jamming and diversity *L*=1.

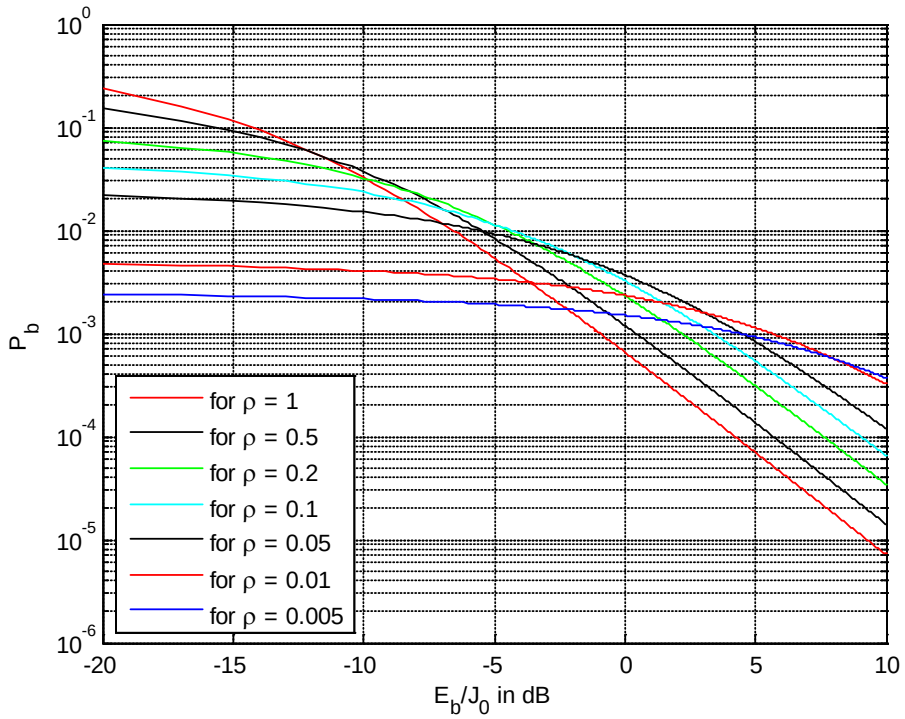

Figure 35. BER of DS QPSK system for pulsed jamming and diversity *L*=2.

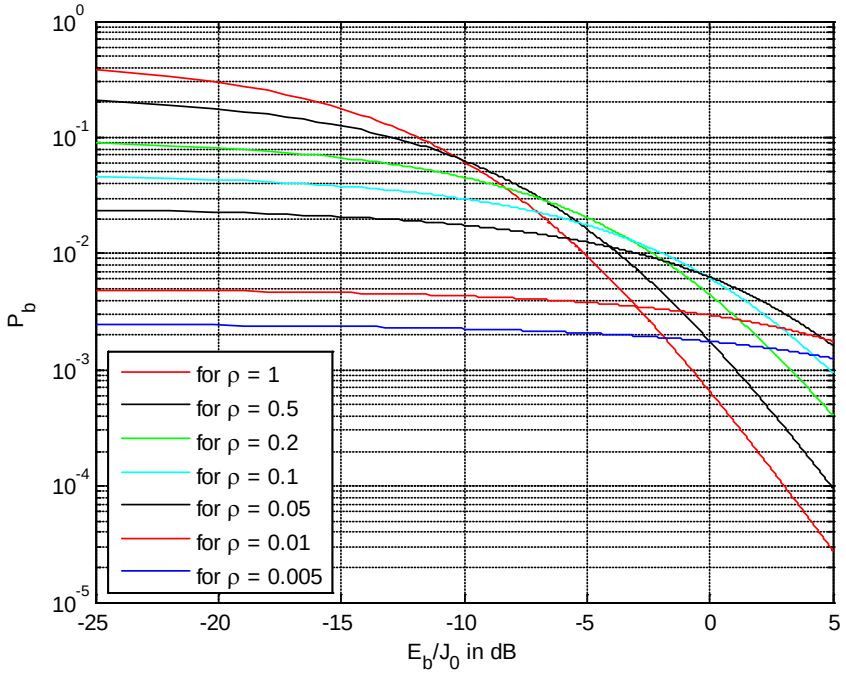

Figure 36. BER of DS QPSK system for pulsed jamming and diversity *L*=3.

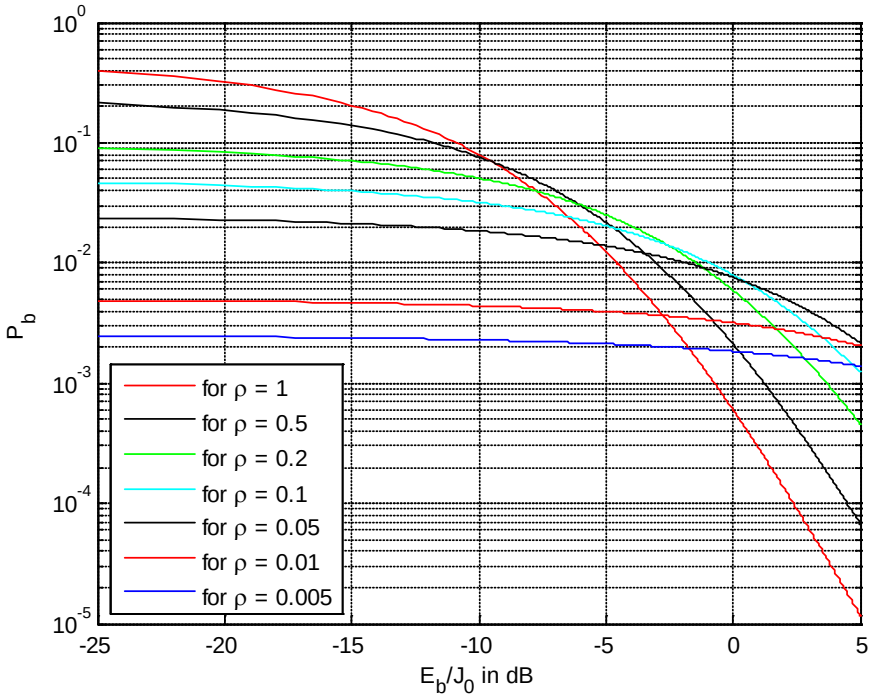

Figure 37. BER of DS QPSK system for pulsed jamming and diversity *L*=4.

2. 16QAM

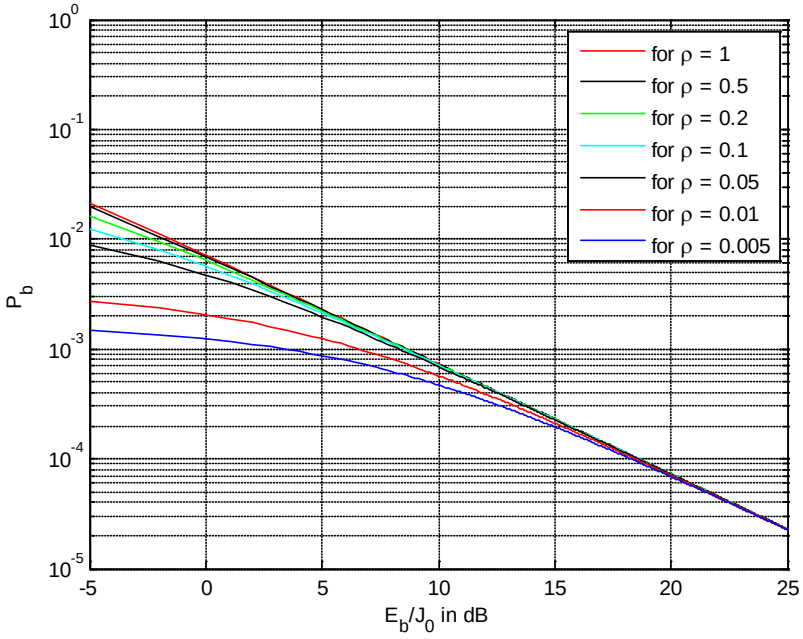

Figure 38. BER of DS 16QAM system for pulsed jamming and diversity *L*=1.

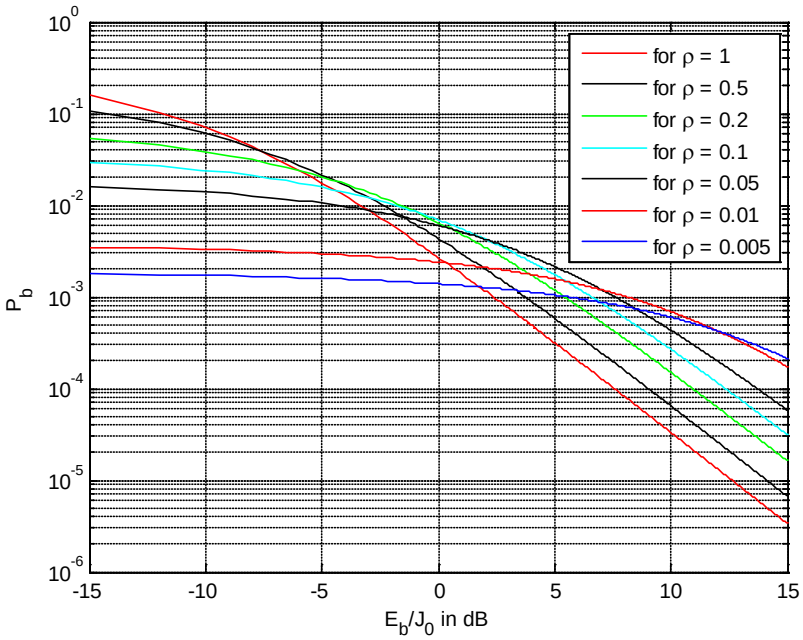

Figure 39. BER of DS 16QAM system for pulsed jamming and diversity L=2.

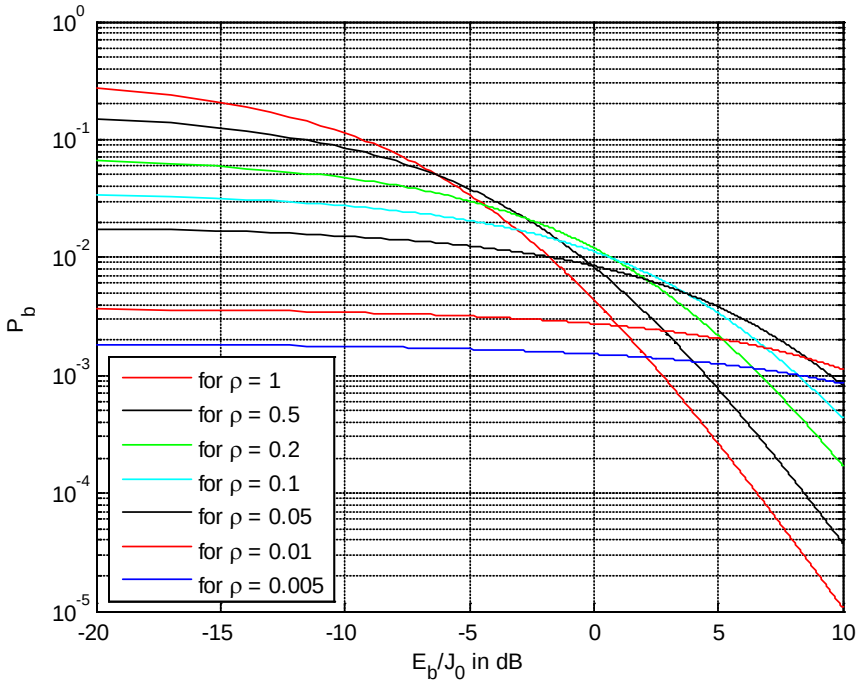

Figure 40. BER of DS 16QAM system for pulsed jamming and diversity L=3.

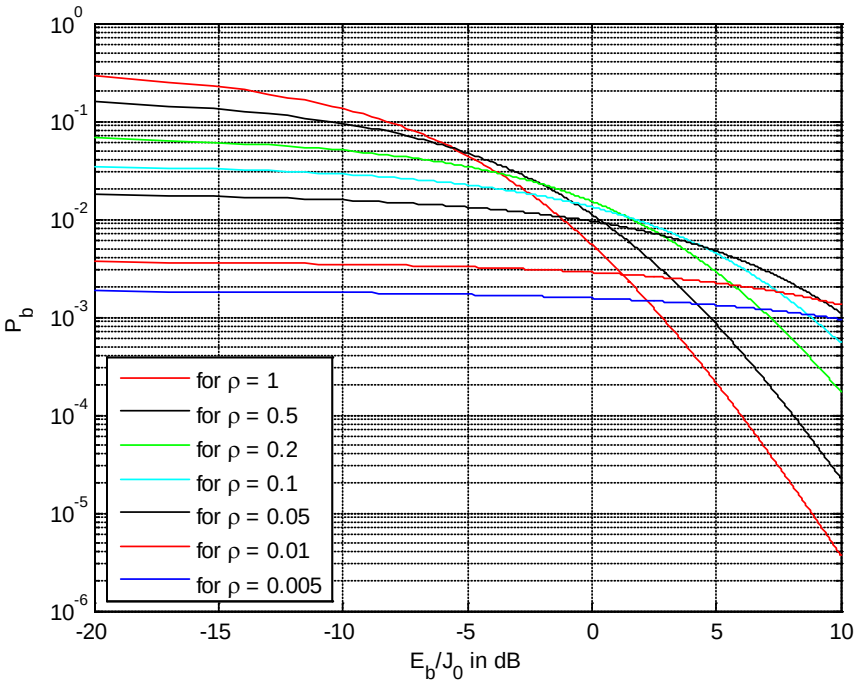

Figure 41. BER of DS 16QAM system for pulsed jamming and diversity *L*=4.

3. 64QAM

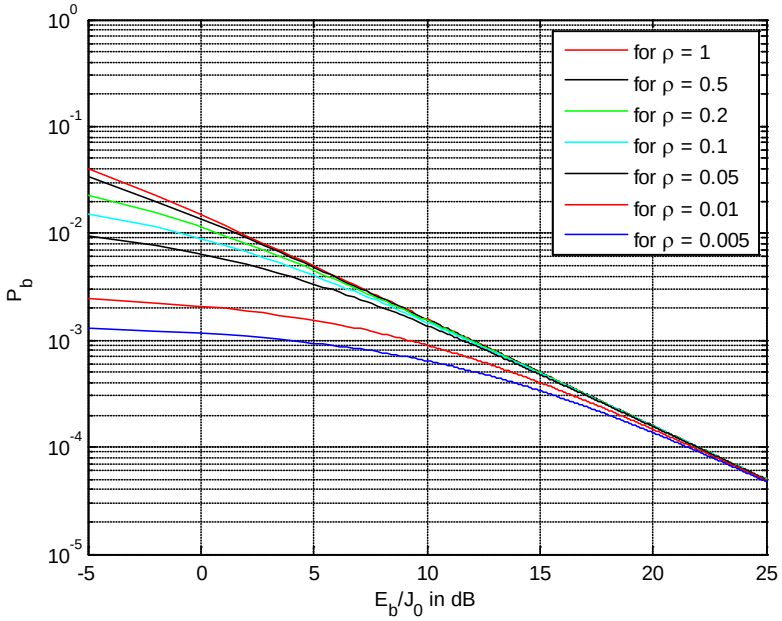

Figure 42. BER of DS 64QAM system for pulsed jamming and diversity *L*=1.

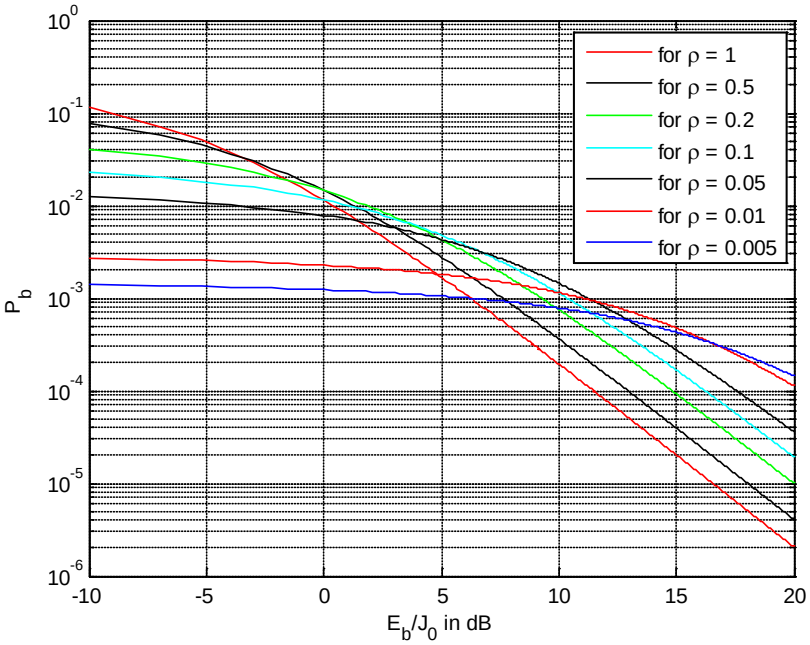

Figure 43. BER of DS 64QAM system for pulsed jamming and diversity *L*=2.

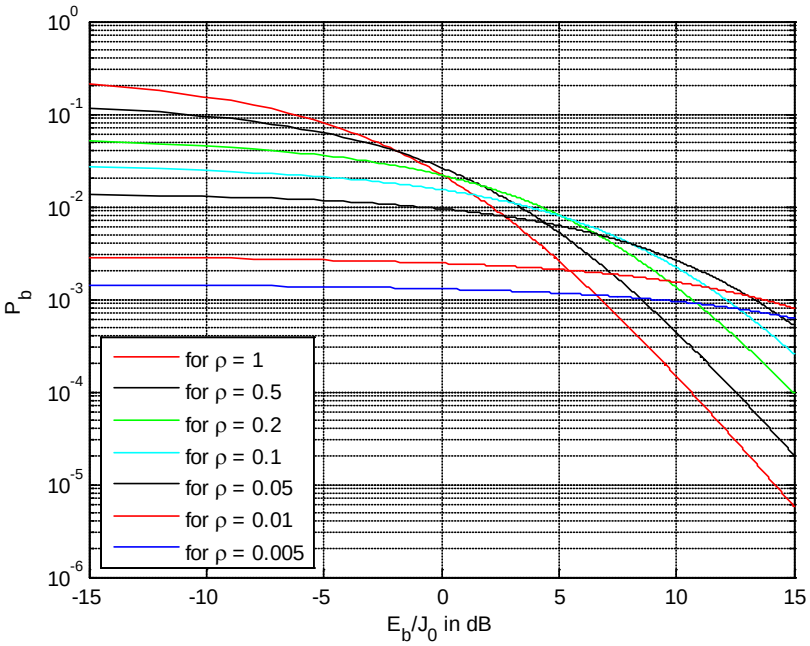

Figure 44. BER of DS 64QAM system for pulsed jamming and diversity *L*=3.

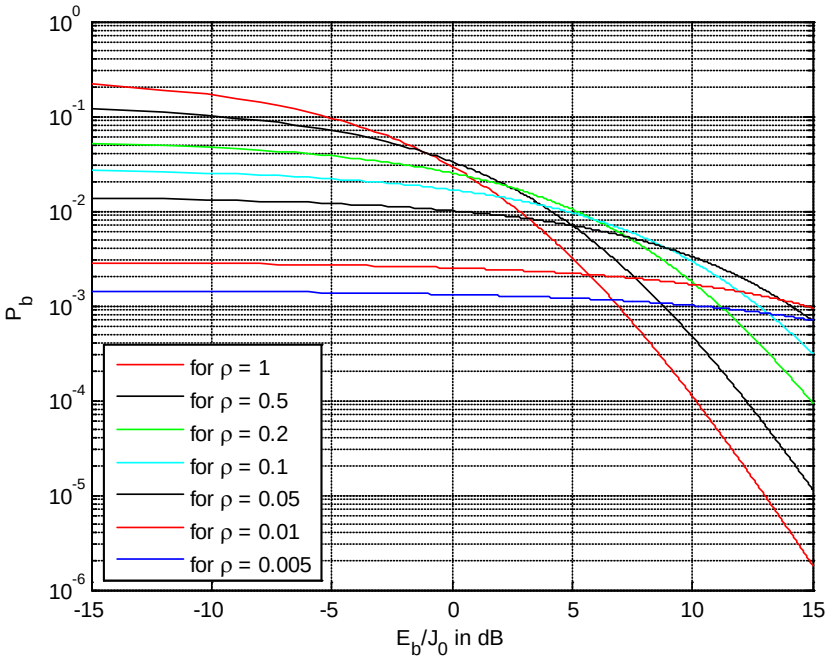

Figure 45. BER of DS 64QAM system for pulsed jamming and diversity L=4.

D. TONE JAMMING

In this section, the jamming signal is assumed to be tone jamming. The system configuration is shown in Figure 21, and the jamming signal is

$$j(t) = A_J \cos(2\pi f_c t + \theta_J), \tag{4.89}$$

where A_J is the amplitude and θ_J is the arbitrary phase of the jamming signal. Thus, the total received signal from the k-th antenna is described by (4.4). After the mixers, the adders and the integrators, we obtain the same decision variables as in (4.19) and (4.20). Based on the results of Section B, Chapter IV, the variances of I-channel and Q-channel noise random variables of AWGN are $N_I^{"} = N_Q^{"} = N_0 / 4$.

For I-channel decision variable, after the mixers, the jamming signal is given by

$$J_I^{'} = \frac{A_J}{2}\cos(2\pi f_c t + \theta_J)\sqrt{\frac{2}{T_S}}\left[c_I(t)\cos(2\pi f_c t + \theta) - c_Q(t)\sin(2\pi f_c t + \theta)\right] \tag{4.90}$$

$$\Rightarrow J_I^{'} = \frac{A_J}{\sqrt{2T_S}}\left[c_I(t)\cos(2\pi f_c t + \theta)\cos(2\pi f_c t + \theta_J) - c_Q(t)\sin(2\pi f_c t + \theta)\cos(2\pi f_c t + \theta_J)\right] \tag{4.91}$$

$$\Rightarrow J_I^{'} = \frac{A_J}{\sqrt{2T_S}}\left\{ c_I(t)\frac{1}{2}\left[\cos(4\pi f_c t + \theta + \theta_J) + \cos(\theta - \theta_J)\right] \right.$$
$$\left. -c_Q(t)\frac{1}{2}\left[\sin(4\pi f_c t + \theta + \theta_J) + \sin(\theta - \theta_J)\right]\right\} \tag{4.92}$$

The high frequency terms are neglected [11, p. 451], and we let $\theta - \theta_J = \theta'$. Then, we obtain

$$J_I^{'} = \frac{A_J}{2\sqrt{2T_S}}\left[c_I(t)\cos\theta' - c_Q(t)\sin\theta' \right]. \tag{4.93}$$

After the integrator, we have

$$J_I^{"} = \int_0^{T_S} \frac{A_J}{2\sqrt{2T_S}}\left[c_I(t)\cos\theta' - c_Q(t)\sin\theta' \right]dt \tag{4.94}$$

$$\Rightarrow J_I^{"} = \frac{A_J}{2\sqrt{2T_S}}\left[\cos\theta' \int_0^{T_S} c_I(t)dt - \sin\theta' \int_0^{T_S} c_Q(t)dt \right]. \tag{4.95}$$

We consider the *PN* sequences $c_I(t)$ and $c_Q(t)$ maximal sequences and $N = T_s / T_c$. Thus, we obtain

$$J_I^{"} = \frac{A_J}{2\sqrt{2T_S}}\left[\cos\theta' T_c - \sin\theta' T_c\right] \tag{4.96}$$

$$\Rightarrow J_I^{"} = \frac{A_J T_c}{2\sqrt{2T_S}}\left[\cos\theta' - \sin\theta'\right]. \tag{4.97}$$

We calculate the variance of the jamming signal to be

$$\sigma_{J_I^{"}}^2 = \overline{J_I^{"} \cdot J_I^{"*}} = E\left\{ \left[\frac{A_J T_c}{2\sqrt{2T_S}}\left(\cos\theta' - \sin\theta'\right) \right]^2 \right\} \tag{4.98}$$

$$\Rightarrow \sigma_{J_I^{"}}^2 = \frac{A_J^2 T_c^2}{8T_s} E\left\{\cos^2\theta' - 2\sin\theta'\cos\theta' + \sin^2\theta'\right\} \tag{4.99}$$

$$\Rightarrow \sigma_{J_I^{"}}^2 = \frac{A_J^2 T_c^2}{8T_s}\left(\frac{1}{2} + \frac{1}{2}\right) = \frac{A_J^2 T_c}{8N}. \tag{4.100}$$

Similarly, we derive $\sigma_{J_Q}^2 = \sigma_{J_I}^2 = (A_J^2 T_c)/(8N)$. Therefore, the total variance of AWGN and the jamming signal is

$$\sigma_T^2 = \sigma_{N_I}^2 + \sigma_{N_Q}^2 + \sigma_{J_I}^2 + \sigma_{J_Q}^2 = \frac{N_0}{2} + \frac{A_J^2 \cdot T_c}{4N}. \tag{4.101}$$

For QPSK, based on (2.16), we recall that

$$P_b = \left(\frac{1-\mu}{2}\right)^L \sum_{l=0}^{L-1} \binom{L-1+l}{l} \left(\frac{1+\mu}{2}\right)^l, \tag{4.102}$$

where

$$\mu = \sqrt{\frac{aSJNR}{1+aSJNR}}, \tag{4.103}$$

and

$$aSJNR = \frac{1}{2}\left(\frac{d_{\min}}{2\sigma_T}\right)^2, \tag{4.104}$$

where $d_{\min} = \sqrt{2\varepsilon_s}$ and $\varepsilon_s = E_s / L$. Thus, we obtain

$$aSJNR = \frac{1}{2}\left(\frac{d_{\min}}{2\sigma_T}\right)^2 = \frac{1}{2}\cdot\frac{2\cdot\varepsilon_s}{4\cdot\left(\frac{N_0}{2}+\frac{A_J^2\cdot T_c}{4N}\right)} = \frac{\varepsilon_s}{2N_0+\frac{A_J^2\cdot T_c}{N}} \tag{4.105}$$

$$\Rightarrow aSJNR = \frac{E_s}{L\left(2N_0+\frac{A_J^2\cdot T_c}{N}\right)} = \frac{1}{L\left[\left(\frac{E_b}{N_0}\right)^{-1}+\frac{A_J^2\cdot T_c}{2N\cdot E_b}\right]}. \tag{4.106}$$

We know that the bit energy equals [11, p. 18]

$$E_b = \frac{1}{2}A^2 T_b \tag{4.107}$$

where *A* is the amplitude of the information signal. Thus, by using equation (4.107) and replacing the E_b in the second term of the denominator of equation (4.106), we obtain

$$aSJNR = \frac{1}{L\left[\left(\frac{E_b}{N_0}\right)^{-1}+\left(\frac{A^2}{A_J^2}\right)^{-1}\cdot\frac{1}{N^2}\right]}. \tag{4.108}$$

Therefore, we have

$$\mu = \sqrt{\frac{1}{\frac{1}{aSJNR}+1}} = \sqrt{\frac{1}{L\left[\left(\frac{E_b}{N_0}\right)^{-1}+\left(\frac{A^2}{A_J^2}\right)^{-1}\cdot\frac{1}{N^2}\right]+1}}. \tag{4.109}$$

Similarly, for MQAM we have

$$P_{b_{J+N}} = \frac{4-4/\sqrt{M}}{\log_2 M}\left(\frac{1-\mu}{2}\right)^L \sum_{l=0}^{L-1}\binom{L-1+l}{l}\left(\frac{1+\mu}{2}\right)^l \tag{4.110}$$

where

$$aSJNR = \frac{1}{2}\frac{d_{\min}^2}{4\sigma_T^2} = \frac{3\log_2 M}{2L(M-1)\left[\left(\frac{E_b}{N_0}\right)^{-1} + \left(\frac{A}{A_J}\right)^{-2}\frac{1}{N^2}\right]}, \tag{4.111}$$

and

$$\mu = \sqrt{\frac{1}{\frac{1}{aSJNR}+1}} = \sqrt{\frac{1}{\frac{2(M-1)}{3\log_2 M}L\left[\left(\frac{E_b}{N_0}\right)^{-1} + \left(\frac{A^2}{A_J^2}\right)^{-1}\frac{1}{N^2}\right]+1}}. \tag{4.112}$$

We illustrate the performance of the system for three different *I*-*Q* modulation schemes. We utilize QPSK, 16-QAM and 64-QAM. By using (4.112), (4.110), (4.109) and (4.102), we calculate the BER versus the information signal-to-jamming signal amplitude ratio (A_J / A) for various diversities (*L* transmit antennas) and obtain Figures 46-57. We use the same OSTBCs that were used in Chapter III, Section B. All the plots are for spread factor *N*=64.

1. QPSK

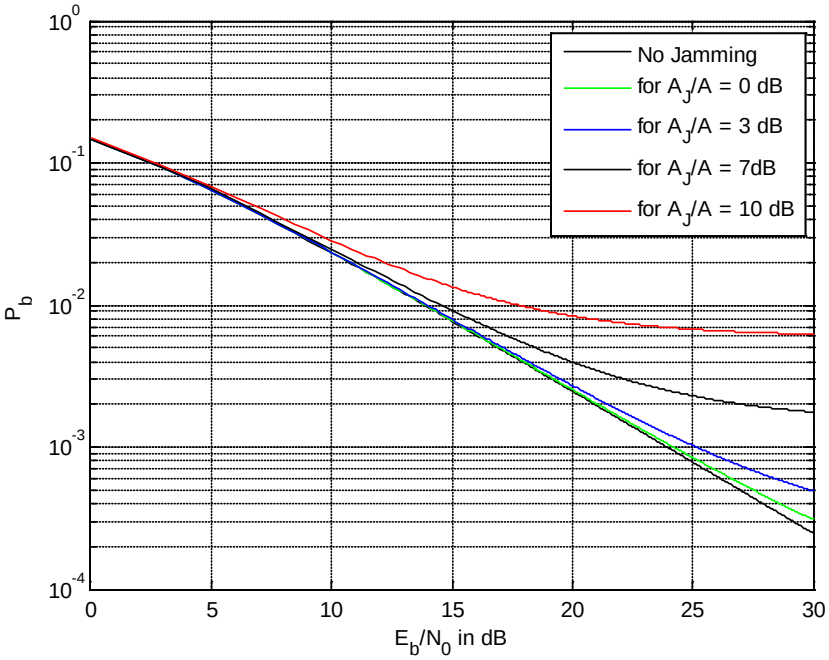

Figure 46. BER of DS QPSK system for tone jamming and diversity *L*=1.

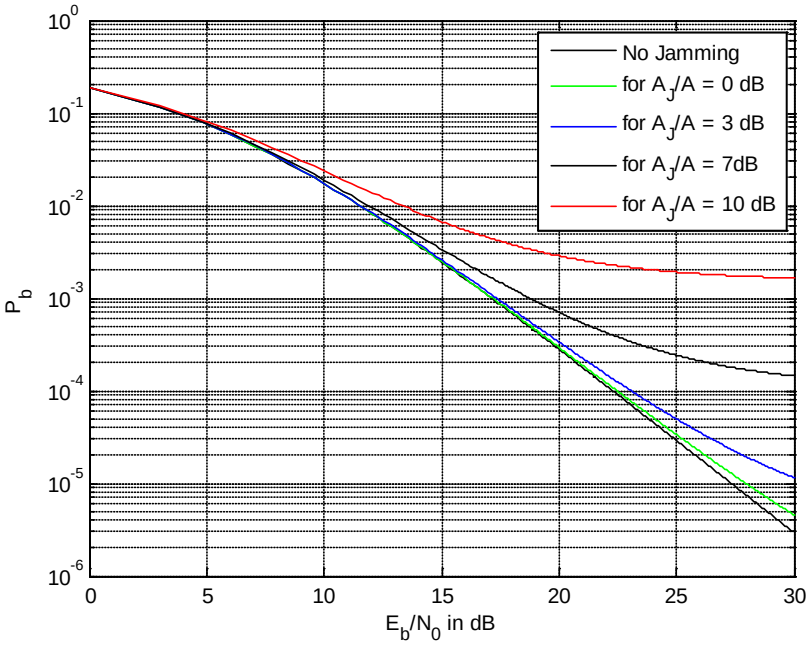

Figure 47. BER of DS QPSK system for tone jamming and diversity L=2.

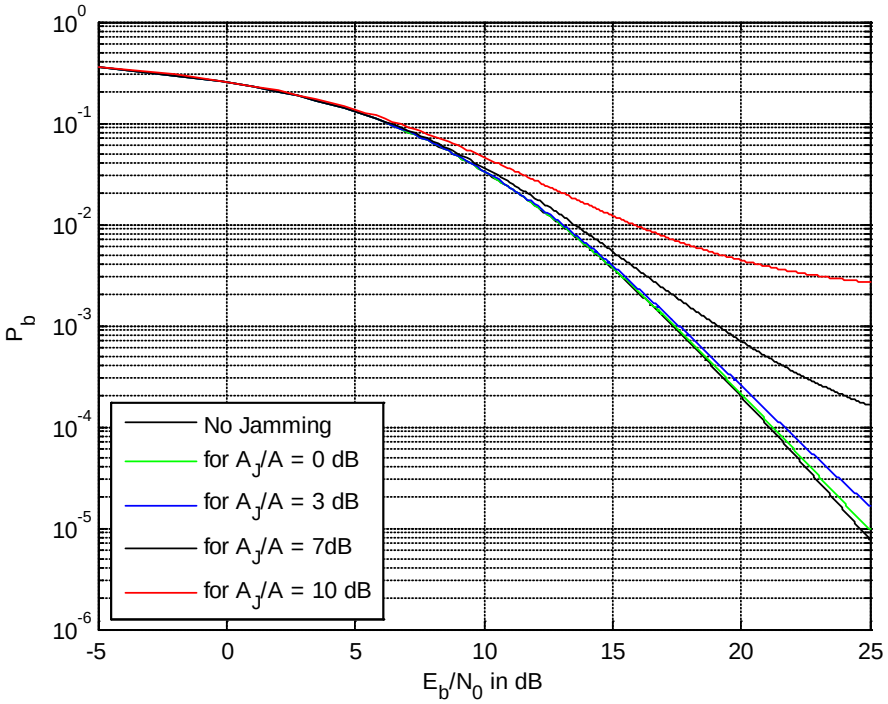

Figure 48. BER of DS QPSK system for tone jamming and diversity L=3.

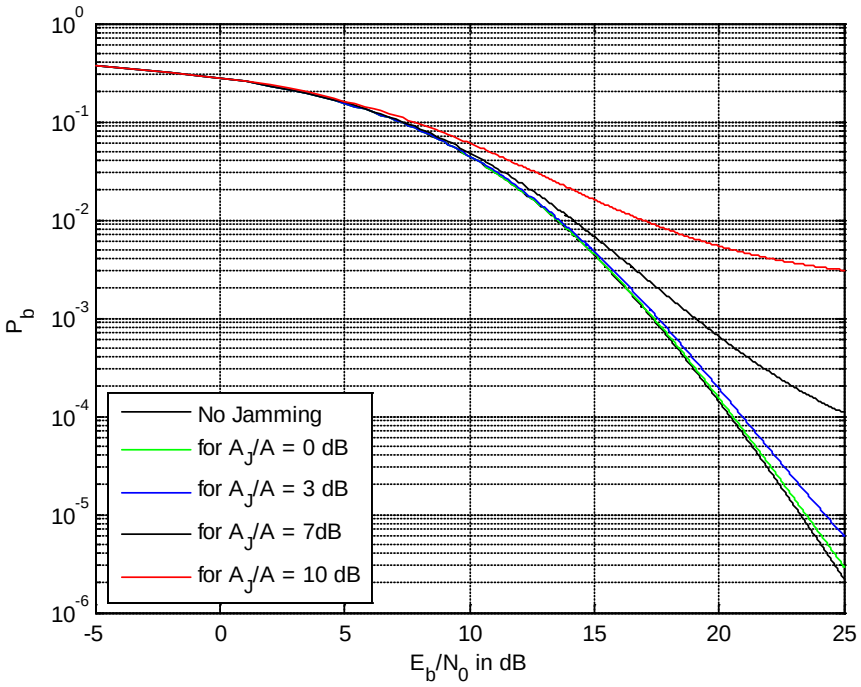

Figure 49. BER of DS QPSK system for tone jamming and diversity L=4.

2. 16QAM

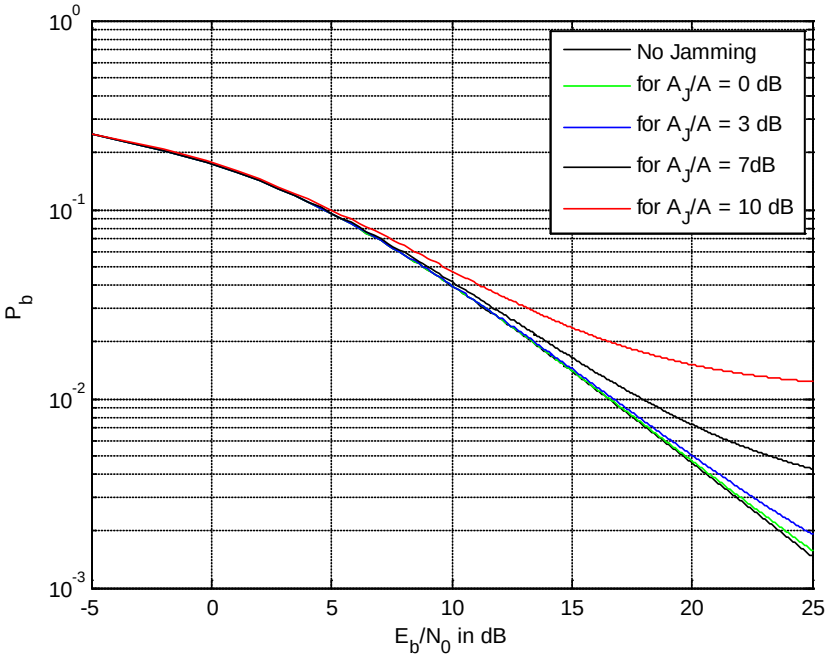

Figure 50. BER of DS 16QAM system for tone jamming and diversity L=1.

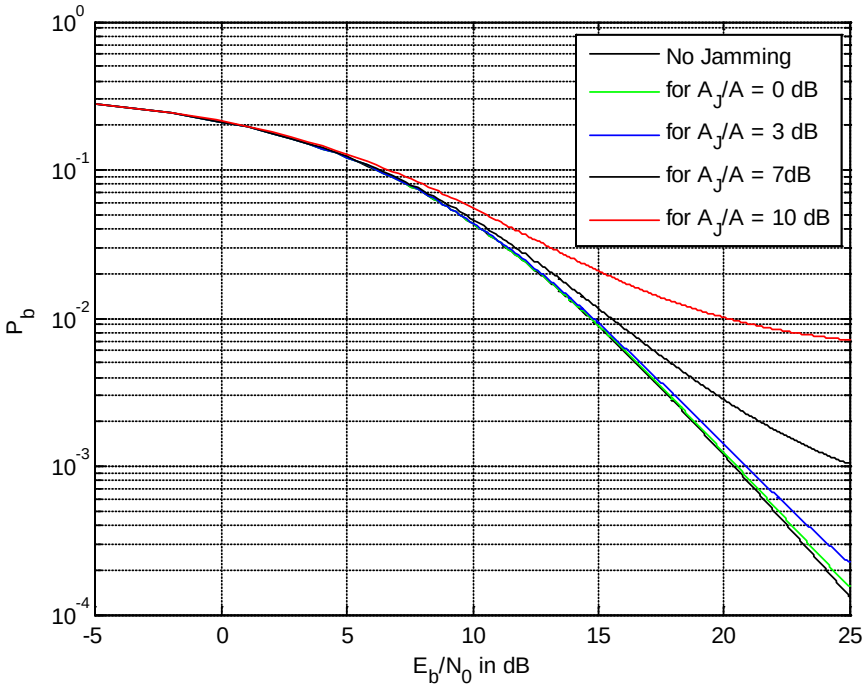

Figure 51. BER of DS 16QAM system for tone jamming and diversity *L*=2.

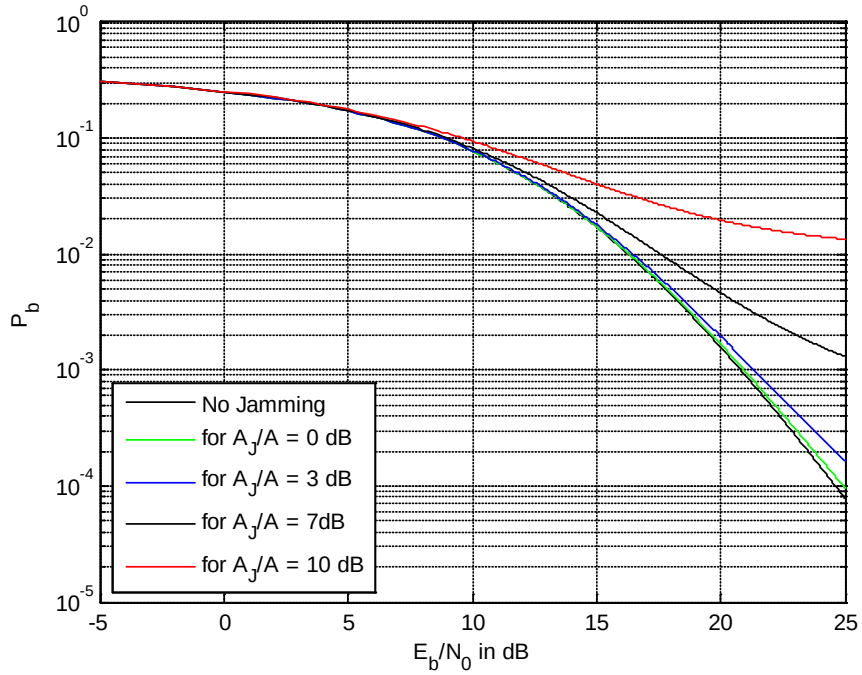

Figure 52. BER of DS 16QAM system for tone jamming and diversity *L*=3.

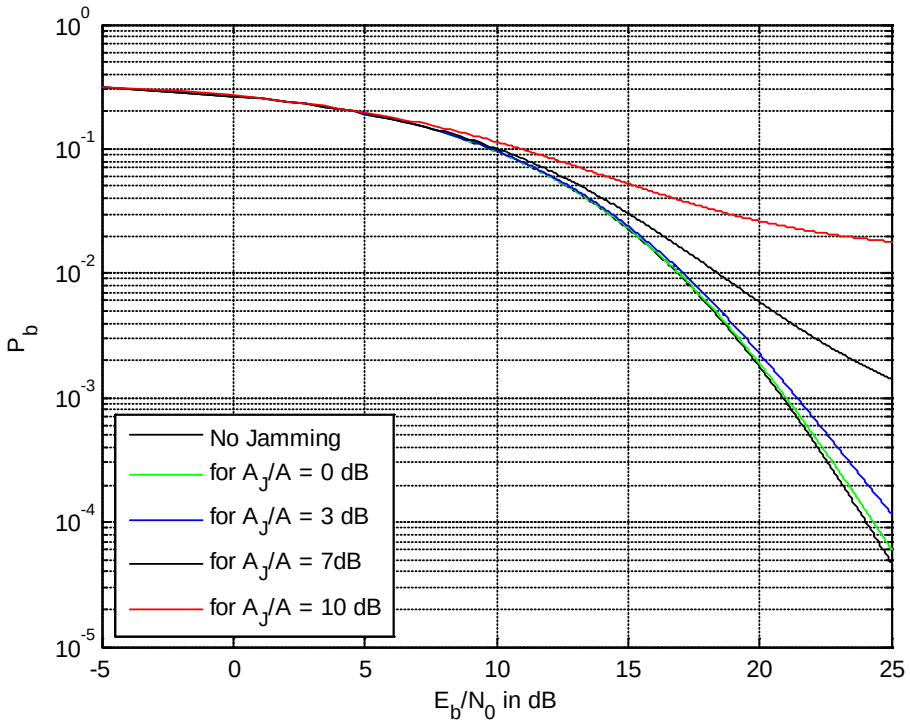

Figure 53. BER of DS 16QAM system for tone jamming and diversity *L*=4.

3. 64QAM

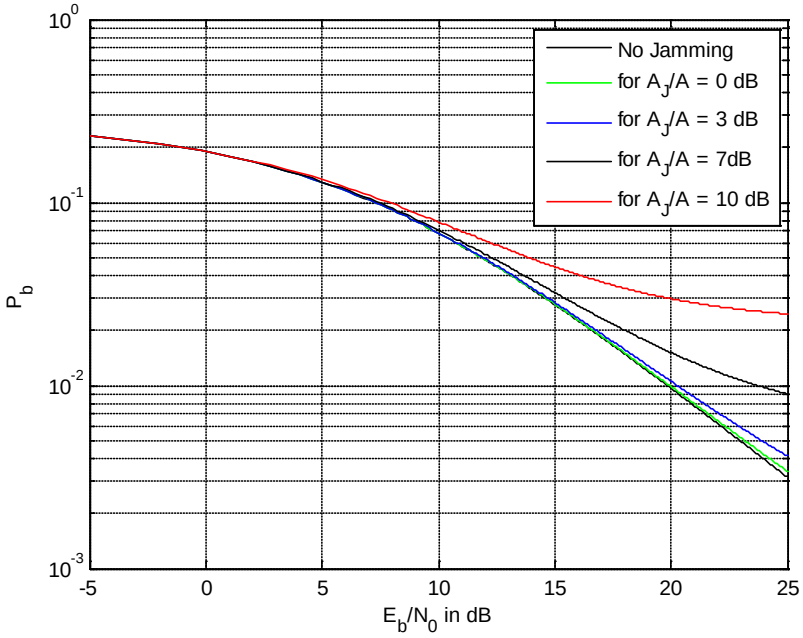

Figure 54. BER of DS 64QAM system for tone jamming and diversity *L*=1.

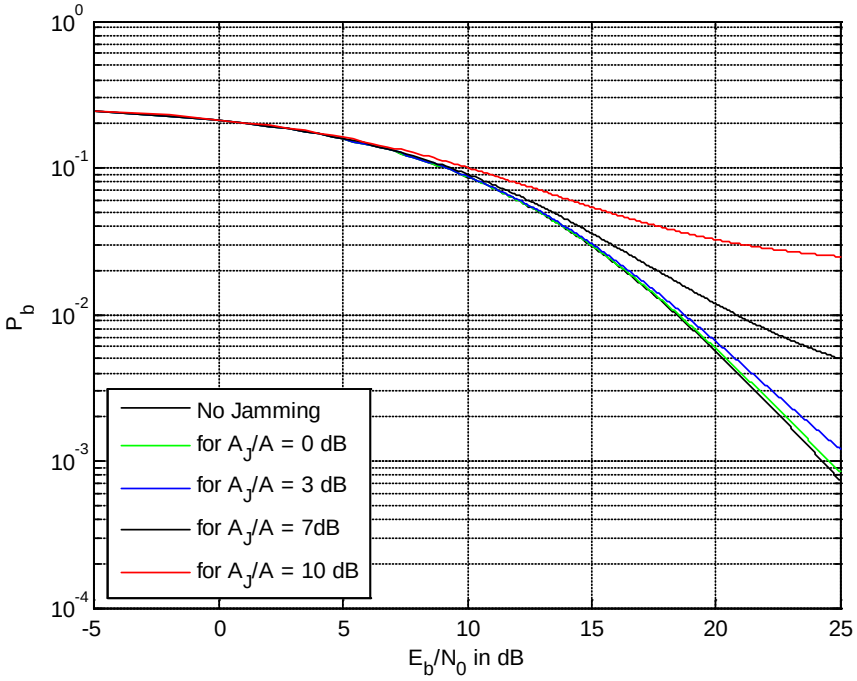

Figure 55. BER of DS 64QAM system for tone jamming and diversity *L*=2.

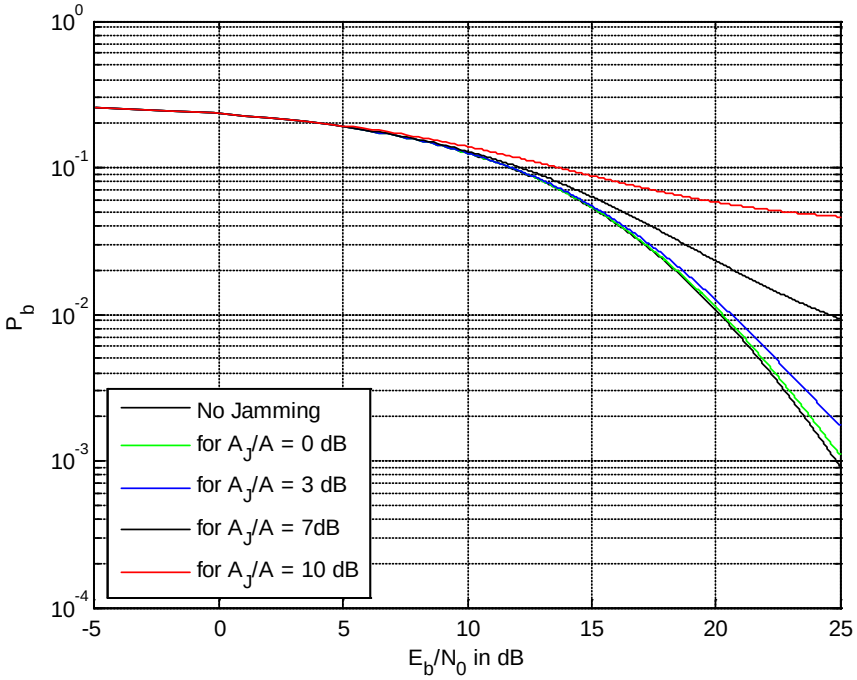

Figure 56. BER of DS 64QAM system for tone jamming and diversity *L*=3.

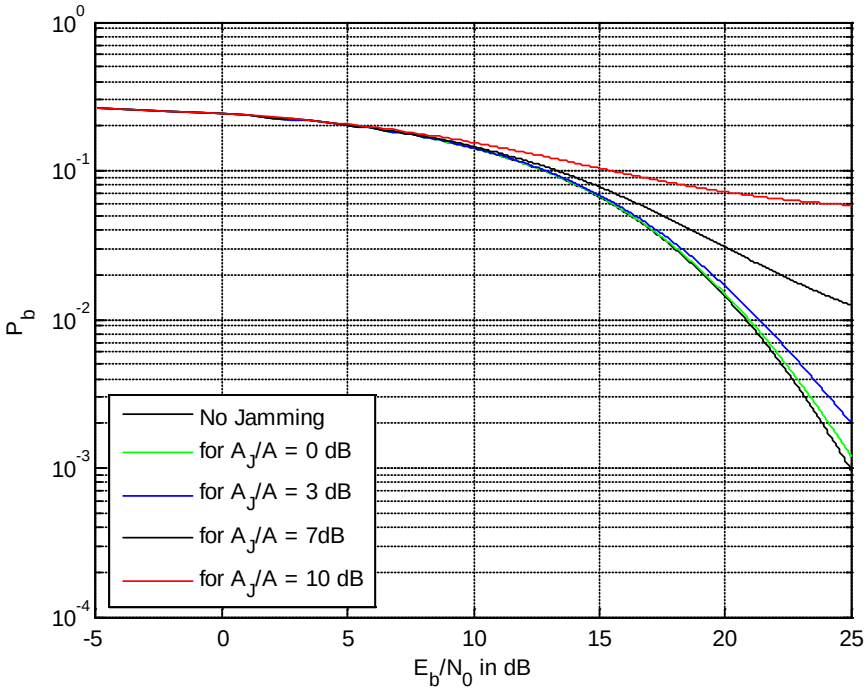

Figure 57. BER of DS 64QAM system for tone jamming and diversity L=4.

In this chapter, we studied MISO systems, which use *I-Q* modulation schemes. More specifically, we utilized QPSK, 16QAM and 64QAM. In the next chapter, we introduce MIMO systems for the same modulation schemes. We evaluate their performance and apply exploitation of full diversity of the systems for three types of jamming: broadband, pulsed-noise and tone.

THIS PAGE INTENTIONALLY LEFT BLANK

V. PERFORMANCE ANALYSIS OF IQ COMPLEX SPREADING MIMO SYSTEM

A. SYSTEM DESCRIPTION

In this chapter, we analyze the configuration of a MIMO system and the benefits of its use. We also evaluate the performance of a general *I-Q* complex spreading MIMO system. We examine the system for various modulation schemes under three types of jamming: broadband, pulsed-noise and tone. We also use MRC. The system is assumed to experience Rayleigh fading and we assume perfect channel estimation. The system configuration is shown in Figure 58.

The basic advantage for the use of a MIMO system is that we can exploit an increased diversity from both transmit and receive antennas. We implement transmit diversity via OSTBC with a complex $L_s \times L_t$ code matrix $\boldsymbol{G}$ which provides L_t-fold diversity via L_t transmit antennas for m complex symbols transmitting over L_s symbol times. Therefore, the code rate is m / L_s. The receiver diversity comes from L_r receive antennas. We use MRC in order to exploit full diversity of the described system [11, pp. 578-580], [11, pp. 605-608]. The final diversity is $L = L_t \times L_r$.

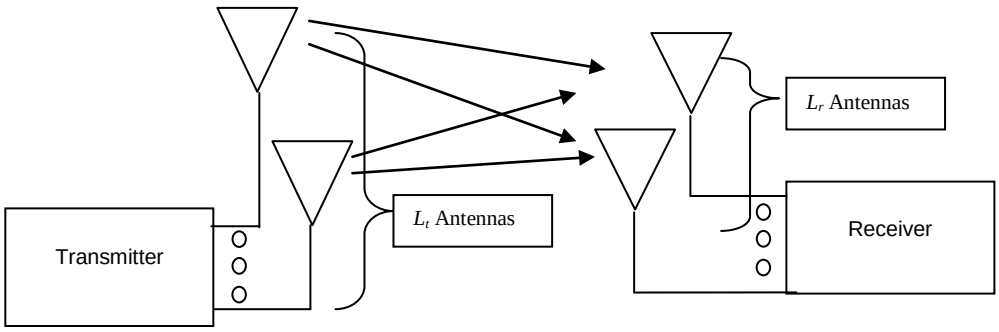

Figure 58. Configuration of a MIMO system.

B. MIMO SYSTEM FULL DIVERSITY FOR *I-Q* MODULATION

1. MIMO 2X2, 2X3 2X4

Firstly, we consider a two-T_x (transmitter), two-T_r (receiver) antenna system for general *I-Q* modulation. We apply an Alamouti code, which has a code rate of *R*=1. Thus, we have $L_t = 2, L_s = 2, L_r = 2$, and the code matrix is [14, pp. 103-105]

$$G = \begin{bmatrix} s_1 & s_2 \\ -s_2^* & s_1^* \end{bmatrix}. \tag{5.1}$$

As mentioned before, in order to do a proper comparison of the performances of the various systems examined, we consider fixed transmitted power. Because of the transmit antennas diversity, the symbol energy is divided by two. In addition, we have two symbols transmitted over two symbol times (code rate *R*=1). Thus, the symbol energy becomes $E_s^{'} = E_s / 2$. By using proper MRC and assuming perfect channel estimation, we achieve a full diversity of $L = L_t \cdot L_r = 4$. Assuming that we use the same Alamouti OSTBC, we can show that for MIMO systems of $2T_x$-$3T_r$ (2X3) and $2T_x$-$4T_r$ (2X4), the symbol energy becomes $E_s^{'} = E_s / 2$, and the diversities are $L = L_t \cdot L_r = 6$ and $L = L_t \cdot L_r = 8$, respectively.

2. MIMO 3X2, 3X3 3X4

We now consider a 3 T_x 2 T_r antenna system for general *I-Q* modulation. We apply an OSTBC with code rate *R*=3/4. Therefore, we have $L_t = 3, L_s = 4, L_r = 2$, and the code matrix is [14, pp. 103-105]

$$G = \begin{vmatrix} s_1 & 0 & -s_2^* \\ 0 & s_1 & -s_3 \\ s_2 & s_3^* & s_1^* \\ -s_3 & s_2^* & 0 \end{vmatrix}. \tag{5.2}$$

We consider fixed transmitted power and because of transmit diversity, the symbol energy is divided by three. In addition, we have three symbols transmitted over four symbol times (code rate $R = 3/4$). Thus, the symbol energy is $E_s^{'} = E_s / 3$. In order

to maintain the same throughput, we have to increase the symbol rate 4/3. Thus, the symbol energy is degraded by 3/4, and we obtain $E_s^{"} = E_s^{'} = (E_s / 3)(3/4) = E_s / 4$. By using proper MRC and assuming perfect channel estimation, we achieve a diversity of $L = L_t \cdot L_r = 6$. Assuming that we use the same OSTBC, we can show that for MIMO systems of $3T_x$-$3T_r$ (3X3) and $3T_x$-$4T_r$ (3X4), the symbol energy is $E_s^{'} = E_s / 4$, and the diversities are $L = L_t \cdot L_r = 9$ and $L = L_t \cdot L_r = 12$, respectively.

3. MIMO 4X2, 4X3 4X4

Finally, we consider a $4T_x$-$2T_r$ antenna system for general *I*-*Q* modulation. We apply an OSTBC with code rate *R*=3/4. Therefore, we have $L_t = 4, L_s = 4, L_r = 2$, and the code matrix is [14, pp. 103-105]

$$G = \begin{vmatrix} s_1 & 0 & -s_2^* & s_3^* \\ 0 & s_1 & -s_3 & -s_2 \\ s_2 & s_3^* & s_1^* & 0 \\ -s_3 & s_2^* & 0 & s_1^* \end{vmatrix}. \tag{5.3}$$

We consider fixed transmitted power and, because of transmit diversity, the symbol energy is divided by four. In addition, we have three symbols transmitted over four symbol times (code rate $R = 3/4$). Thus, the symbol energy is $E_s^{'} = E_s / 4$,. Therefore, in order to maintain the same throughput, we have to increase the symbol rate by 4/3. Thus, the symbol energy is degraded by 3/4, and $E_s^{"} = E_s^{'} = (E_s / 4) \cdot (3/4) = (3/16)E_s$. By using proper MRC and assuming perfect channel estimation, we achieve a diversity of $L = L_t \cdot L_r = 8$. Assuming that we use the same OSTBC, we can similarly prove that for MIMO systems of $4T_x$-$3T_r$ (4X3) and $4T_x$-$4T_r$ (4X4), the symbol energy is $E_s^{'} = 3E_s / 16$, and the diversities are $L = L_t \cdot L_r = 12$ and $L = L_t \cdot L_r = 16$, respectively.

C. BROADBAND JAMMING

Based on the analysis of Section B of this chapter and the results and the performance analysis for *I-Q* modulation in the previous chapter, we use the same expressions for the BER using the full diversity obtained by the equivalent MIMO configuration. The results are shown in Figures 59-85. We use spread factor N=64.

1. QPSK

a. MIMO 2X2, 2X3 2X4

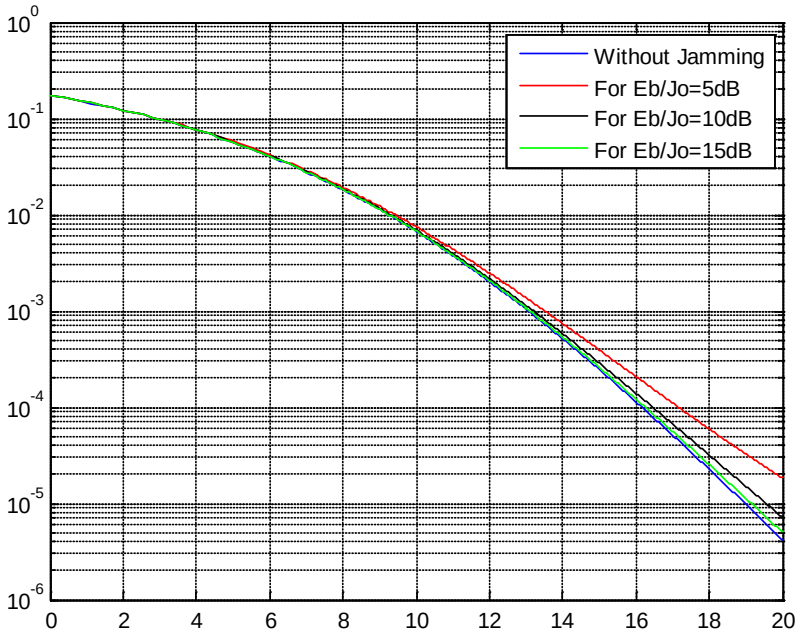

Figure 59. BER of DS QPSK MIMO for broadband jamming and diversity L=4.

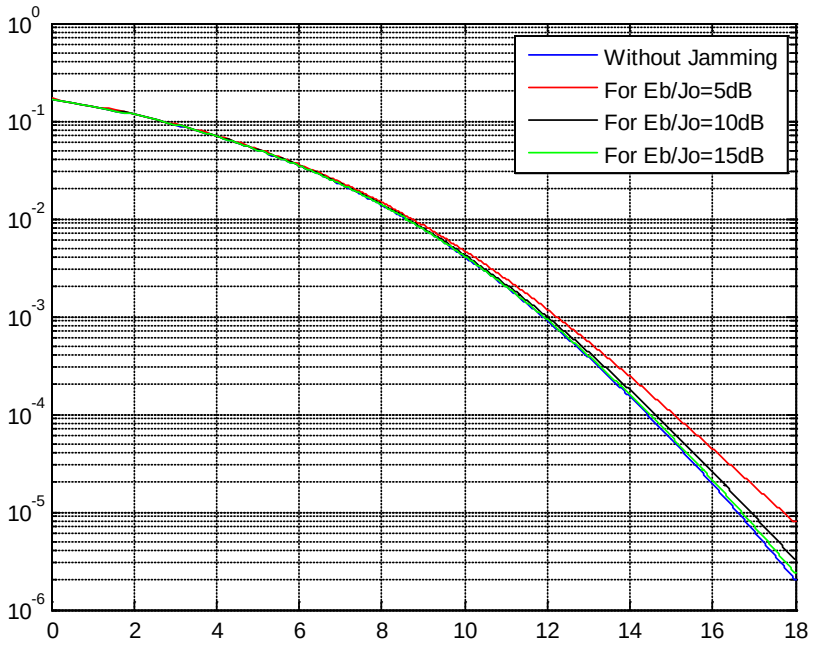

Figure 60. BER of DS QPSK MIMO for broadband jamming and diversity *L*=6.

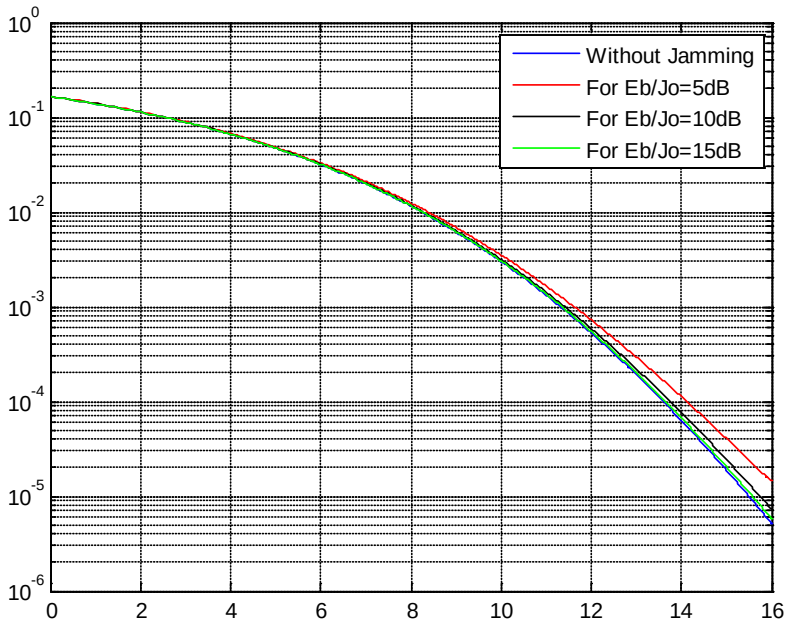

Figure 61. BER of DS QPSK MIMO for broadband jamming and diversity *L*=8.

b. MIMO 3X2, 3X3 3X4

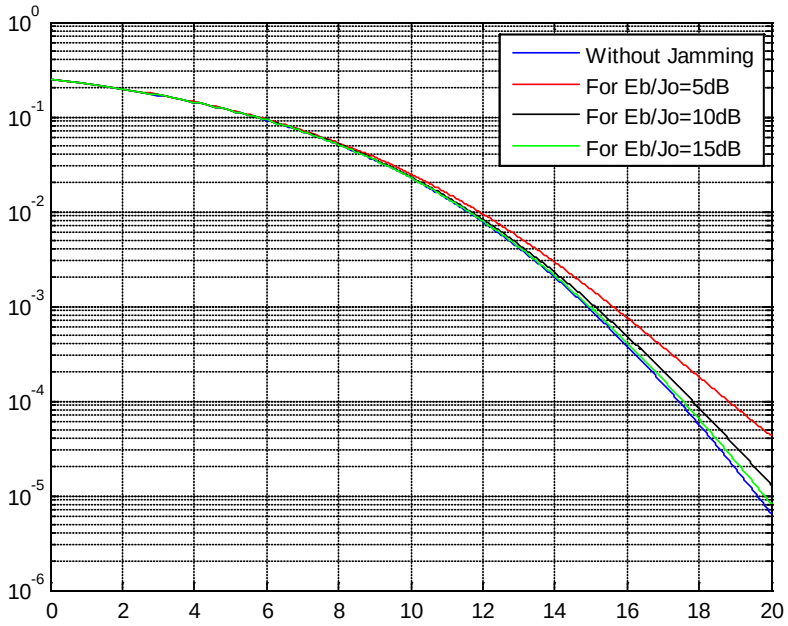

Figure 62. BER of DS QPSK MIMO for broadband jamming and diversity *L*=6.

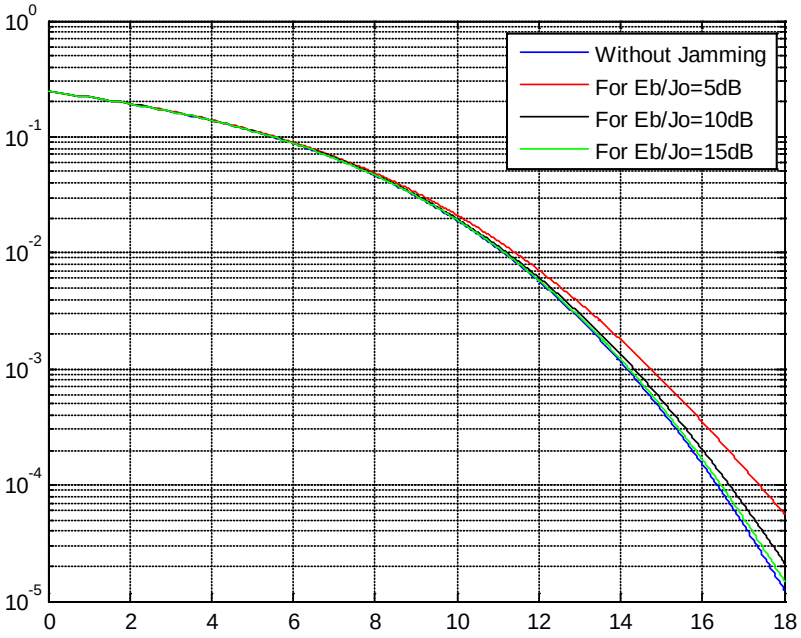

Figure 63. BER of DS QPSK MIMO for broadband jamming and diversity *L*=9.

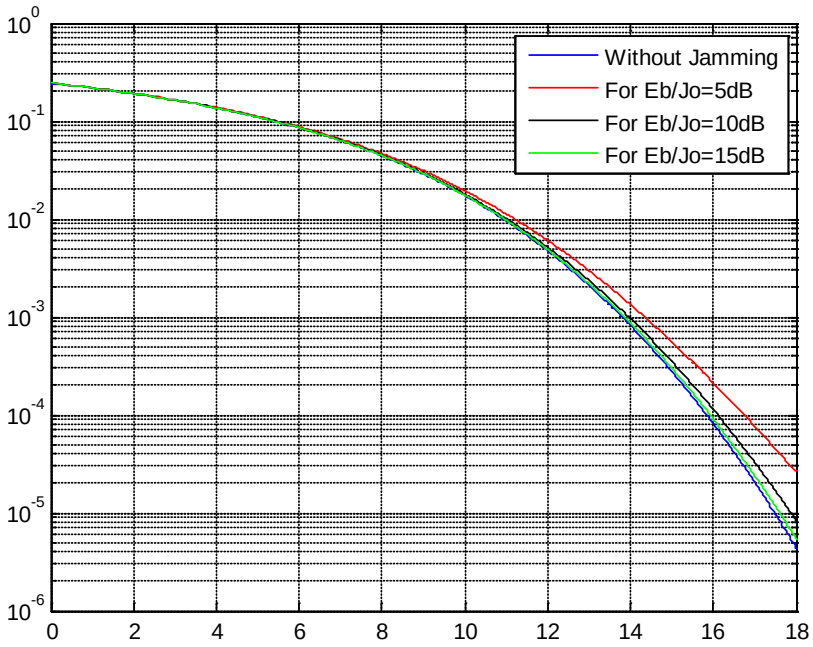

Figure 64. BER of DS QPSK MIMO for broadband jamming and diversity *L*=12.

c. MIMO4X2, 4X3 4X4

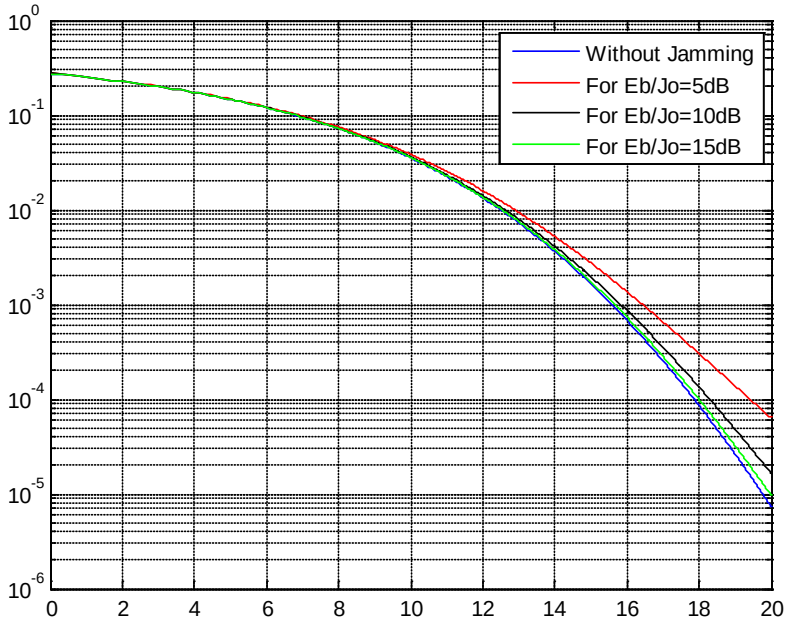

Figure 65. BER of DS QPSK MIMO for broadband jamming and diversity *L*=8.

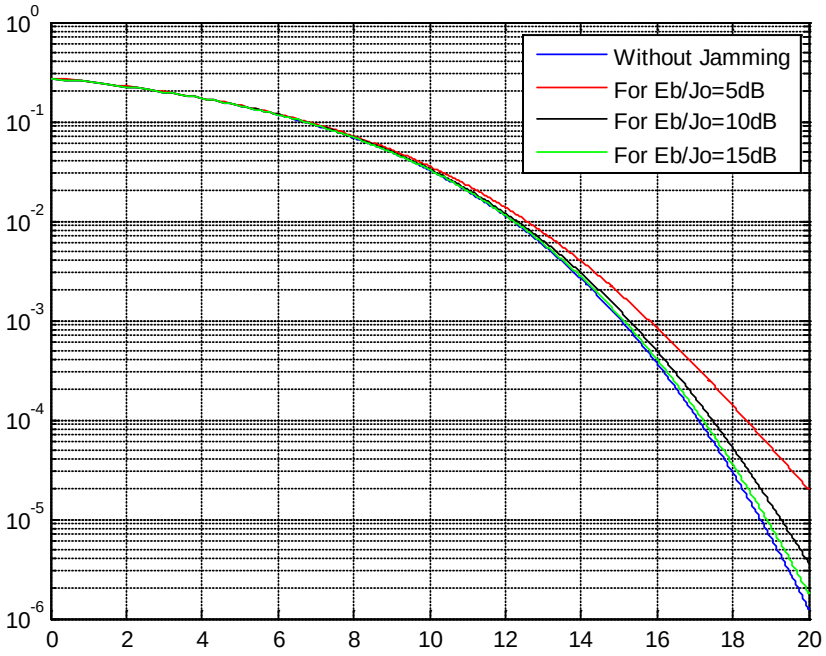

Figure 66. BER of DS QPSK MIMO for broadband jamming and diversity L=12.

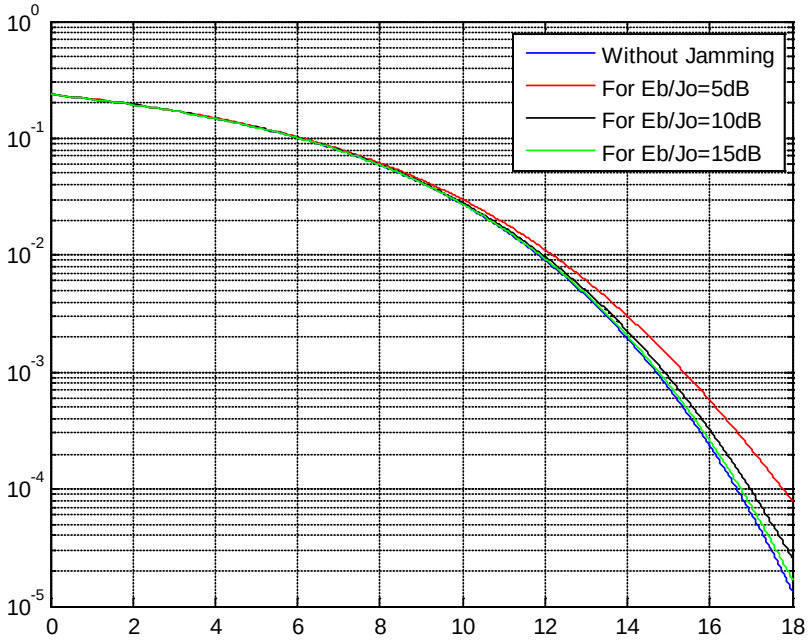

Figure 67. BER of DS QPSK MIMO for broadband jamming and diversity L=16.

2. 16-QAM

a. MIMO 2X2, 2X3 2X4

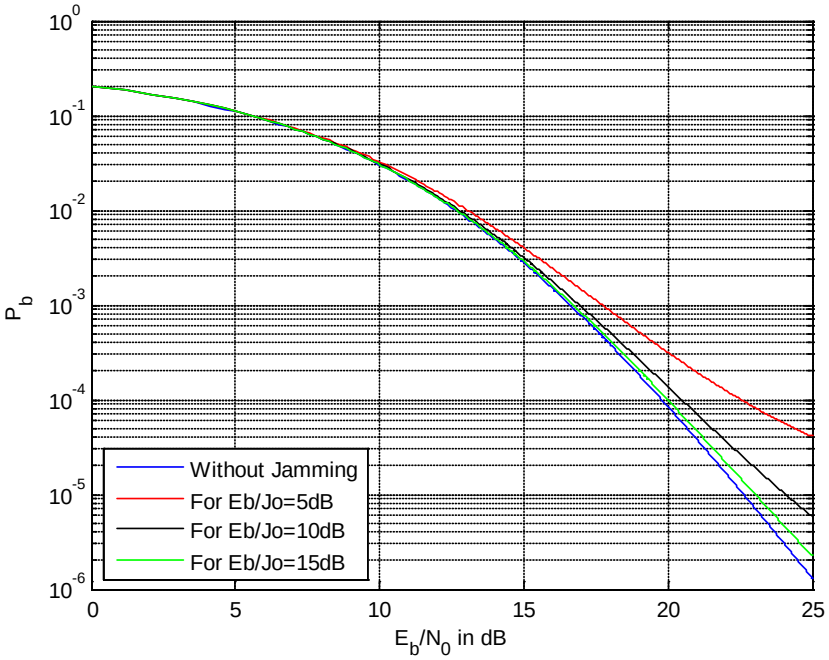

Figure 68. BER of DS 16QAM MIMO for broadband jamming and diversity *L*=4.

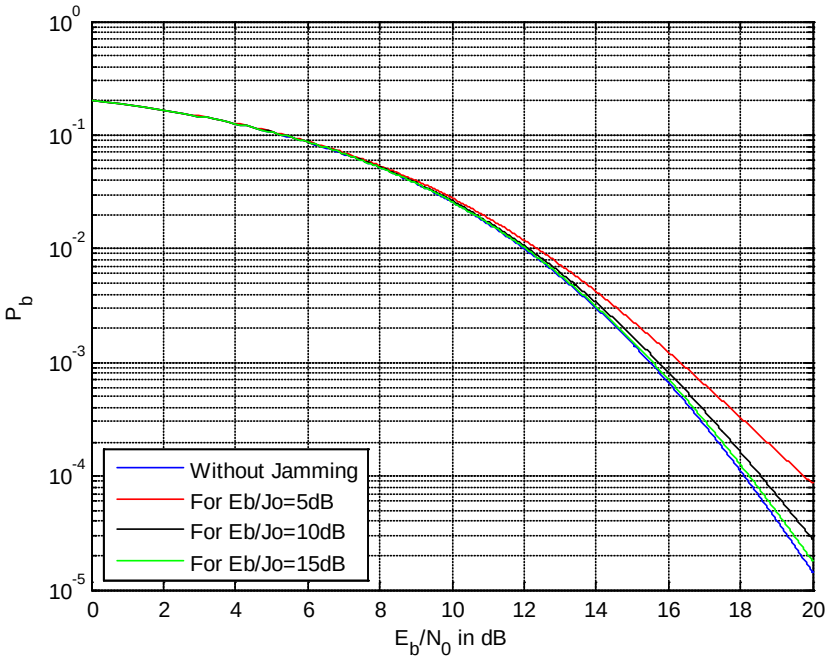

Figure 69. BER of DS 16QAM MIMO for broadband jamming and diversity *L*=6.

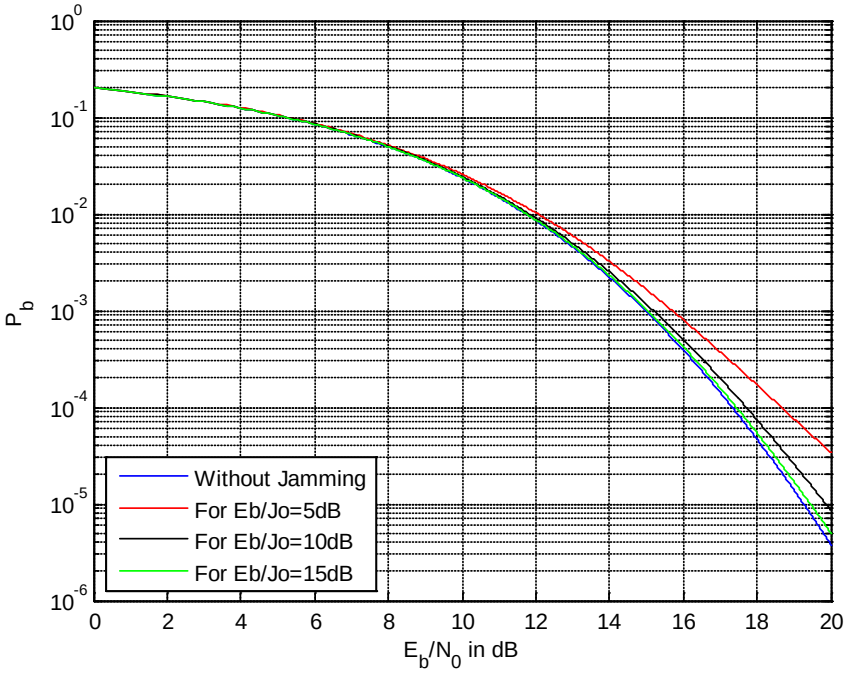

Figure 70. BER of DS 16QAM MIMO for broadband jamming and diversity *L*=8.

b. MIMO 3X2, 3X3 3X4

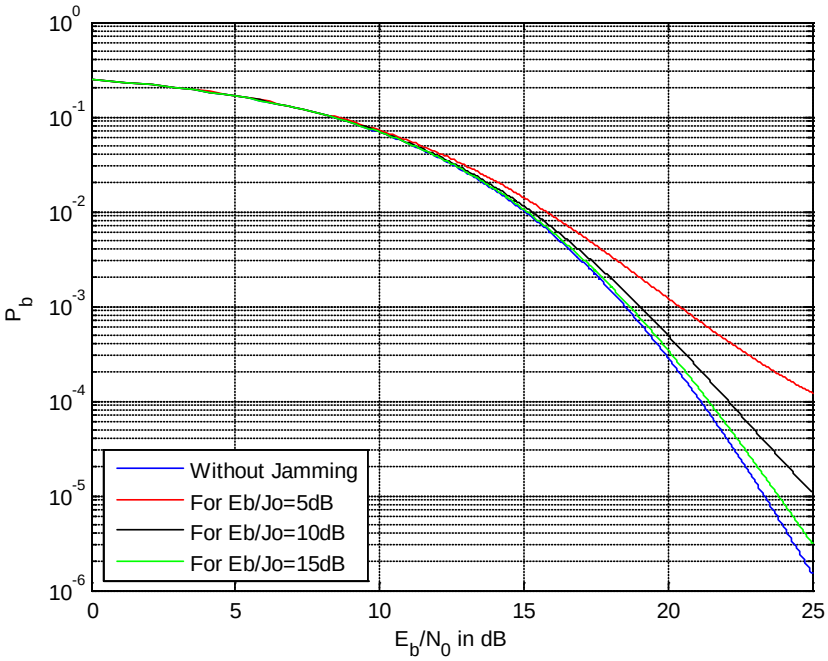

Figure 71. BER of DS 16QAM MIMO for broadband jamming and diversity *L*=6.

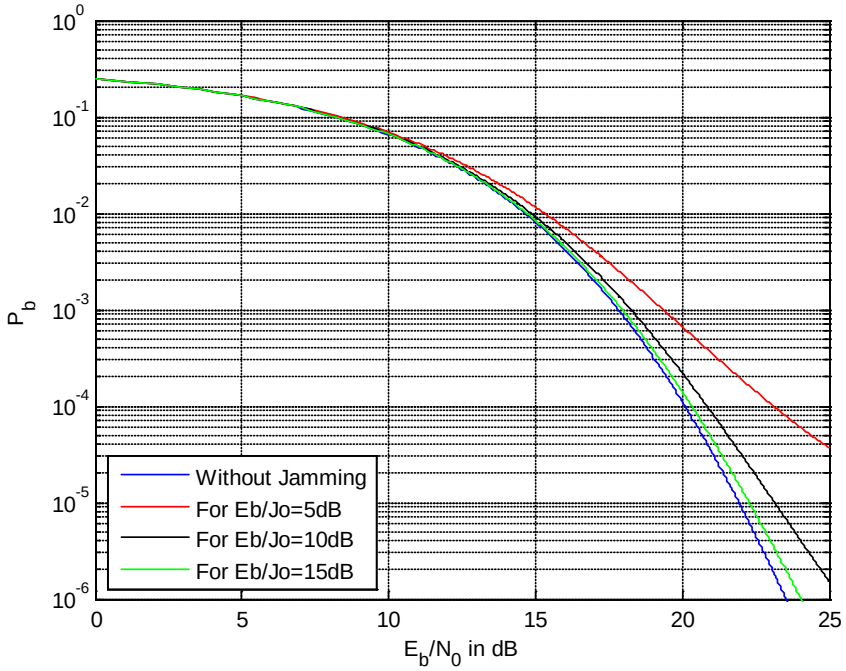

Figure 72. BER of DS 16QAM MIMO for broadband jamming and diversity *L*=9.

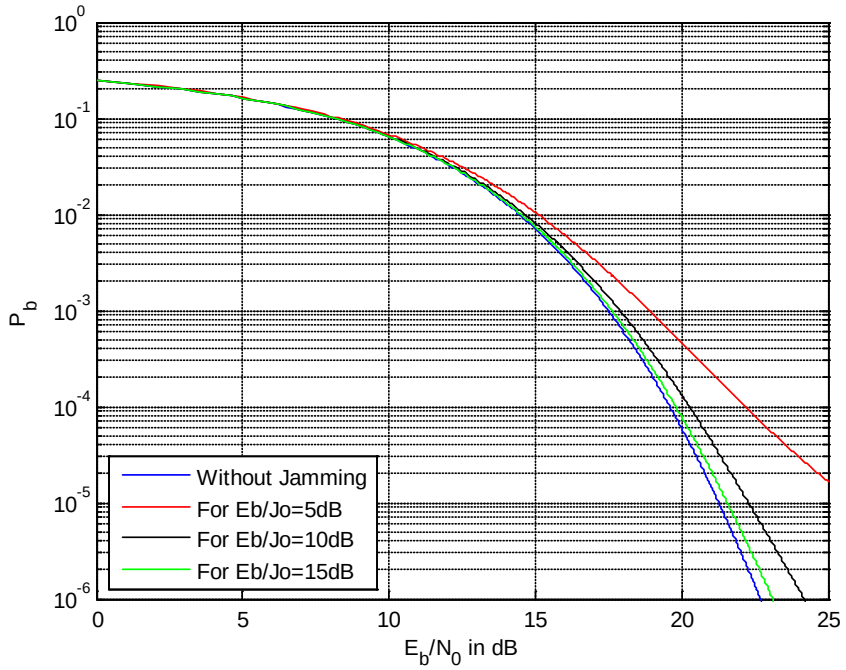

Figure 73. BER of DS 16QAM MIMO for broadband jamming and diversity *L*=12.

c. MIMO 4X2, 4X3 4X4

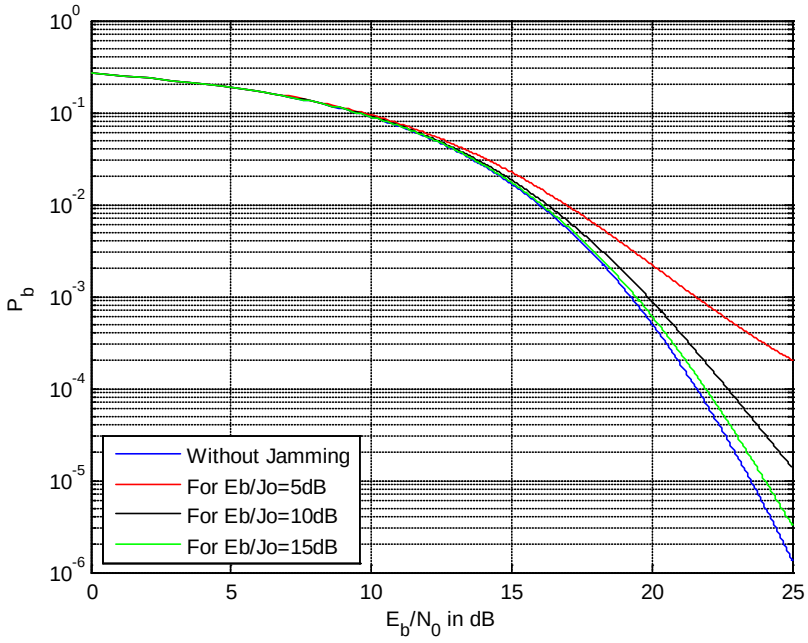

Figure 74. BER of DS 16QAM MIMO for broadband jamming and diversity *L*=8.

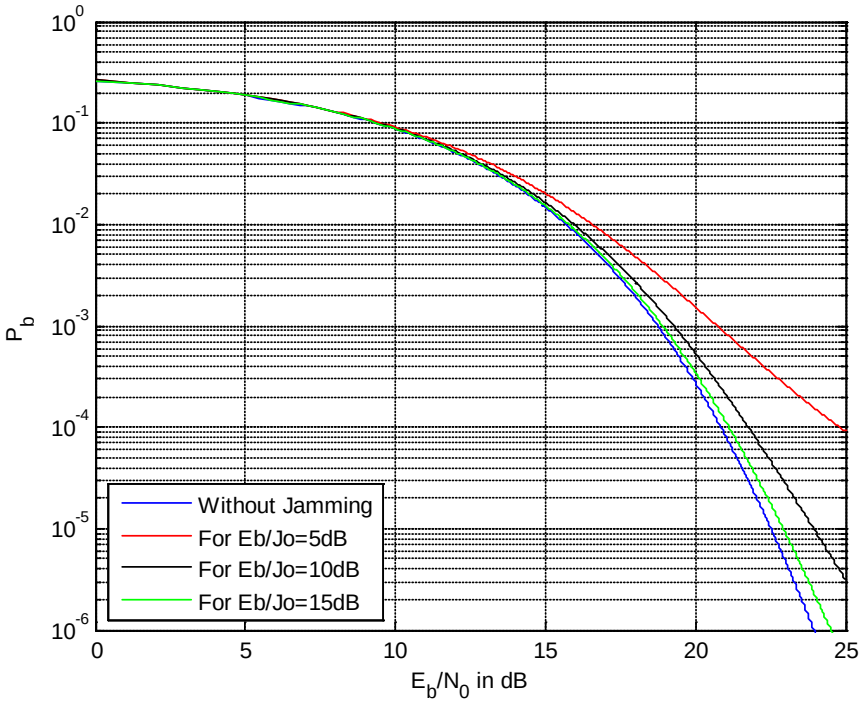

Figure 75. BER of DS 16QAM MIMO for broadband jamming and diversity *L*=12.

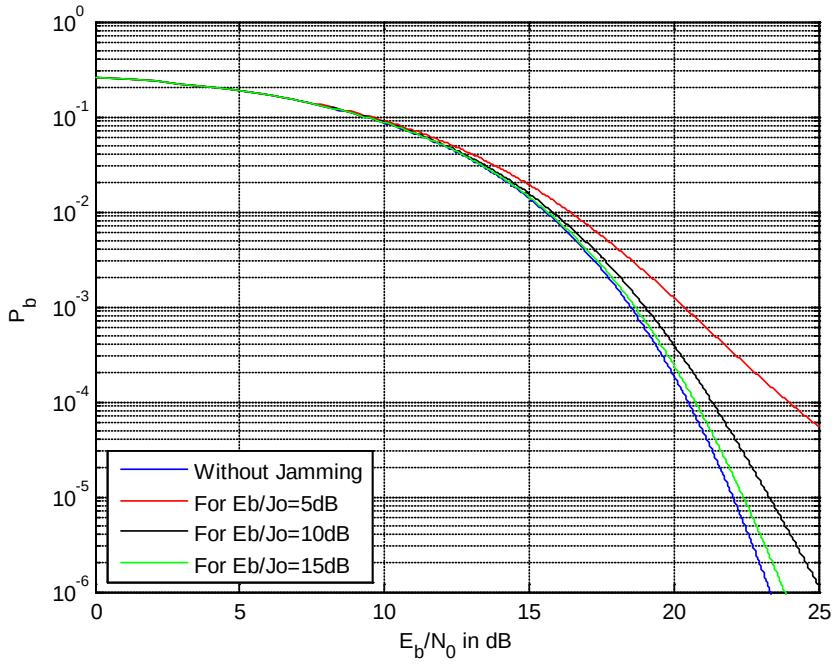

Figure 76. BER of DS 16QAM MIMO for broadband jamming and diversity *L*=16.

3. 64-QAM

a. MIMO 2X2, 2X3 2X4

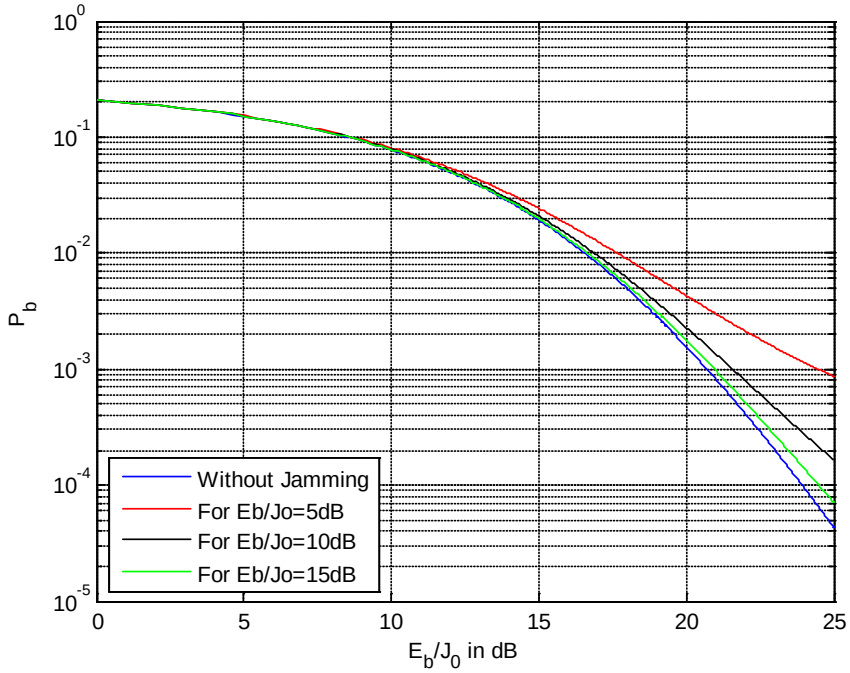

Figure 77. BER of DS 64QAM MIMO for broadband jamming and diversity *L*=4.

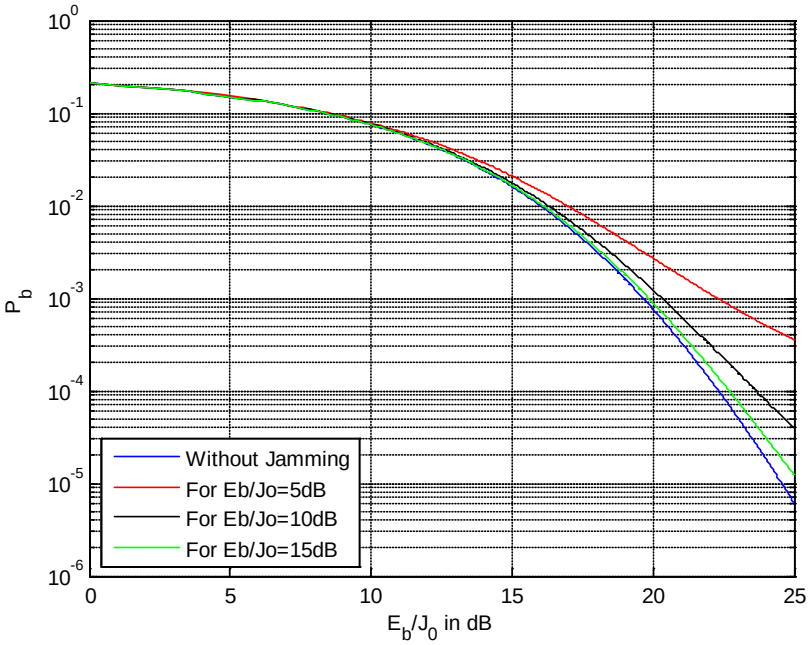

Figure 78. BER of DS 64QAM MIMO for broadband jamming and diversity *L*=6.

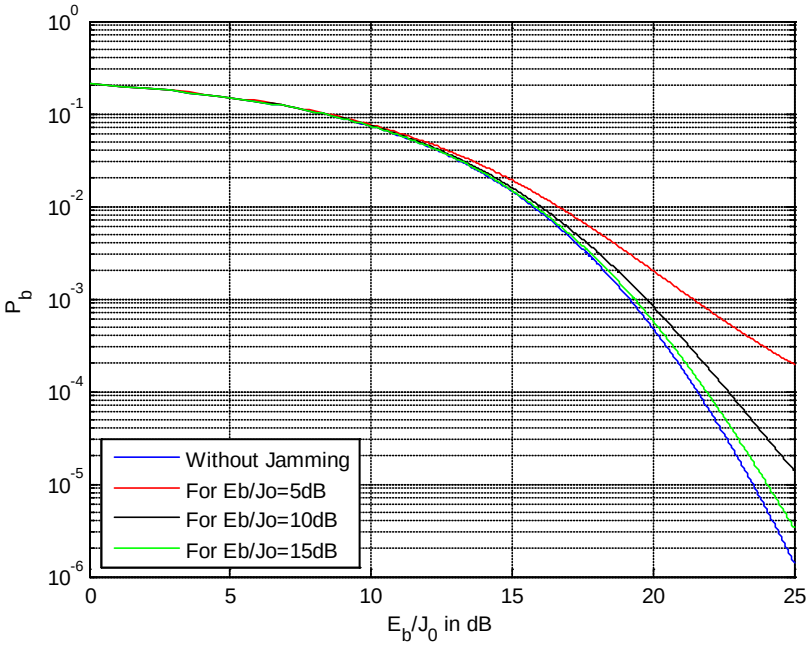

Figure 79. BER of DS 64QAM MIMO for broadband jamming and diversity *L*=8.

b. MIMO 3X2, 3X3 3X4

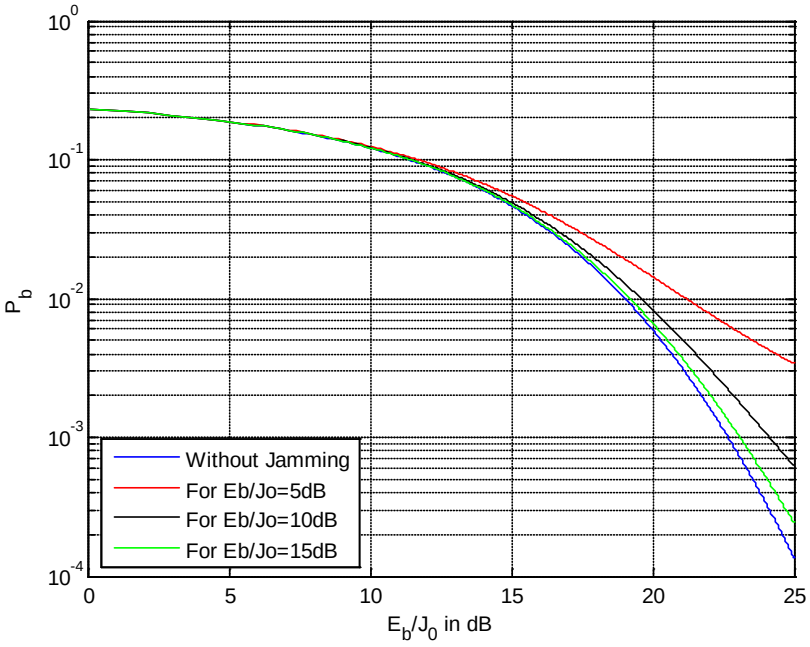

Figure 80. BER of DS 64QAM MIMO for broadband jamming and diversity *L*=6.

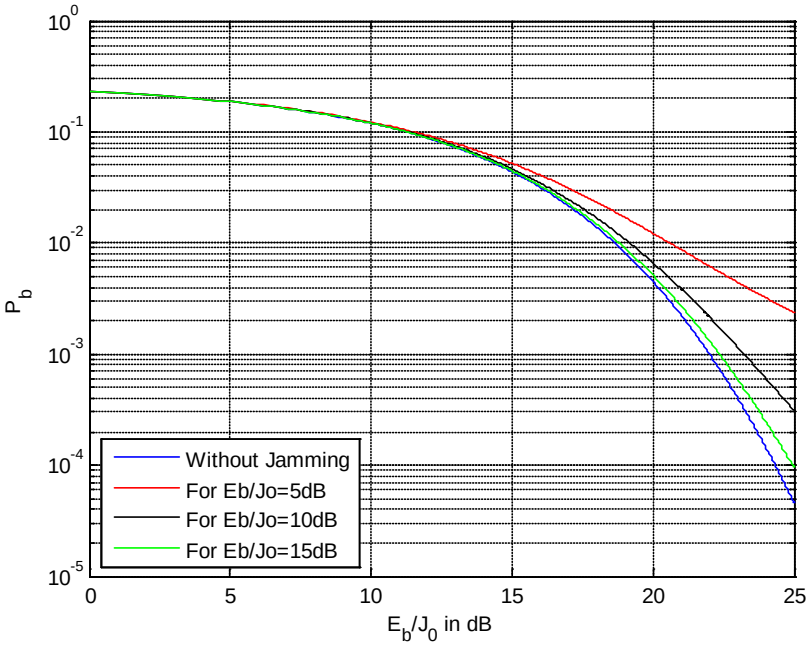

Figure 81. BER of DS 64QAM MIMO for broadband jamming and diversity *L*=9.

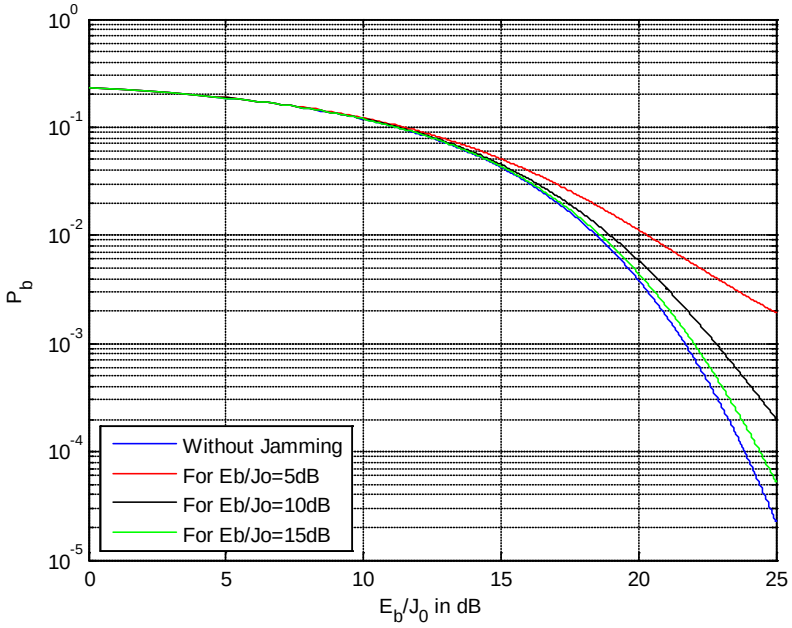

Figure 82. BER of DS 64QAM MIMO for broadband jamming and diversity *L*=12.

c. MIMO 4X2, 4X3 4X4

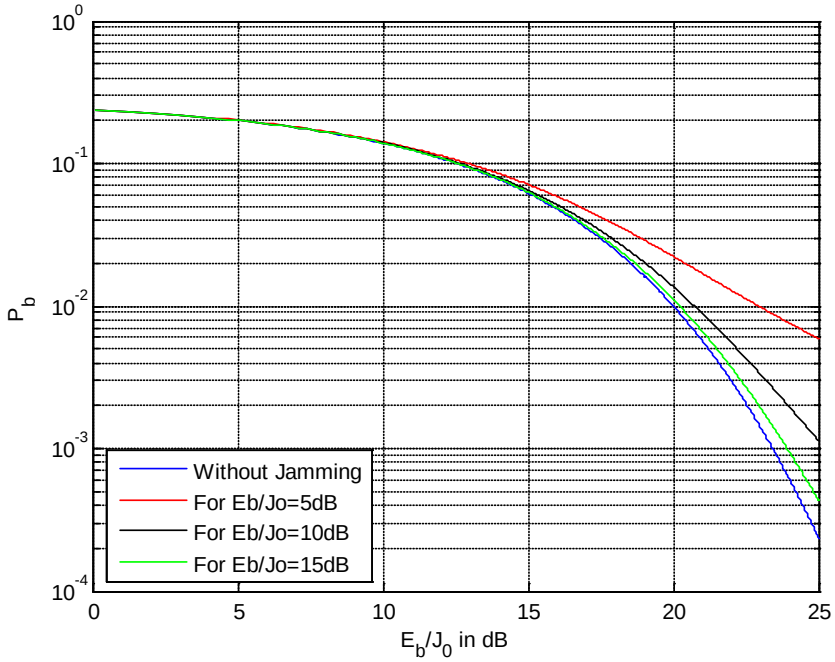

Figure 83. BER of DS 64QAM MIMO for broadband jamming and diversity *L*=8.

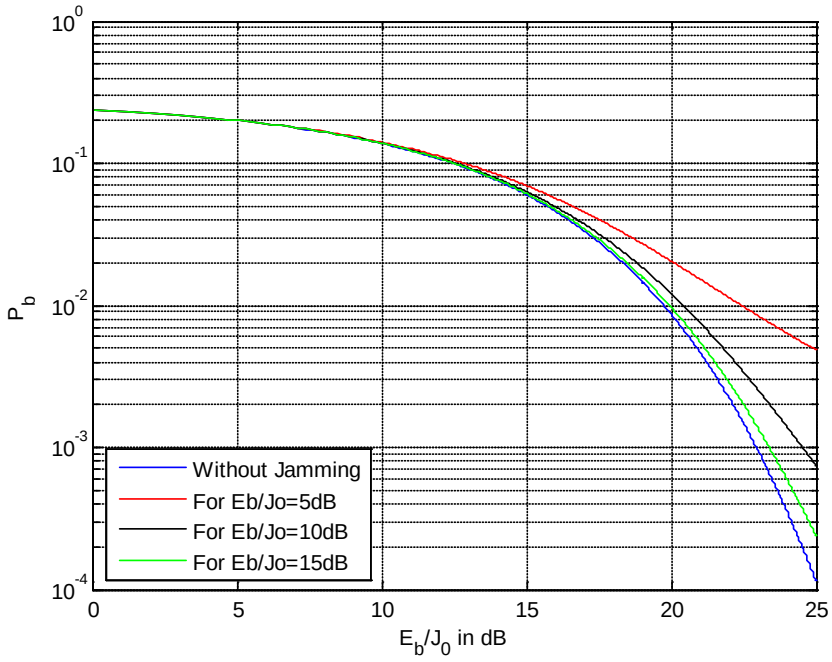

Figure 84. BER of DS 64QAM MIMO for broadband jamming and diversity *L*.=12

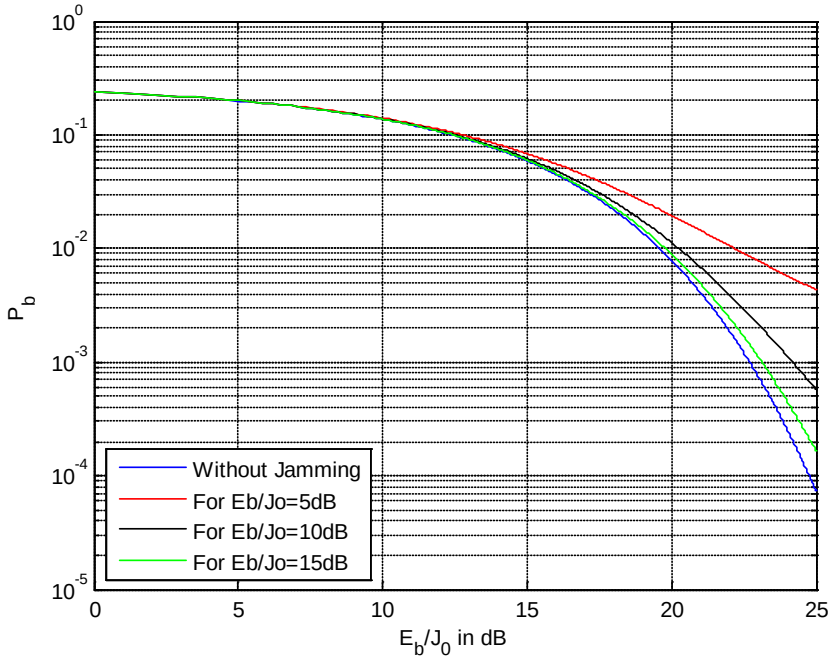

Figure 85. BER of DS 64QAM MIMO for broadband jamming and diversity *L*=16.

D. PULSED JAMMING

Based on the analysis of Section B of this chapter and the results and the performance analysis of *I-Q* modulation in the previous chapter, we use the same expressions for BER using the full diversity obtained by the equivalent MIMO configuration. We present the results in Figures 86-112. We use spread factor N=64.

1. QPSK

a. MIMO 2X2, 2X3 2X4

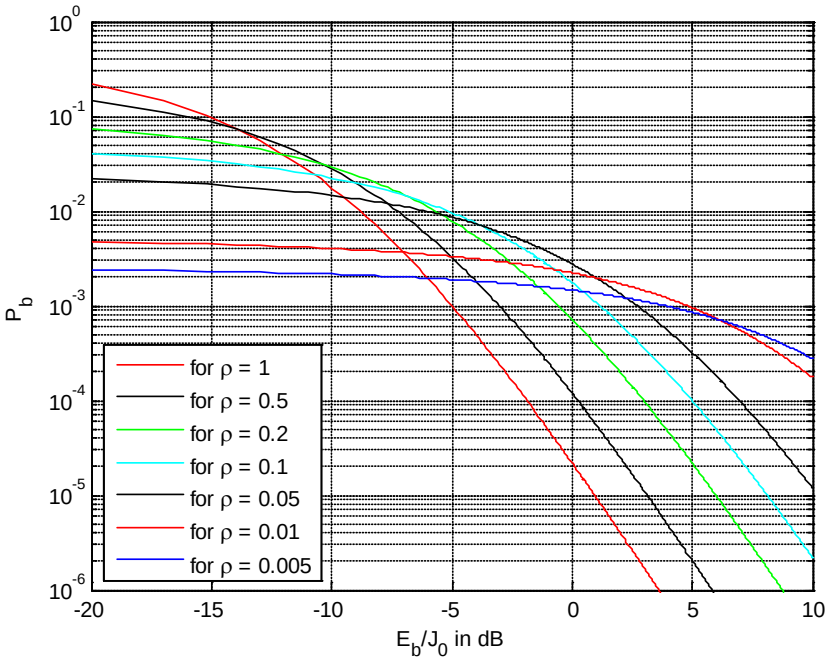

Figure 86. BER of DS QPSK MIMO for pulsed-noise jamming and diversity L=4.

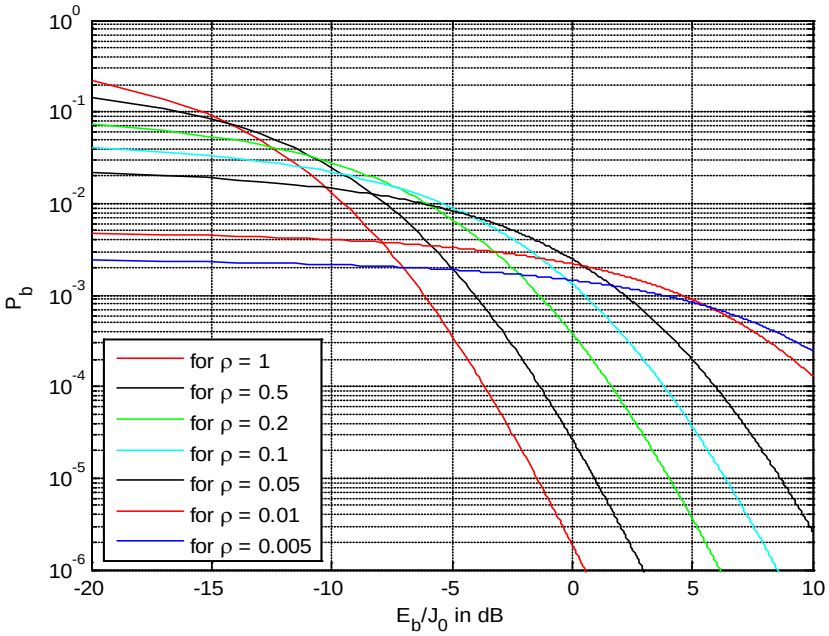

Figure 87. BER of DS QPSK MIMO for pulsed-noise jamming and diversity *L*=6.

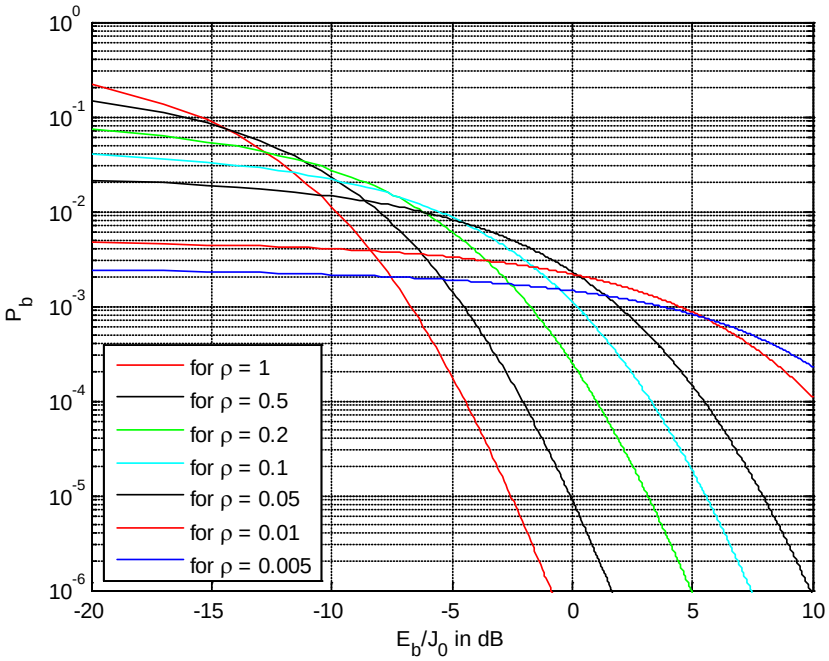

Figure 88. BER of DS QPSK MIMO for pulsed-noise jamming and diversity *L*=8.

b. MIMO 3X2, 3X3 3X4

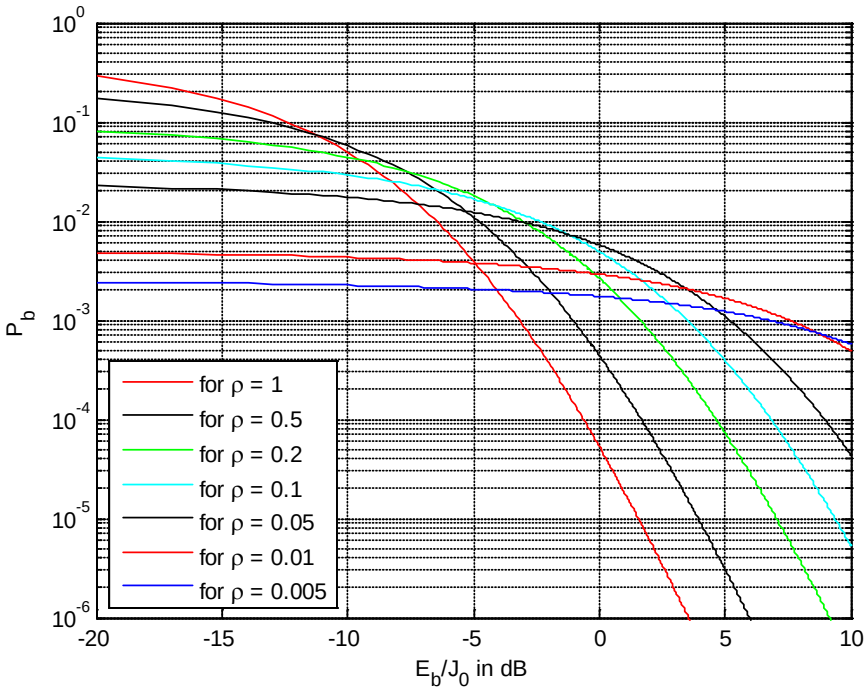

Figure 89. BER of DS QPSK MIMO for pulsed-noise jamming and diversity *L*=6.

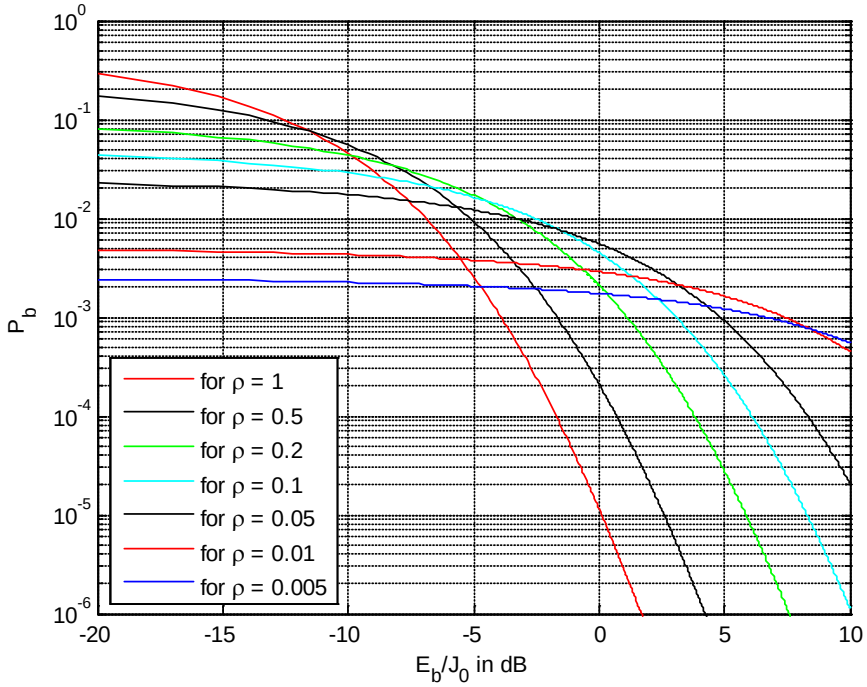

Figure 90. BER of DS QPSK MIMO for pulsed-noise jamming and diversity *L*=9.

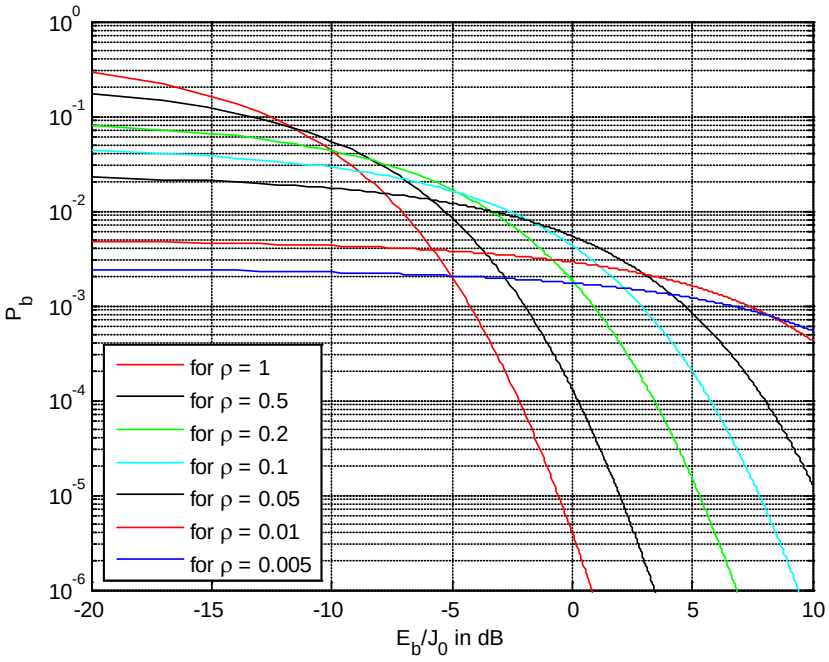

Figure 91. BER of DS QPSK MIMO for pulsed-noise jamming and diversity *L*=12.

c. MIMO 4X2, 4X3 4X4

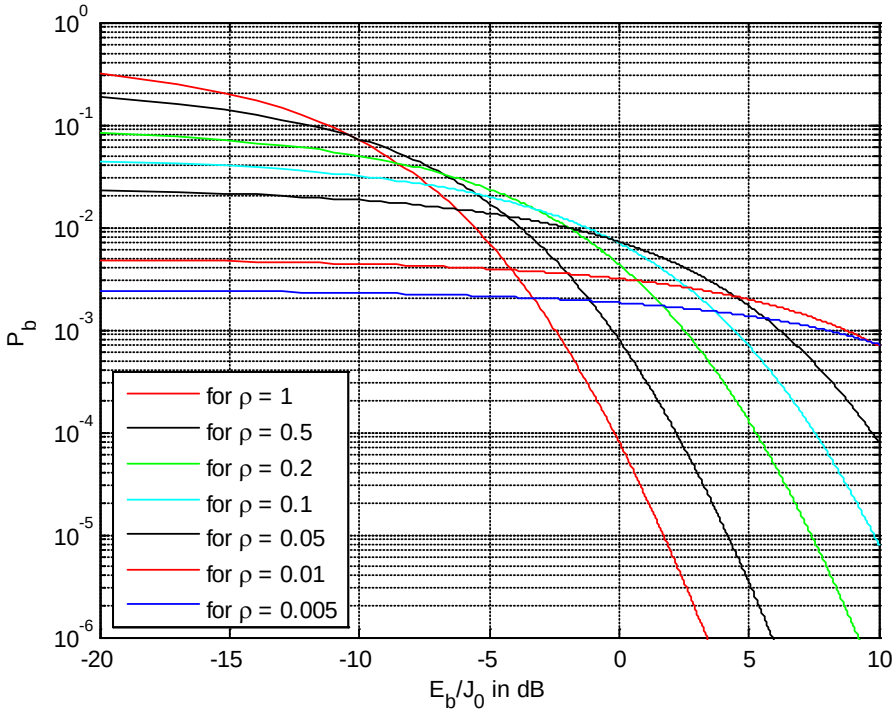

Figure 92. BER of DS QPSK MIMO for pulsed-noise jamming and diversity *L*=8.

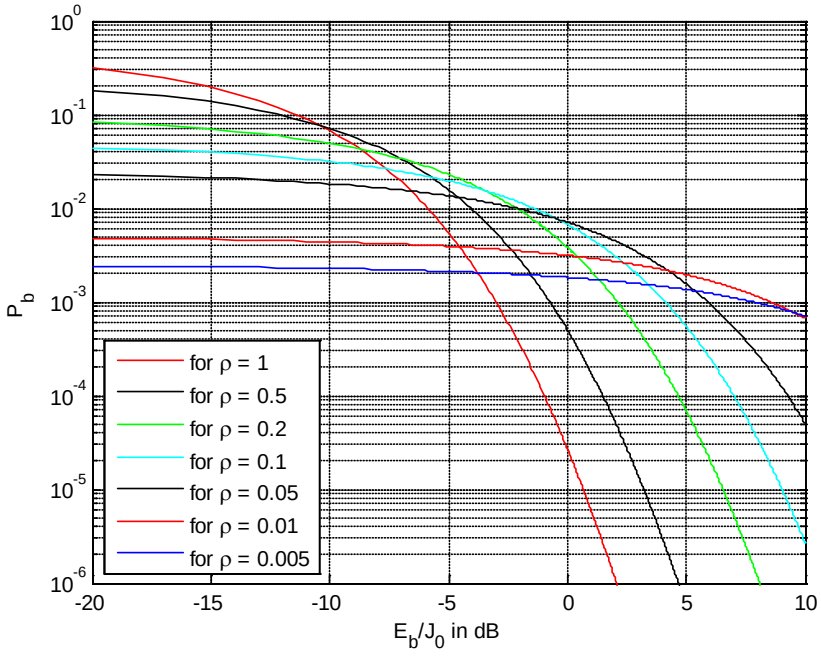

Figure 93. BER of DS QPSK MIMO for pulsed-noise jamming and diversity *L*=12.

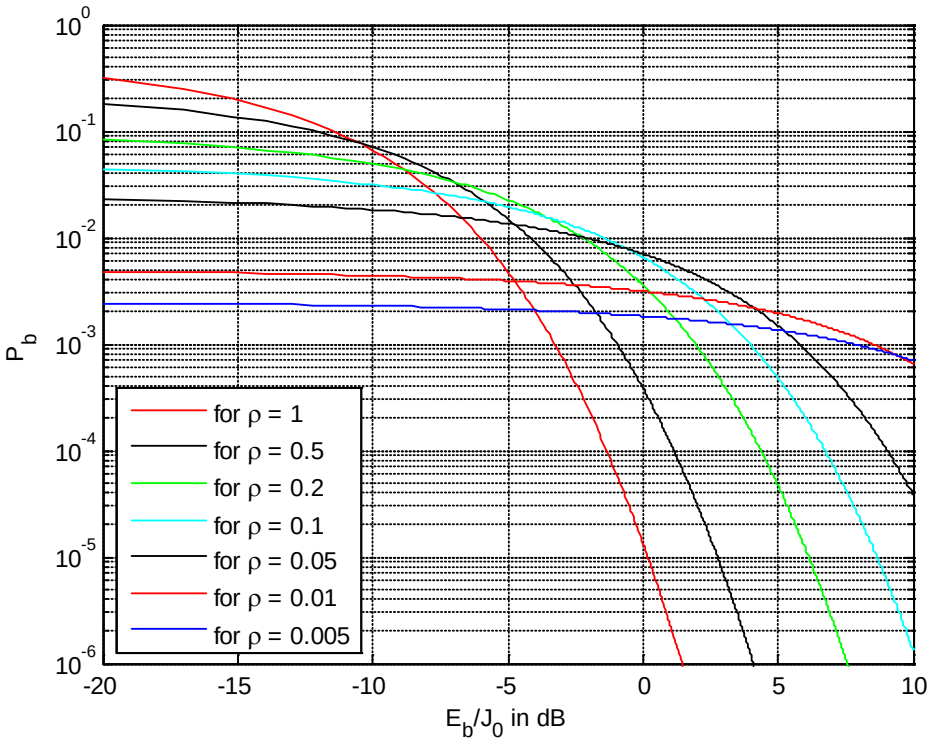

Figure 94. BER of DS QPSK MIMO for pulsed-noise jamming and diversity *L*=16.

2. 16-QAM

a. MIMO 2X2, 2X3 2X4

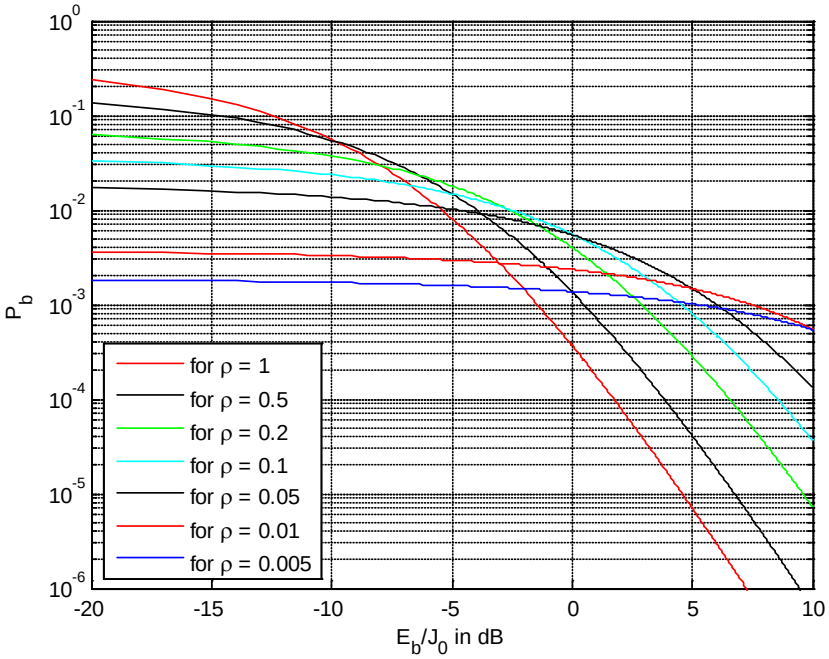

Figure 95. BER of DS 16QAM MIMO for pulsed-noise jamming and diversity *L*=4.

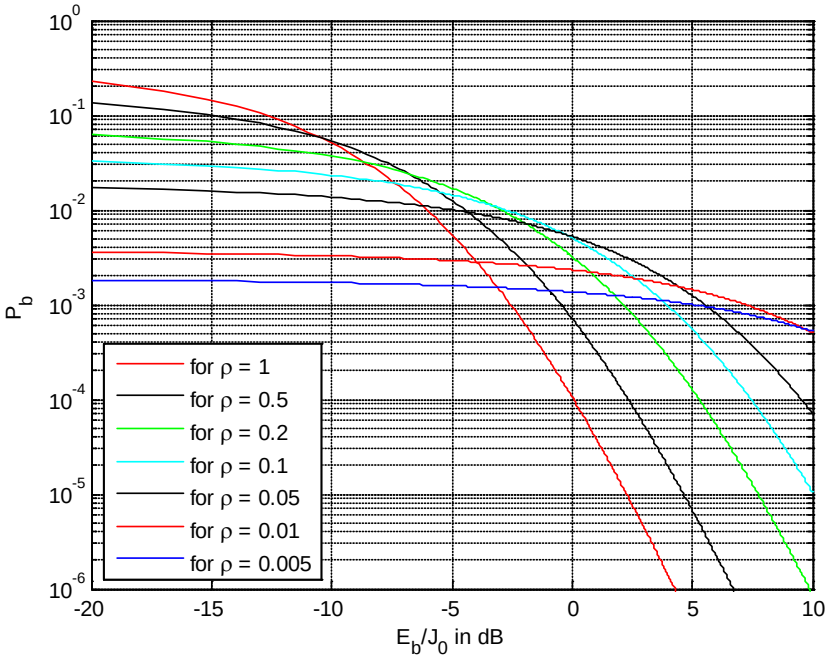

Figure 96. BER of DS 16QAM MIMO for pulsed-noise jamming and diversity *L*=6.

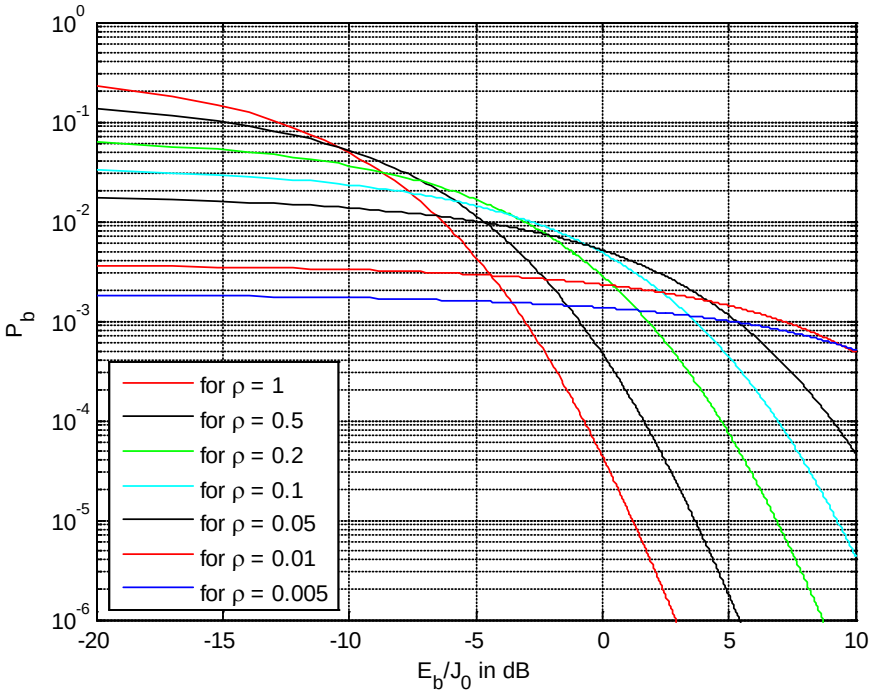

Figure 97. BER of DS 16QAM MIMO for pulsed-noise jamming and diversity *L*=8.

b. MIMO 3X2, 3X3 3X4

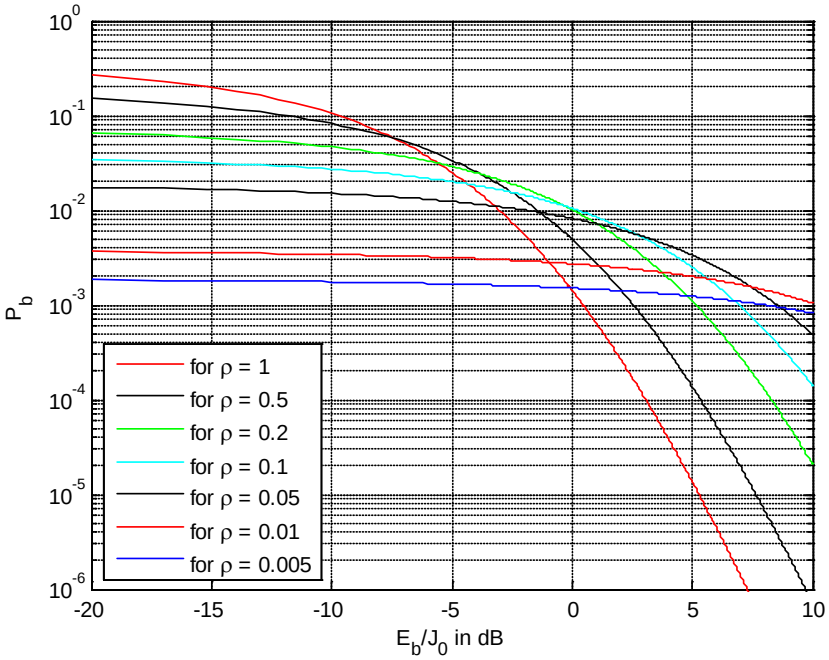

Figure 98. BER of DS 16QAM MIMO for pulsed-noise jamming and diversity *L*=6.

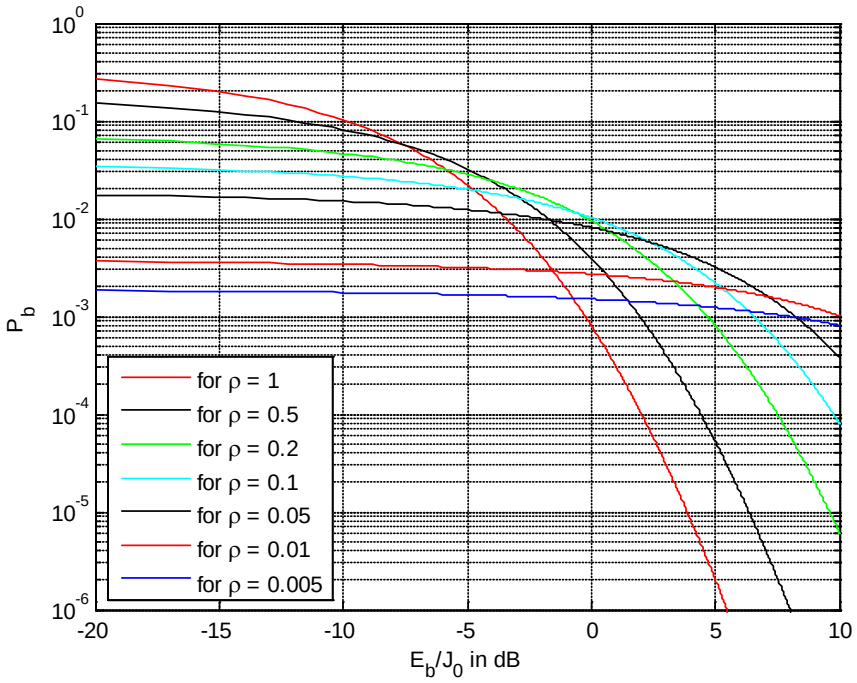

Figure 99. BER of DS 16QAM MIMO for pulsed-noise jamming and diversity *L*=9.

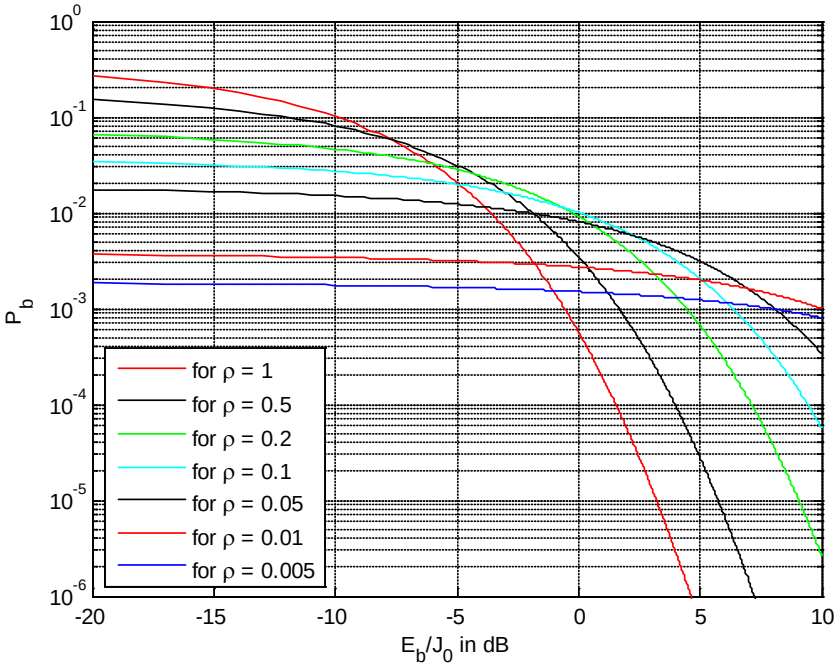

Figure 100. BER of DS 16QAM MIMO for pulsed-noise jamming and diversity *L*=12.

c. MIMO 4X2, 4X3 4X4

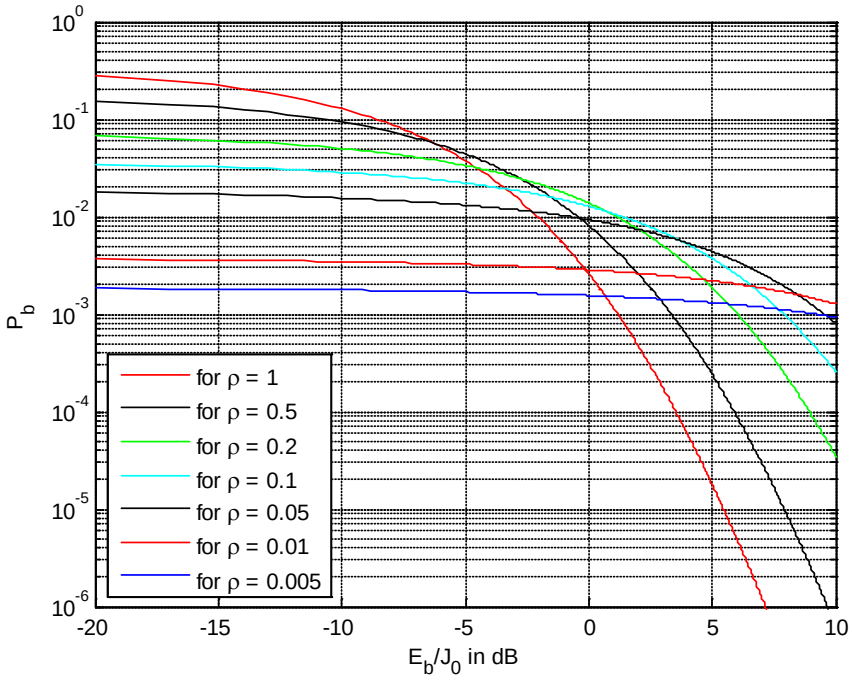

Figure 101. BER of DS 16QAM MIMO for pulsed-noise jamming and diversity *L*=8.

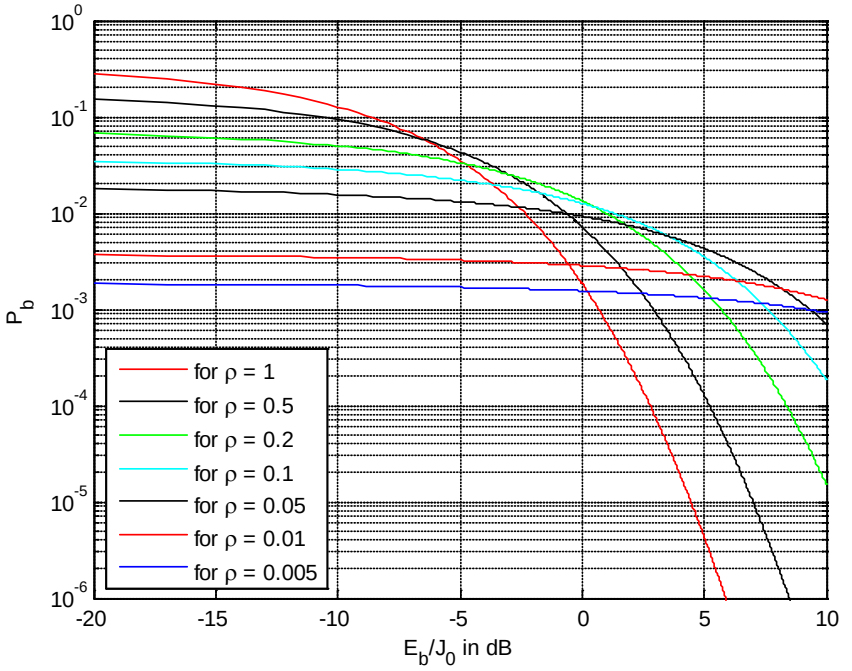

Figure 102. BER of DS 16QAM MIMO for pulsed-noise jamming and diversity *L*=12.

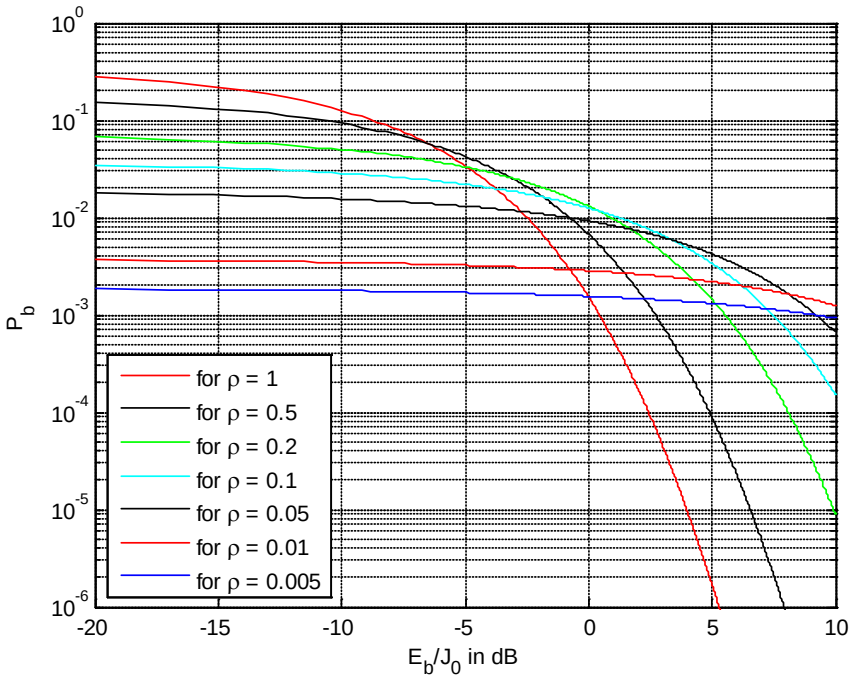

Figure 103. BER of DS 16QAM MIMO for pulsed-noise jamming and diversity *L*=16.

3. 64-QAM

a. MIMO 2X2, 2X3 2X4

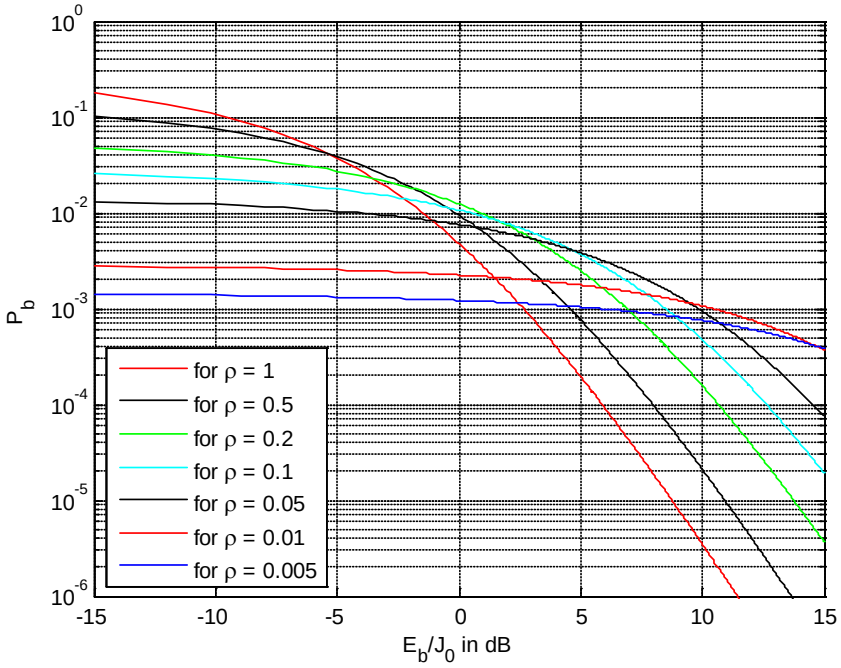

Figure 104. BER of DS 64QAM MIMO for pulsed-noise jamming and diversity *L*=4.

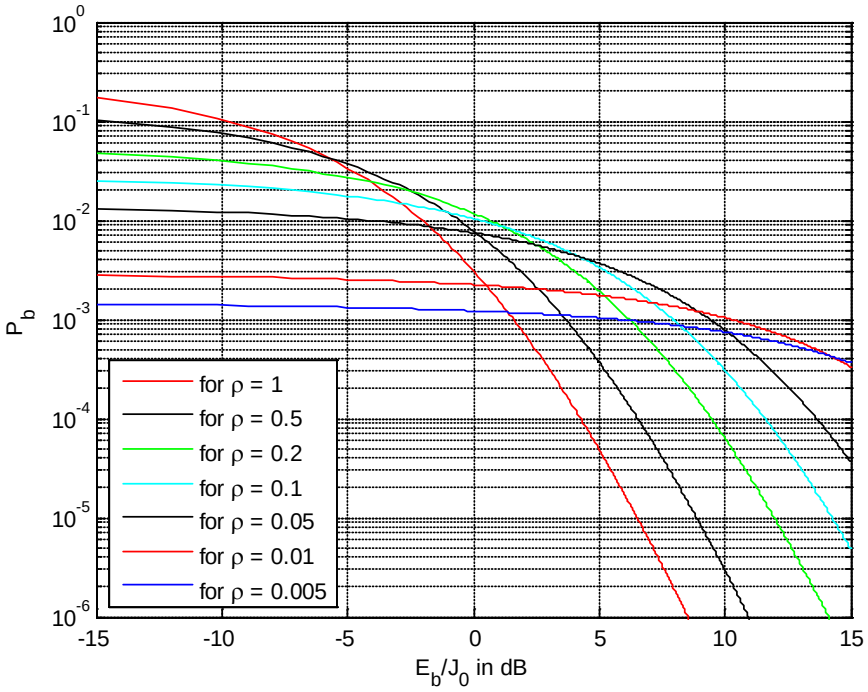

Figure 105. BER of DS 64QAM MIMO for pulsed-noise jamming and diversity *L*=6.

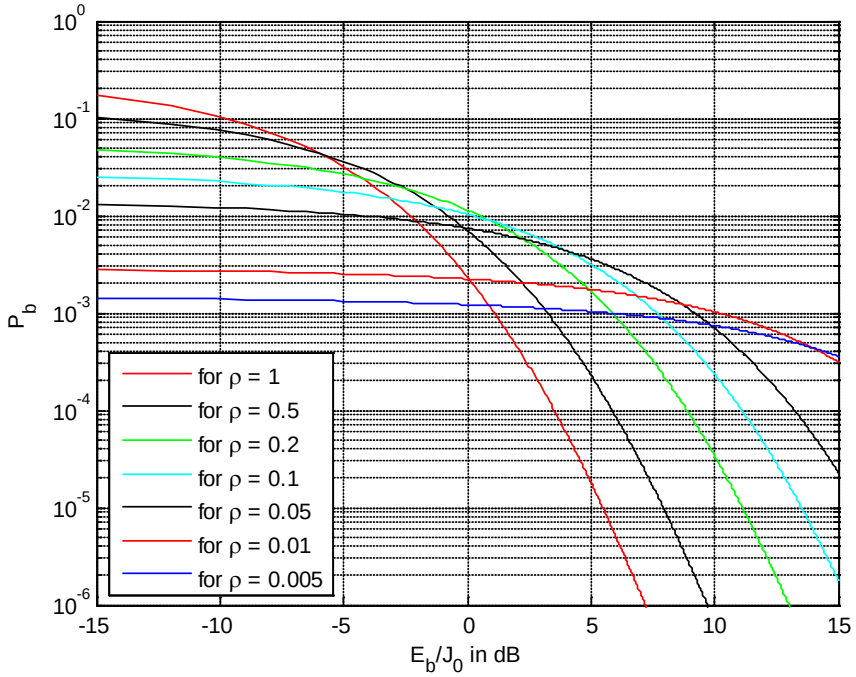

Figure 106. BER of DS 64QAM MIMO for pulsed-noise jamming and diversity *L*=8.

b. MIMO 3X2, 3X3 3X4

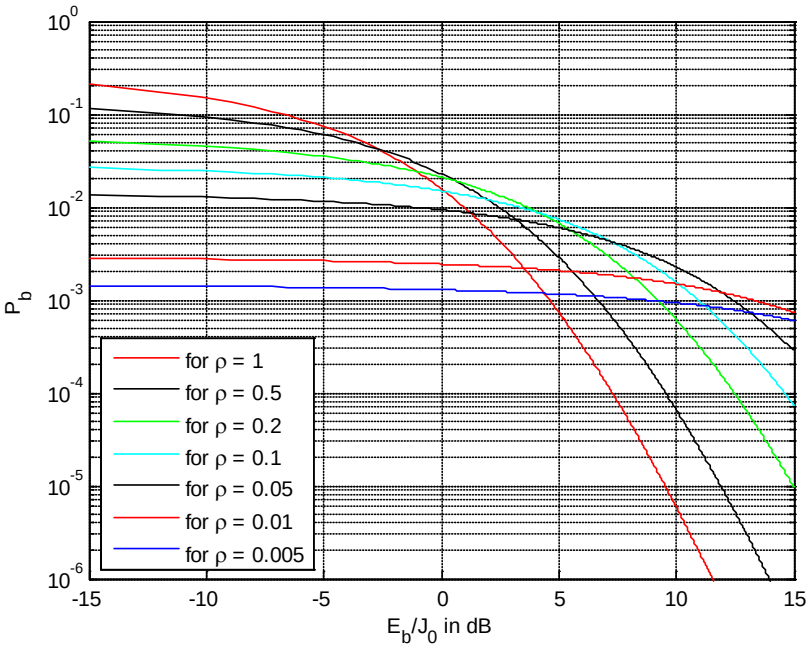

Figure 107. BER of DS 64QAM MIMO for pulsed-noise jamming and diversity *L*=6.

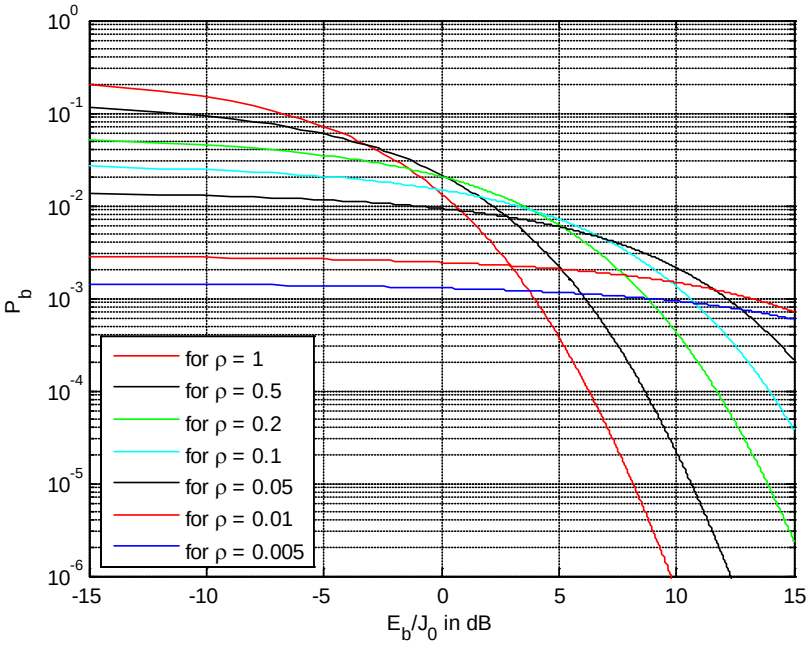

Figure 108. BER of DS 64QAM MIMO for pulsed-noise jamming and diversity *L*=9.

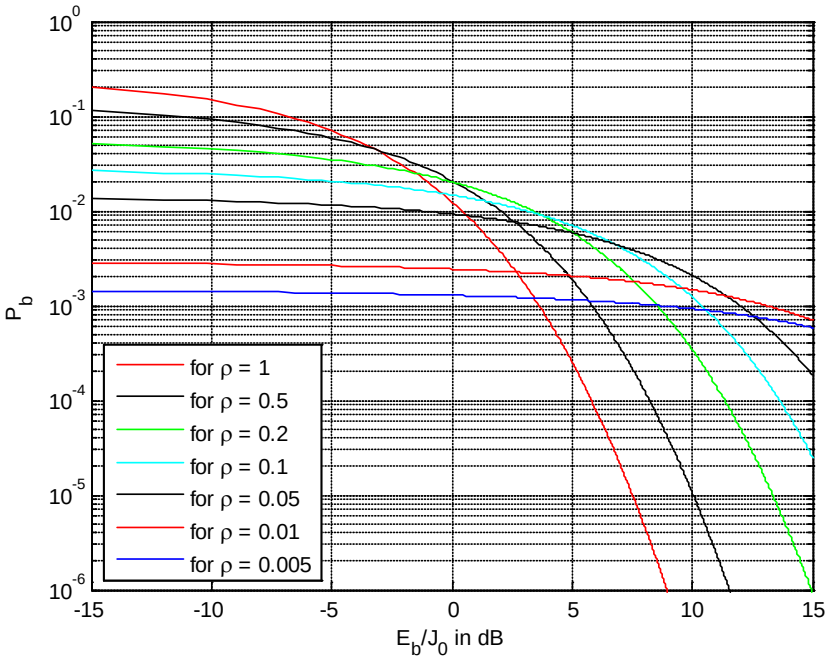

Figure 109. BER of DS 64QAM MIMO for pulsed-noise jamming and diversity *L*=12.

c. MIMO 4X2, 4X3 4X4

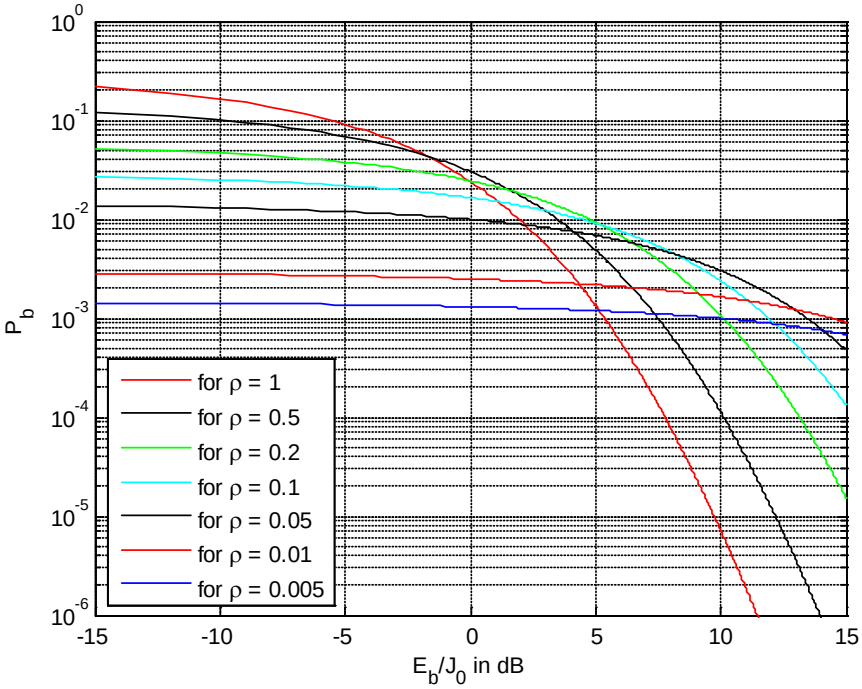

Figure 110. BER of DS 64QAM MIMO for pulsed-noise jamming and diversity *L*=8.

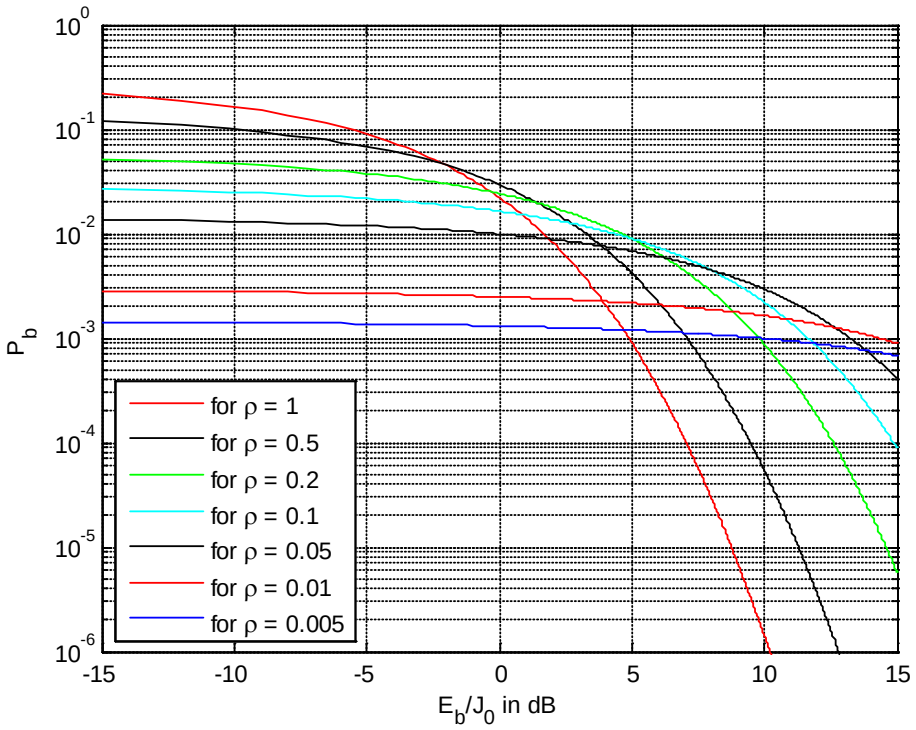

Figure 111. BER of DS 64QAM MIMO for pulsed-noise jamming and diversity *L*=12.

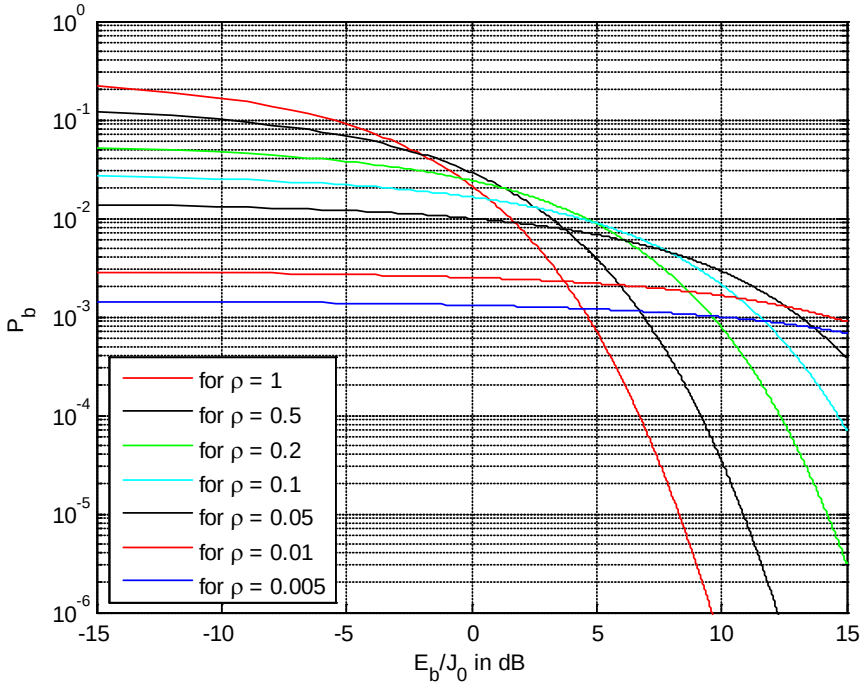

Figure 112. BER of DS 64QAM MIMO for pulsed-noise jamming and diversity *L*=16.

E. TONE JAMMING

Based on the analysis of Section B of this chapter and the results and the performance analysis of *I-Q* modulation in the previous chapter, we use the same expressions for the BER using the full diversity obtained by the equivalent MIMO configuration. We present the results in Figures 113-139. We use spread factor N=64.

1. QPSK

a. MIMO 2X2, 2X3 2X4

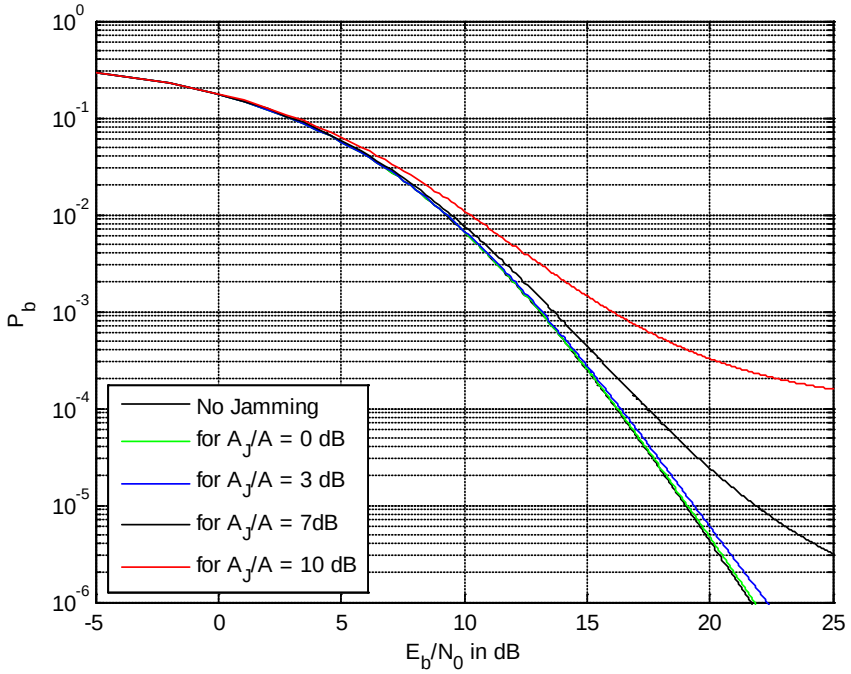

Figure 113. BER of DS QPSK MIMO for tone jamming and diversity L=4.

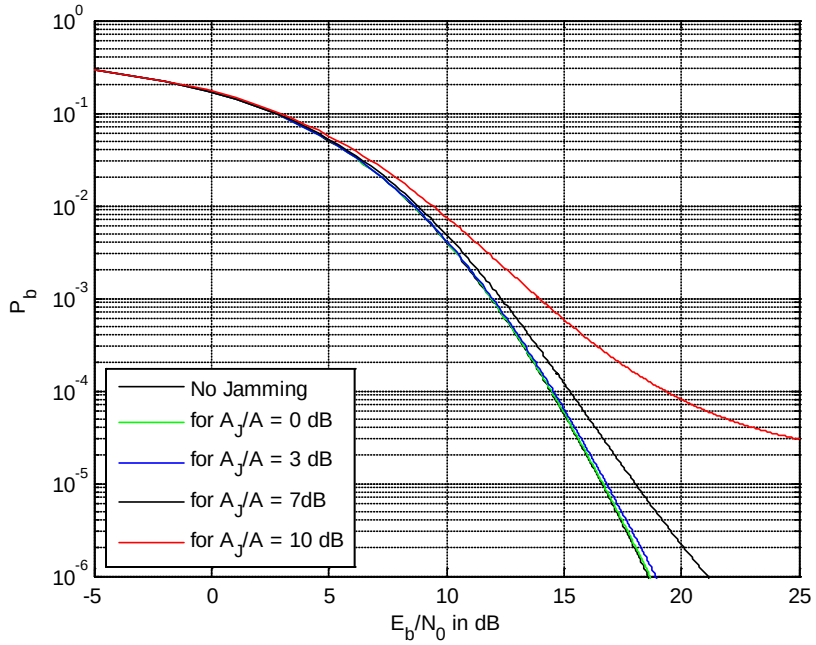

Figure 114. BER of DS QPSK MIMO for tone jamming and diversity *L*=6.

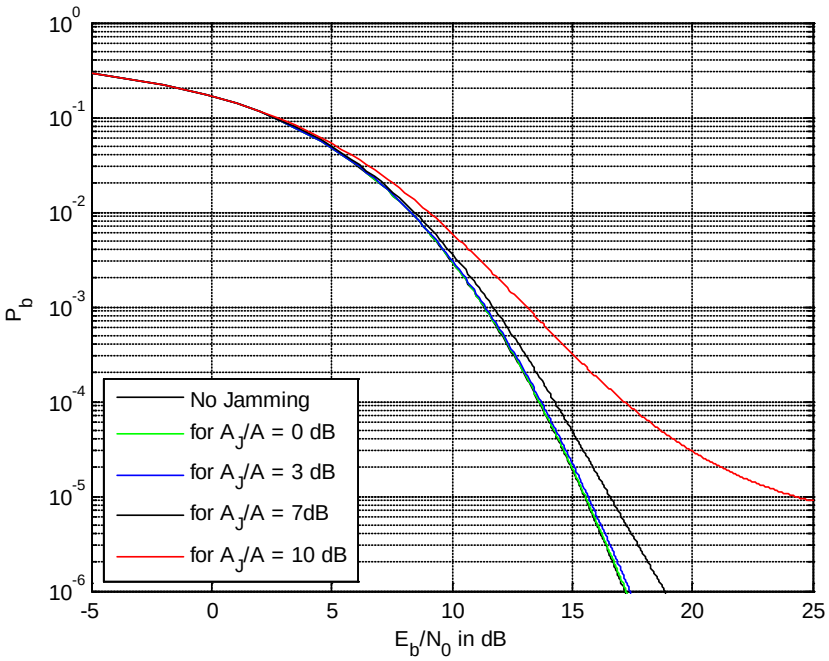

Figure 115. BER of DS QPSK MIMO for tone jamming and diversity *L*=8.

b. MIMO 3X2, 3X3 3X4

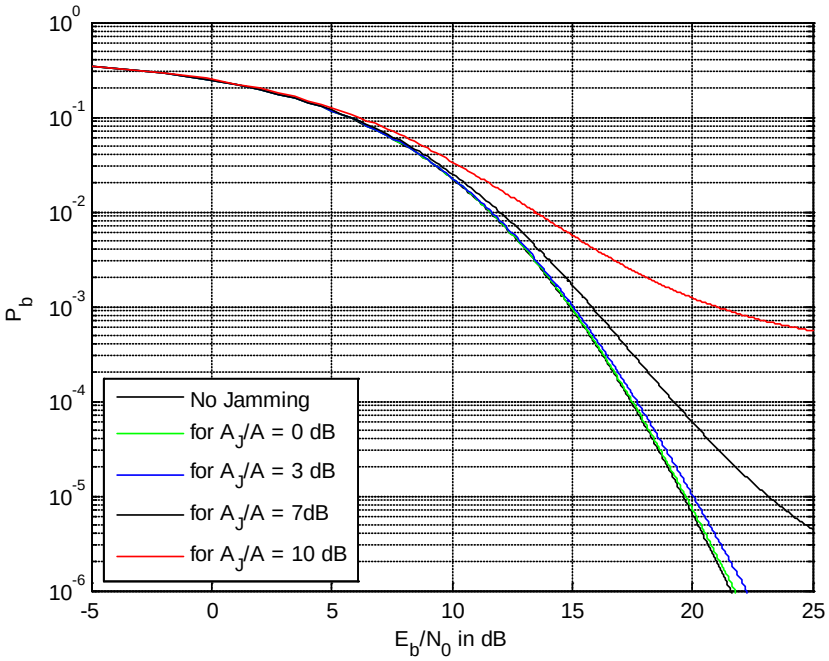

Figure 116. BER of DS QPSK MIMO for tone jamming and diversity *L*=6.

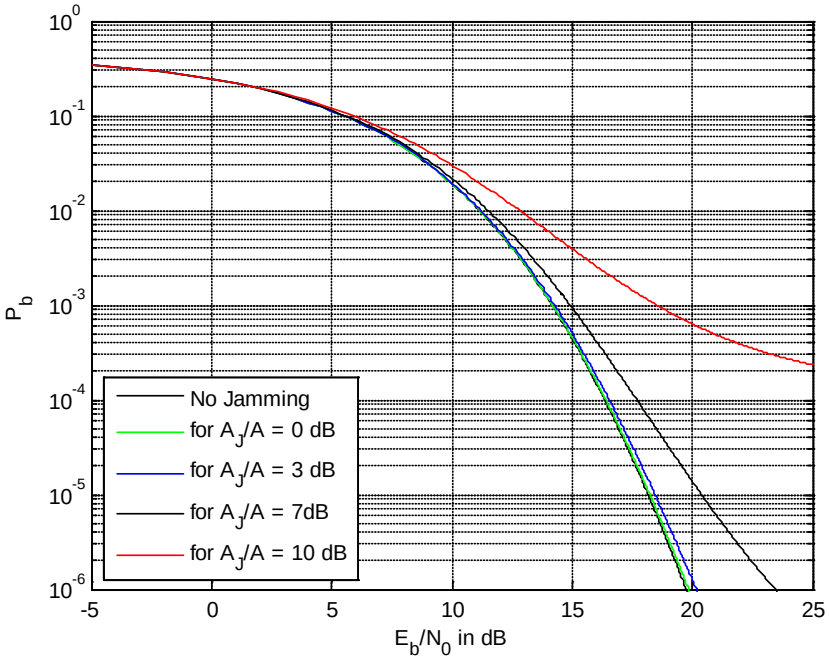

Figure 117. BER of DS QPSK MIMO for tone jamming and diversity *L*=9.

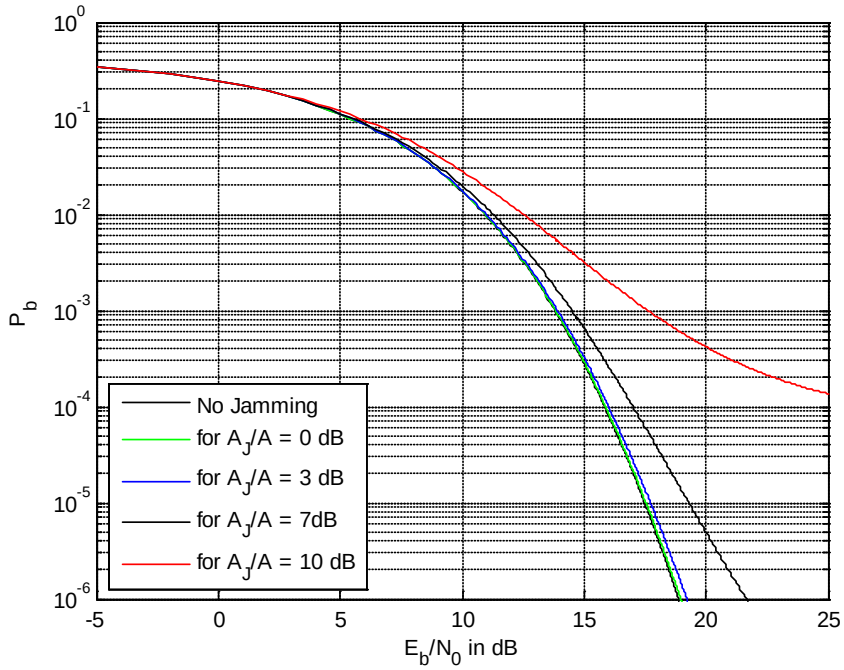

Figure 118. BER of DS QPSK MIMO for tone jamming and diversity *L*=12.

c. MIMO 4X2, 4X3 4X4

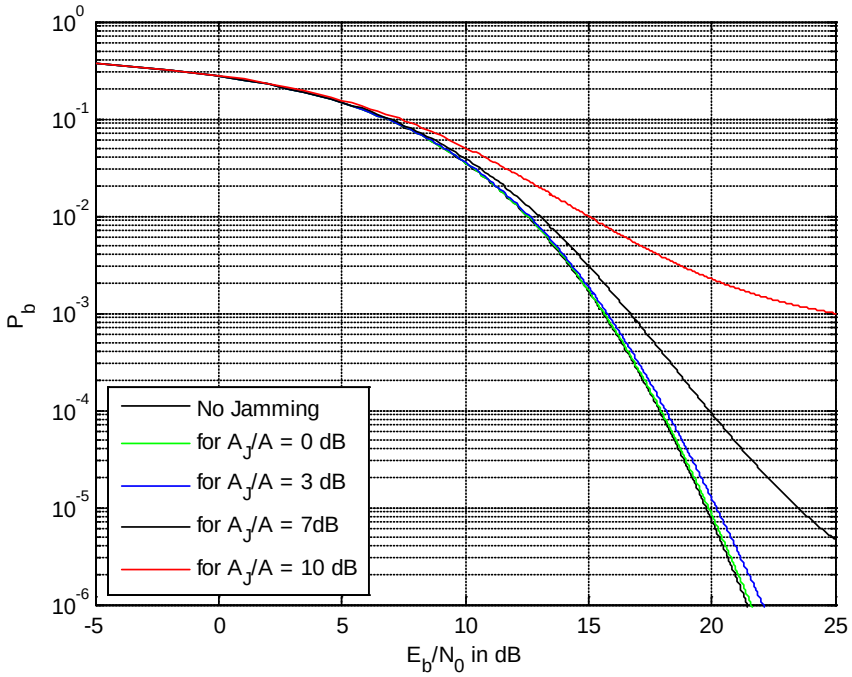

Figure 119. BER of DS QPSK MIMO for tone jamming and total diversity *L*=8.

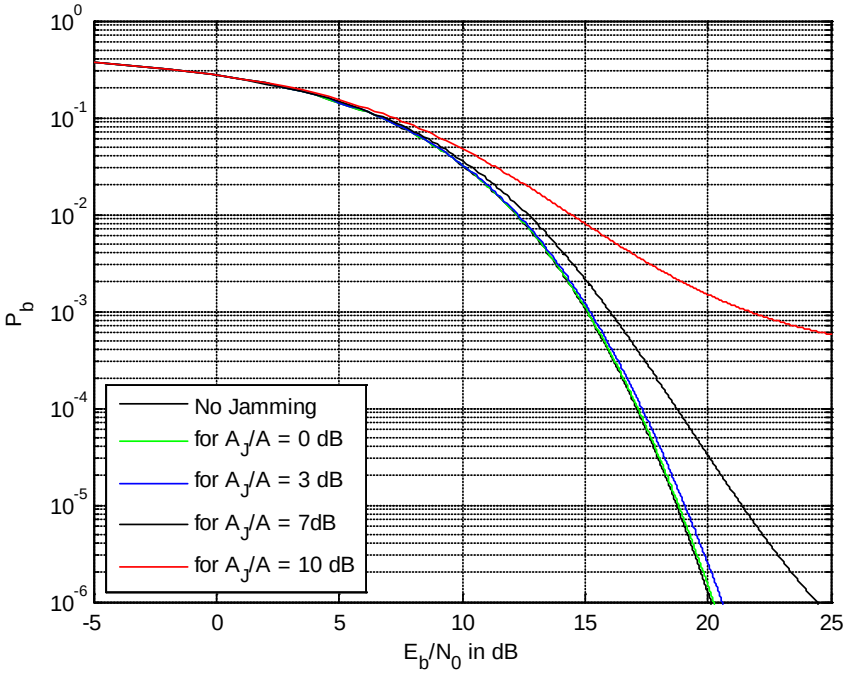

Figure 120. BER of DS QPSK MIMO for tone jamming and diversity *L*=12.

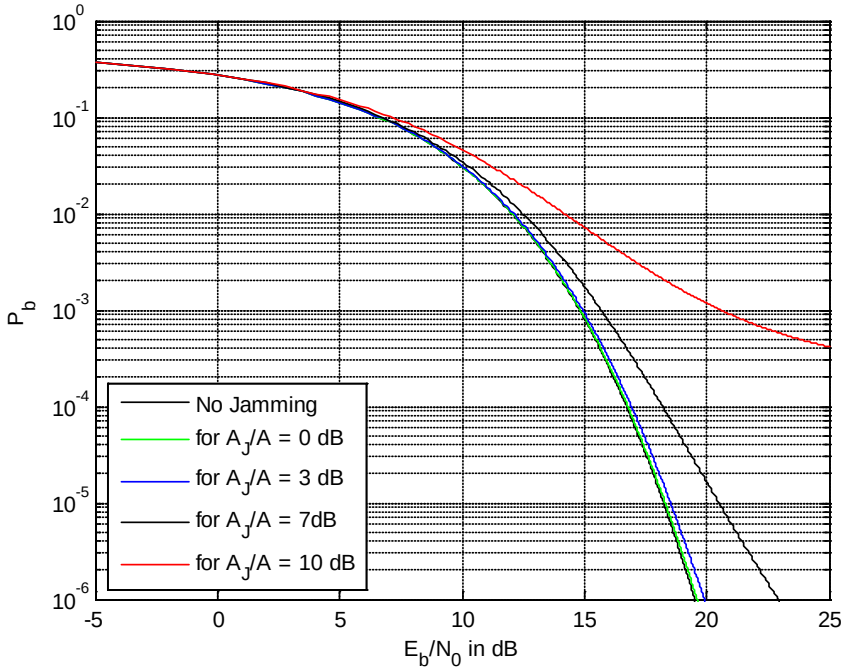

Figure 121. BER of DS QPSK MIMO for tone jamming and diversity *L*=16.

2. 16-QAM

a. MIMO 2X2, 2X3 2X4

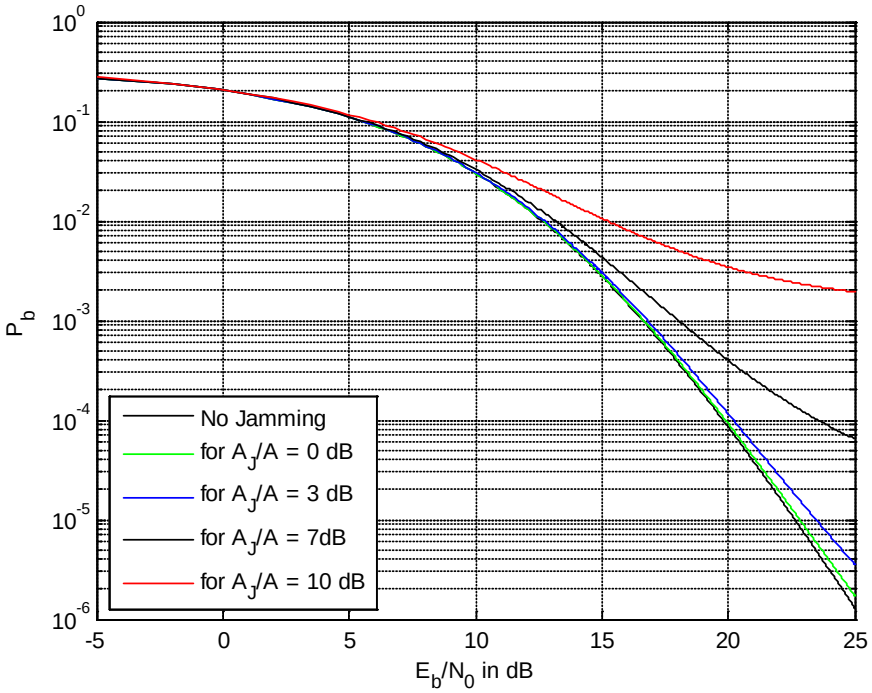

Figure 122. BER of DS 16QAM MIMO for tone jamming and diversity *L*=4.

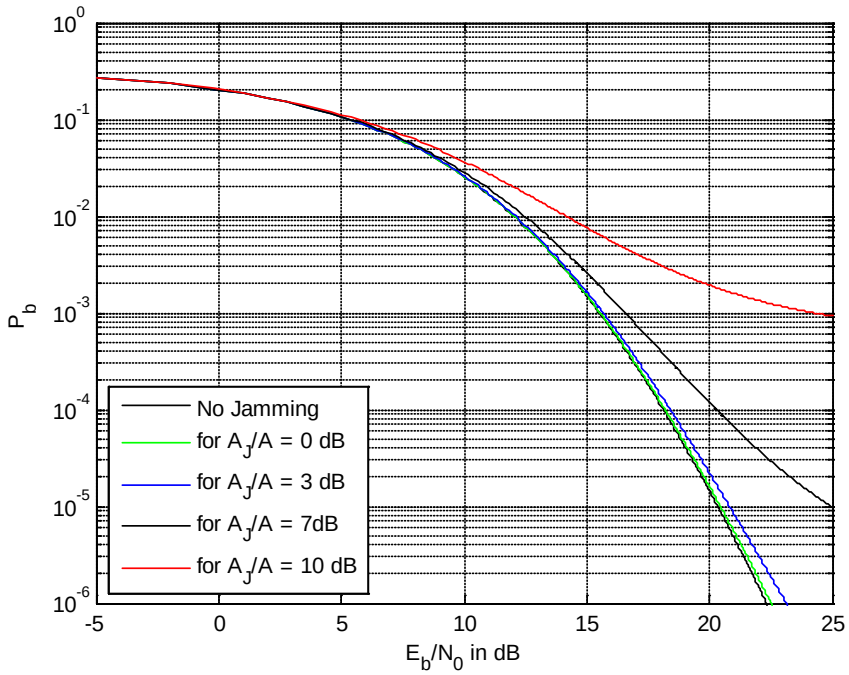

Figure 123. BER of DS 16QAM MIMO for tone jamming and diversity *L*=6.

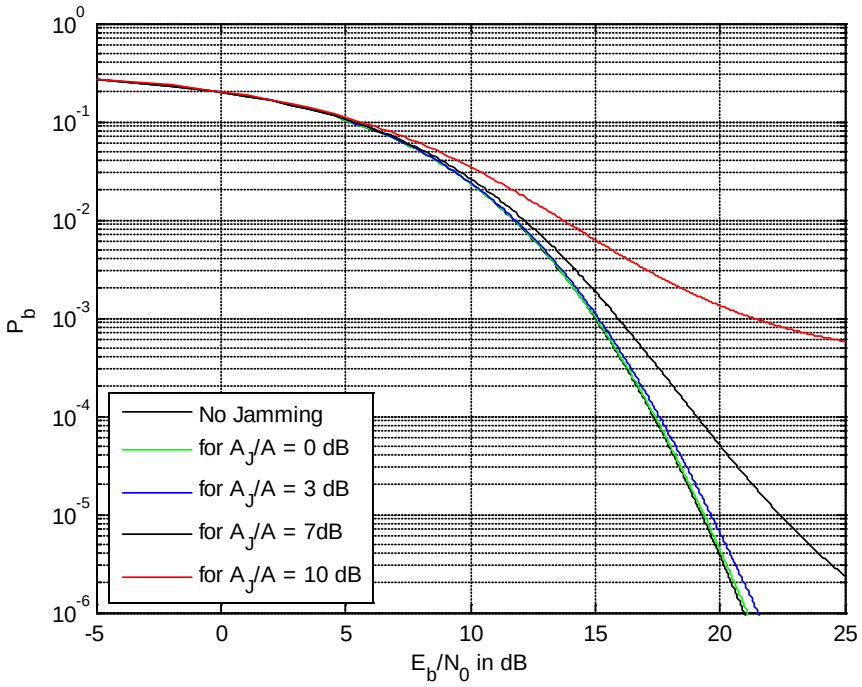

Figure 124. BER of DS 16QAM MIMO for tone jamming and diversity *L*=8.

b. MIMO 3X2, 3X3 3X4

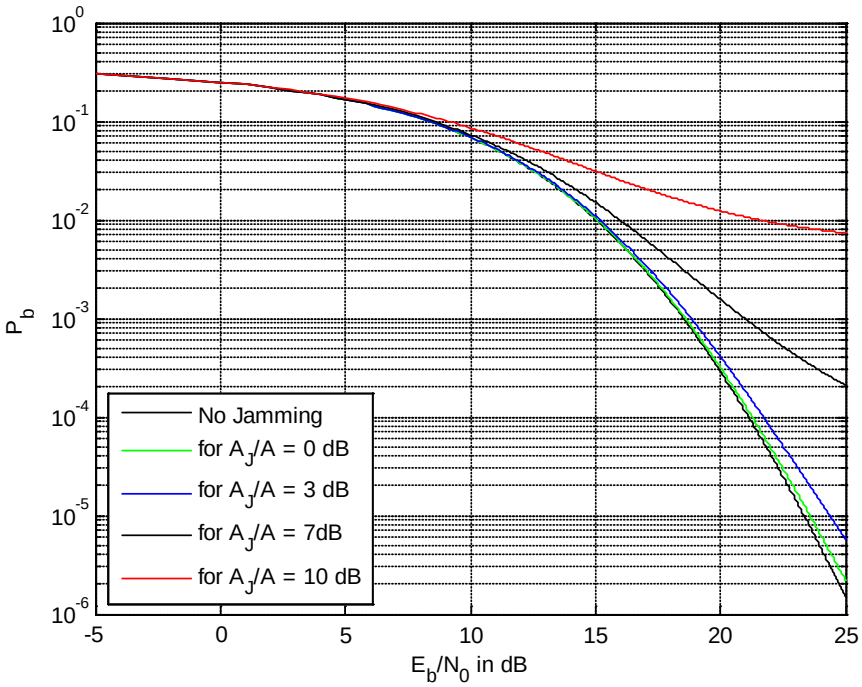

Figure 125. BER of DS 16QAM MIMO for tone jamming and diversity *L*=6.

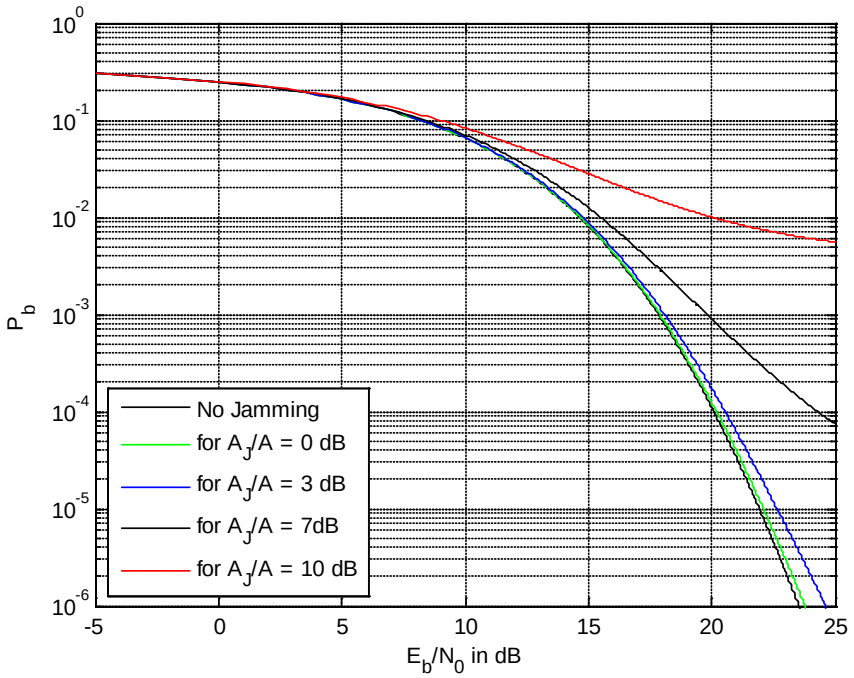

Figure 126. BER of DS 16QAM MIMO for tone jamming and diversity *L*=9.

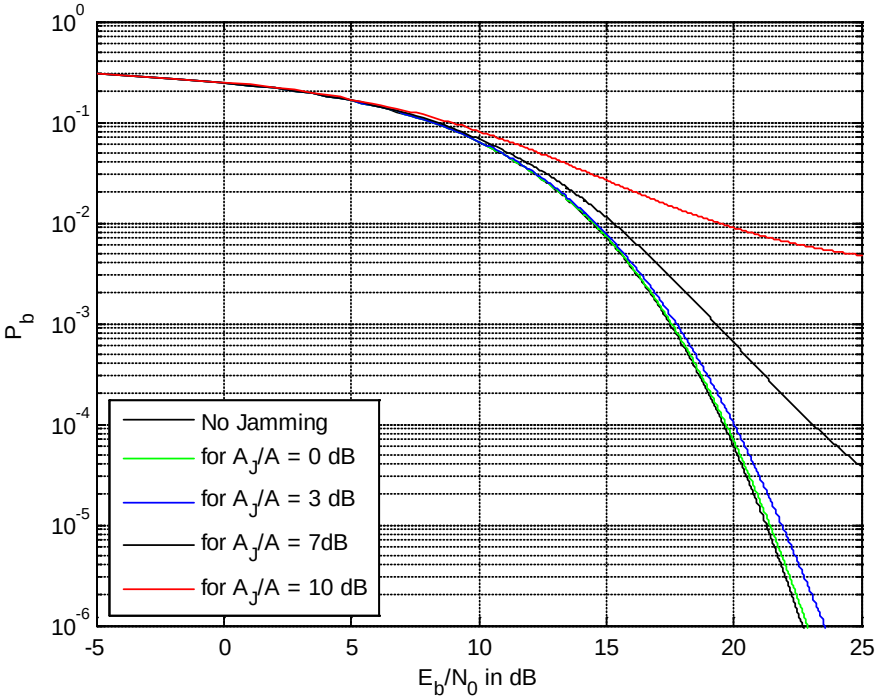

Figure 127. BER of DS 16QAM MIMO for tone jamming and diversity *L*=12.

c. MIMO 4X2, 4X3 4X4

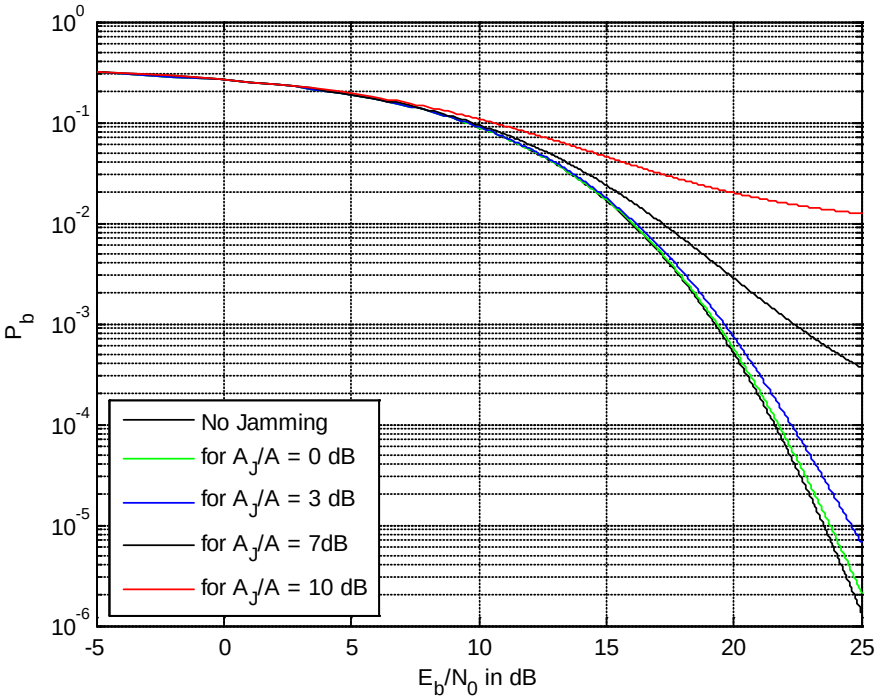

Figure 128. BER of DS 16QAM MIMO for tone jamming and diversity *L*=8.

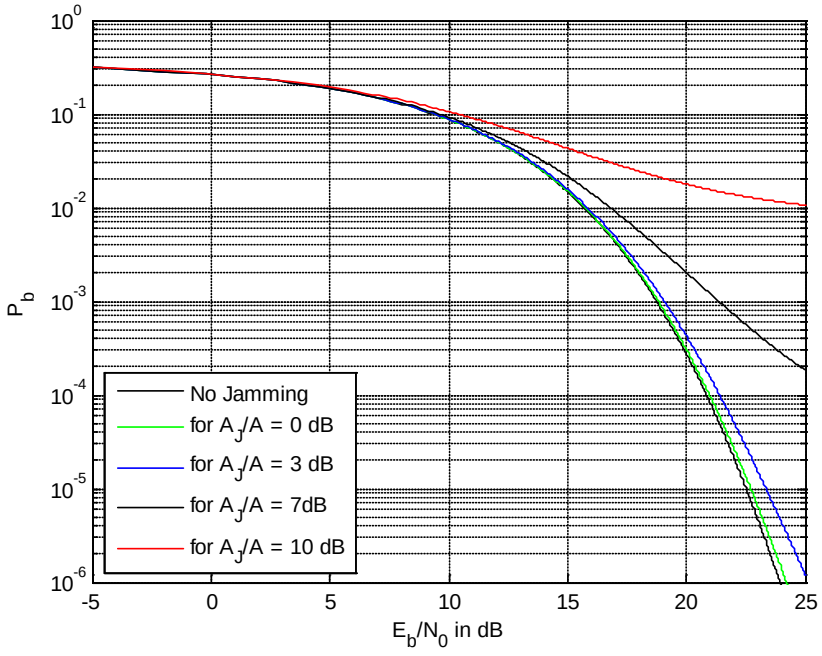

Figure 129. BER of DS 16QAM MIMO for tone jamming and diversity *L*=12.

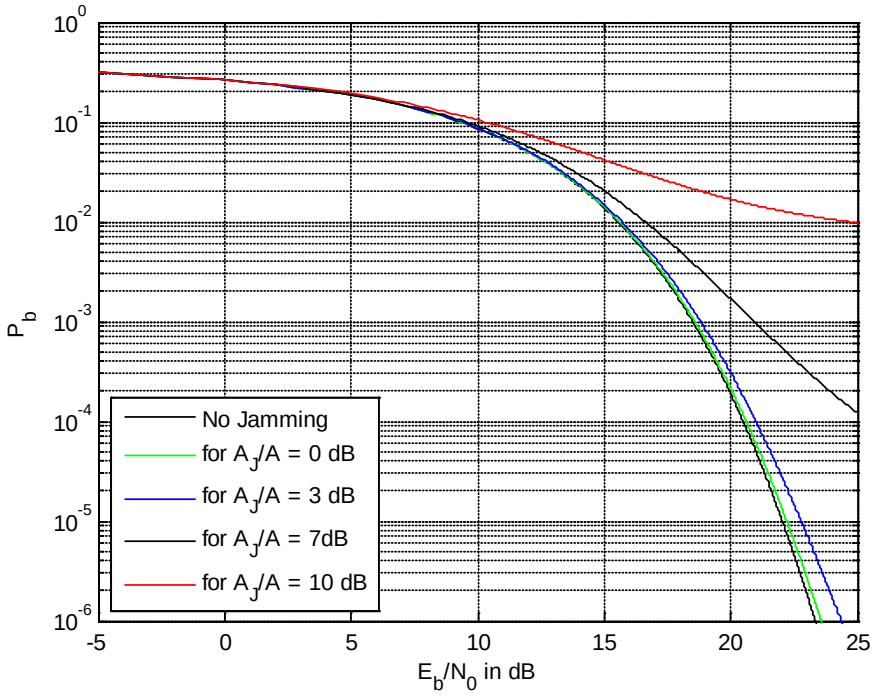

Figure 130. BER of DS 16QAM MIMO for tone jamming and diversity *L*=16.

3. 64-QAM

a. MIMO 2X2, 2X3 2X4

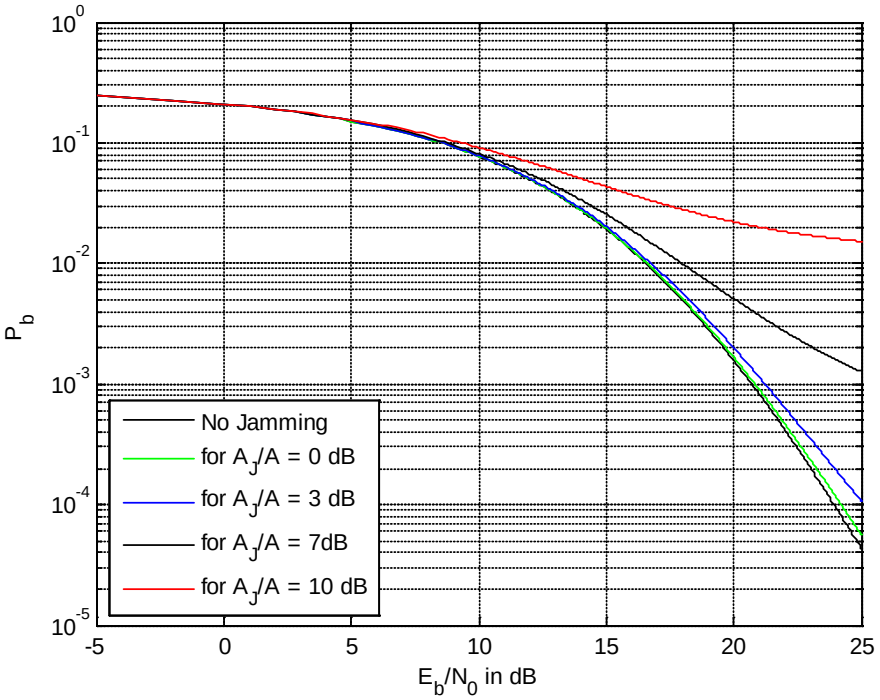

Figure 131. BER of DS 64QAM MIMO for tone jamming and diversity *L*=4.

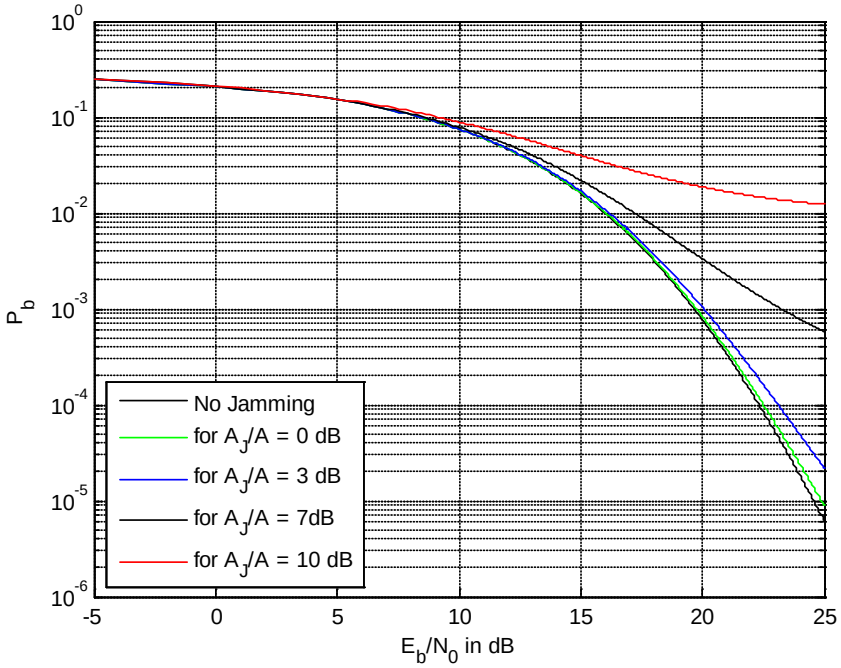

Figure 132. BER of DS 64QAM MIMO for tone jamming and diversity *L*=6.

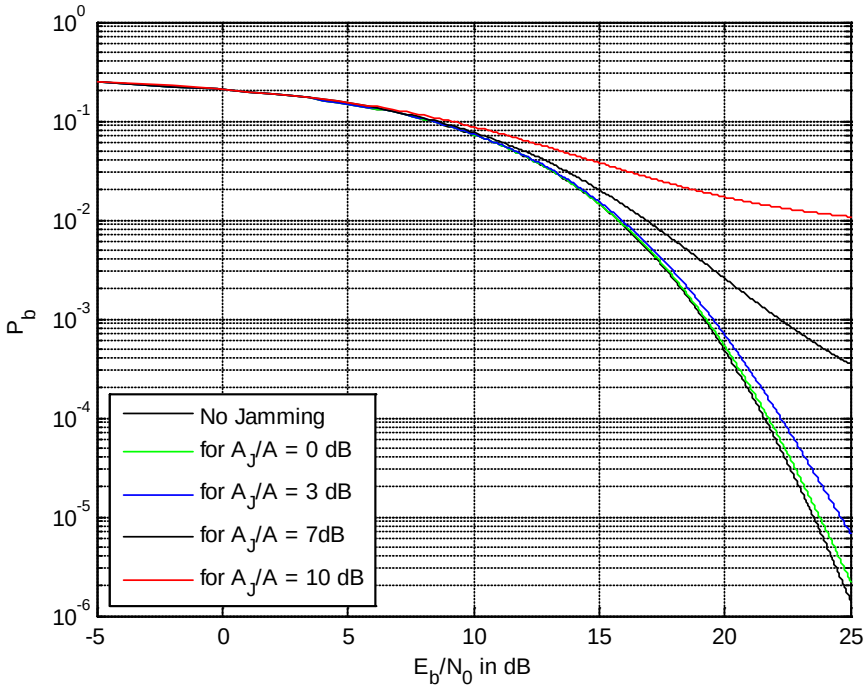

Figure 133. BER of DS 64QAM MIMO for tone jamming and diversity *L*=8.

b. MIMO 3X2, 3X3 3X4

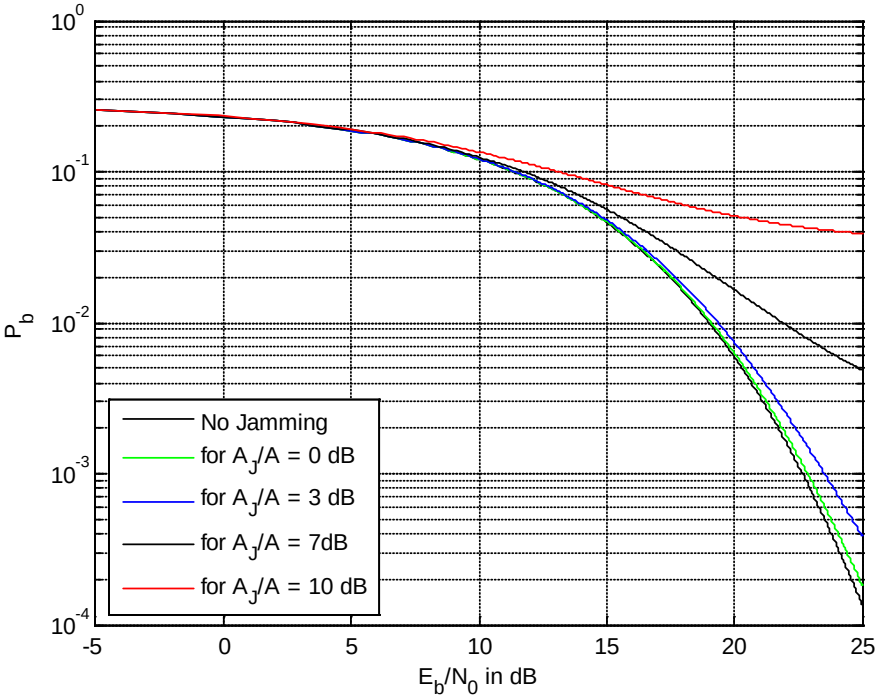

Figure 134. BER of DS 64QAM MIMO for tone jamming and diversity *L*=6.

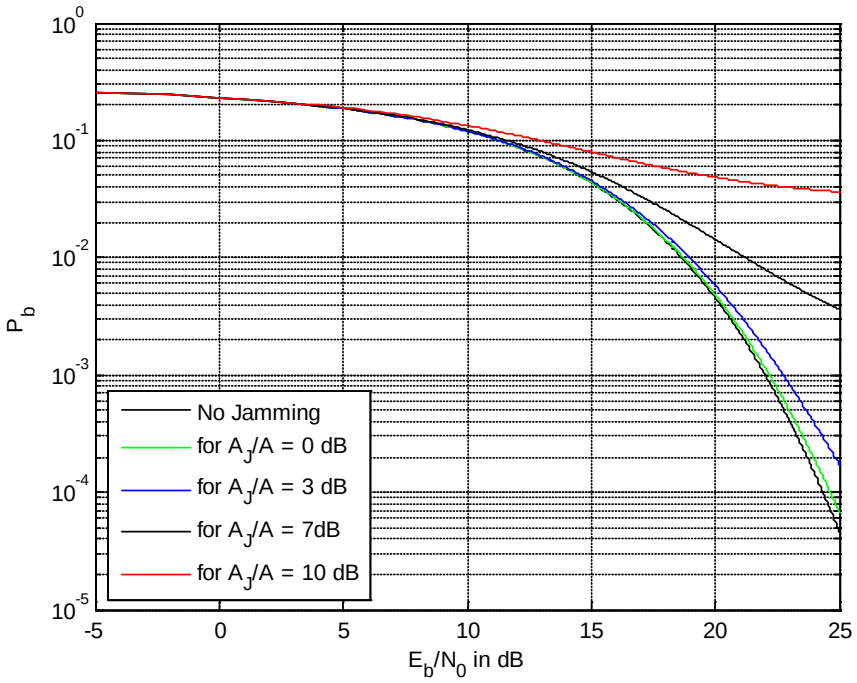

Figure 135. BER of DS 64QAM MIMO for tone jamming and diversity *L*=9.

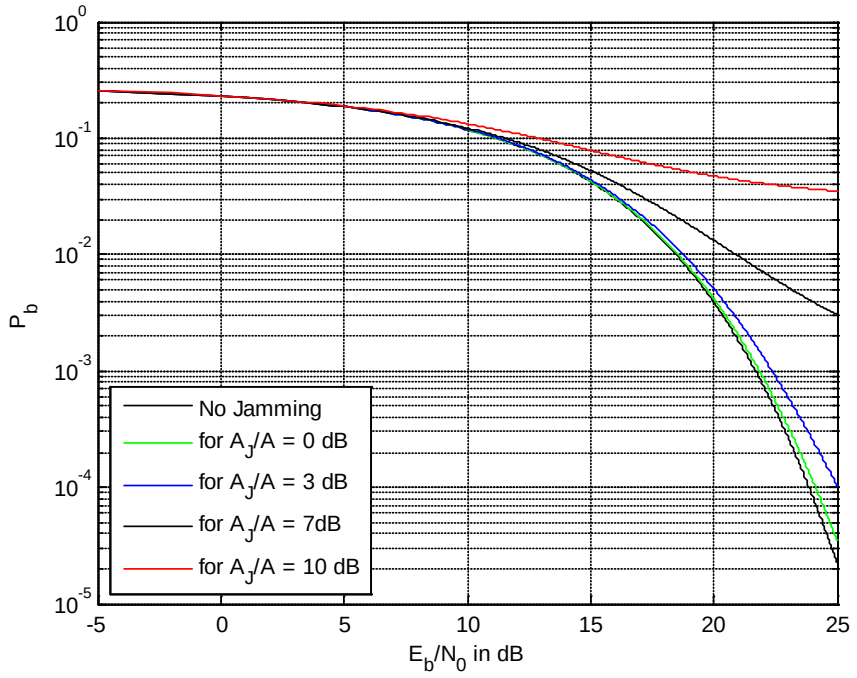

Figure 136. BER of DS 64QAM MIMO for tone jamming and diversity *L*=12.

c. MIMO 4X2, 4X3 4X4

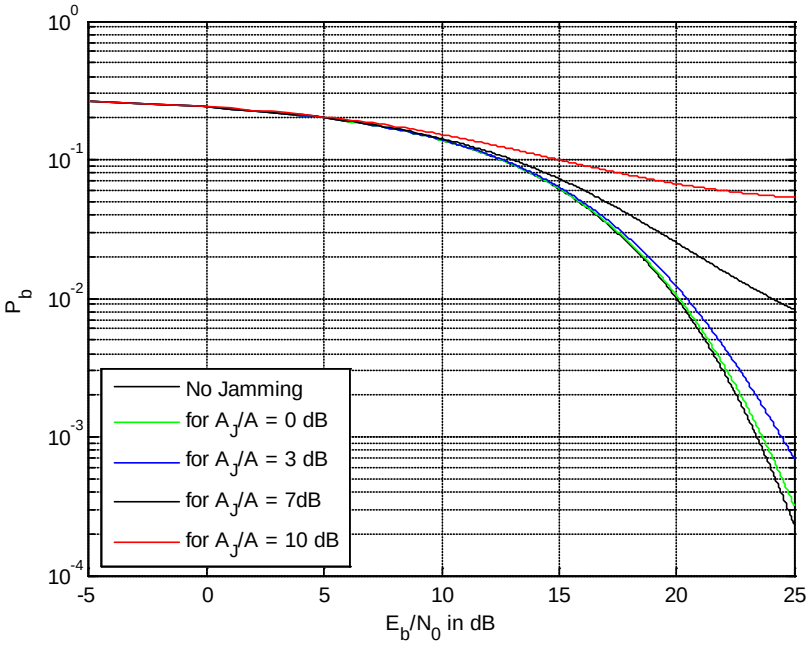

Figure 137. BER of DS 64QAM MIMO for tone jamming and diversity *L*=8.

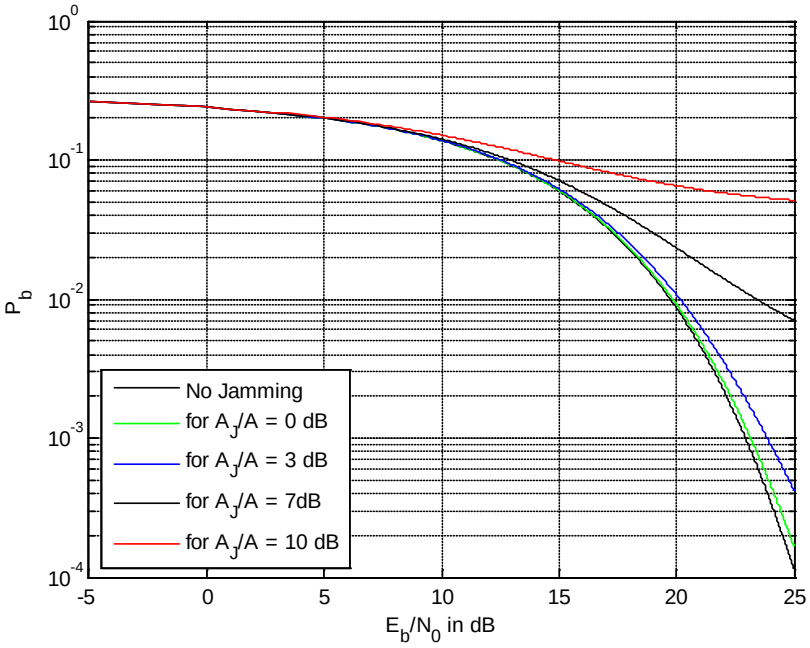

Figure 138. BER of DS 64QAM MIMO for tone jamming and diversity *L*=12.

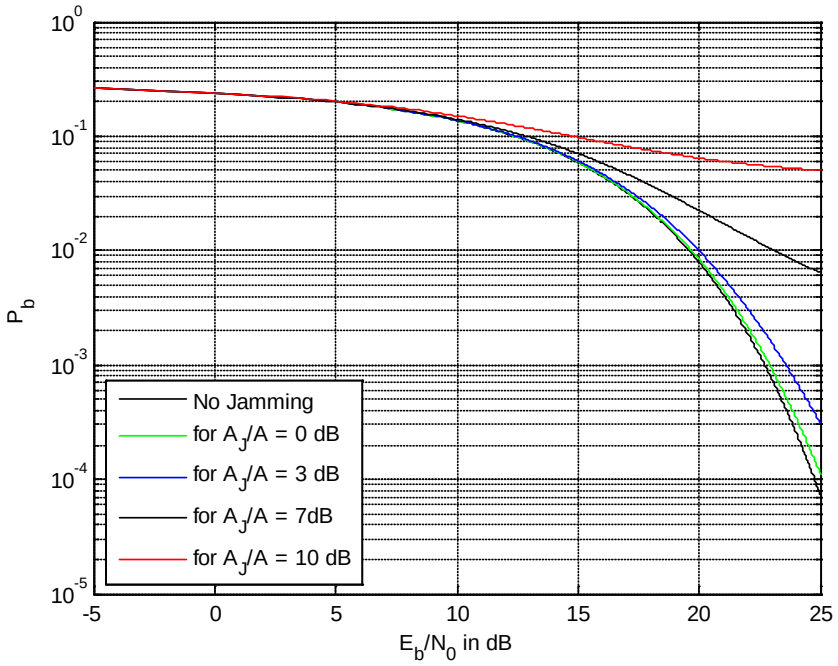

Figure 139. BER of DS 64QAM MIMO for tone jamming and diversity *L*=16.

VI. CONCLUSIONS AND FUTURE WORK

A. CONCLUSIONS

This research focused on the performance analysis of *I-Q* complex spreading communication systems in a Rayleigh fading channel in the presence of three types of interference (broadband, pulsed-noise and tone) for a variety of transmit and receive antenna diversity.

Firstly, we studied MISO systems starting with a binary modulation scheme (DS-PSK) for transmit antenna diversity L=1 to 4. For broadband jamming, the performance improved as the diversity increased. For pulsed jamming, for L=2, the best performance corresponded to the worst case ρ, but as L increased from two to four, the performance degraded. We also noticed that even though the performance for the worst-case ρ decreased, for large ρ, the performance improved. Finally, in the case of tone jamming (0 dB and 3 dB of A_J / A) and in the case of no jamming, as L increased the performance improved. For A_J / A=7dB, performance remained constant. For A_J / A=10 dB, it degraded with respect to E_b / N_0.

We also evaluated MISO systems that employed *I-Q* complex spreading. As expected, the performances of DS-PSK and DS-QPSK were identical. We also noticed that the performance of DS-QPSK was superior to the other modulation schemes (DS-16QAM and DS-64QAM) for all combinations of jamming and diversity. This was the expected result since QPSK is more power efficient than 16QAM, which in turn is more power efficient than 64QAM.

In barrage noise jamming case, 16QAM performance increased as L increased for the no jamming, 15 dB, and 10 dB values of E_b / J_0. For E_b / J_0=5 dB, the improvement was only for L=2. For L=3 and L=4, the performances (for 5 dB) remained almost the same. 64QAM performance improved for diversity L=2; then degraded as L increased. In the case of pulsed-noise jamming, 16QAM and 64QAM had the same performance. For L=2, the BER performance that corresponds to the worst-case ρ remained the same, but

for L=3 and L=4, the performances degraded with respect to E_b / J_0. For other values of ρ, more specifically the large values, the performance increased tremendously. Finally, for the case of tone jamming, 16QAM and 64QAM performances improved for L=2 and as L increased. The performances experienced degradation with respect to E_b / N_0.

We noticed that the system performances were affected by the OSTBCs. In most cases, there was improvement of performance corresponding to diversity L=2. It is because, for that diversity, we used an Alamouti OSTBC which has code rate R=1. For $L = 3$ and $L = 4$, the code rate is $R = 3/4$. This reflects the performance impact of using rates smaller than unity. In order to maintain the same throughput and the same transmit power, we were forced to increase the bit rate. Thus, the bit energy was reduced. The bit rate reduction and the use of code rates smaller than unity are the reasons why, for most cases, the performances did not improve for higher transmit antenna diversities (L=3 and L=4).

We also evaluated the performances of the corresponding MIMO systems. For all the modulation schemes and all the combinations of diversity, we noticed that as the receive antenna diversity increased, the performance increased because there is no power penalty for receive antenna diversity [11, pp. 578-580], [14, pp. 111-114]. The other important point is that for all MIMO configurations, the best overall performance was achieved by 2X4 diversity; this was due to the use of the unity rate $(R = 1)$ Alamouti code.

Finally, we can make some interesting observations about the effectiveness of each jamming technique. By observing the BER plots corresponding to the case of tone jamming, we see that it was relatively ineffective. This can be explained by (4.109) and (4.112), where the spread factor N is raised to the power of two, which reduced the effect of the jamming. For comparison purposes, we mention that for the cases of broadband jamming, in (4.66), (4.69) and (4.72), and pulsed-noise jamming, in (4.88) and (4.85), the corresponding terms are multiplied by a factor of N.

Considering all the performances studied, the most effective type of interference was pulsed-noise jamming. It was very effective against QPSK, 16 and 64QAM for

transmit diversity greater than one. Another important observation about the effectiveness of pulsed-noise jamming is the following: if the hostile interferer has knowledge of the worst-case ρ, then the total diversity L may not be effective. This is because even if L increases, the worst-case ρ BER does not improve. However, if the hostile interferer does not have this information and uses arbitrary ρ, then the total diversity (number of transmit and receive antennas) is a huge advantage such that the effect of jamming can be eliminated, especially for large values of ρ; the MIMO system for large values of ρ experiences tremendous performance improvement.

B. FUTURE RESEARCH AREAS

The area of MIMO systems in fading channels and in the presence of interference is a subject of research in the future for military and civilian applications.

One subject of future research is to consider other types of fading channels such as Rice or Nakagami. Different modulation schemes and configurations can be applied such as W-CDMA or trellis coded modulation (TCM).

Another area of research would be the application of various forward error correction (FEC) techniques to the MIMO systems studied in this research work.

THIS PAGE INTENTIONALLY LEFT BLANK

LIST OF REFERENCES

[1] A. Viterbi, "Spread spectrum communications-Myths and realities," *IEEE Communications Magazine*, vol. 17, p. 11, May 1979.

[2] D. T. Magill, F. D. Natali and G. P. Edwards, "Spread-spectrum technology for commercial applications," *Proceedings of the IEEE*, vol. 82, p. 572, April 1994.

[3] R. Dixon, "Why spread spectrum?," *Communications Society*, vol. 13, p. 21, July 1975.

[4] Y. J. Choi, N. H. Lee and S. Bahk, "IEEE 802.11 Performance enhancement by MIMO spatial multiplexing," *Personal, Indoor and Mobile Radio Communications, 2005. IEEE 16th International Symposium*, vol. 1, p. 87, September 2005.

[5] B. A. Bjerke and J. G. Proakis, "Multiple-antenna diversity techniques for transmission over fading channels," *Proc. IEEE WCNC 98*, pp. 1038-1042, October 1998.

[6] A. Belhouji, C. Decroze, D. Carsenat, M. Mouhamadou, S. Reynaud and T. Monediere, "A MIMO WiMax-OFDM based system measurements in real environments," *Antennas and Propagation, 2009. EuCAP, 3rd European Conference*, p. 1106, March 2009.

[7] L. Qinghua et al. "MIMO techniques in WiMAX and LTE: a feature overview," *IEEE Communications Magazine*, vol. 48, p. 86, May 2010.

[8] A. Richardson, *WCDMA Design Handbook*. Cambridge: Cambridge University Press, 2005.

[9] C. Yeonho and S. Kihong, "Adaptive QAM modulation with complex spreading for high-speed mobile multimedia communications," *IEEE Vehicular Technology Conference, 2000*, vol. 1, p. 384, 2000.

[10] J. Xiangdong, Y. Jing and L. Xiong, "Study on the characteristic of WCDMA uplink complex spreading and modulation," *Wireless Communications, Networking and Mobile Computing, WiCom '09. 5th International Conference*, p. 1, September 2009.

[11] T. T. Ha, "Theory and Design of Digital Communication Systems," Cambridge: Cambridge University Press, 2011.

[12] R. L. Peterson, R. E. Ziemer and D. E. Borth, *Introduction to Spread Spectrum Communications*. New Jersey: Prentice-Hall Inc, 1995.

[13] National Instruments Developer Zone, “Understanding Spread Spectrum for Communications,” April 2011.http://zone.ni.com/devzone/cda/tut/p/id/4450

[14] E. G. Larsson and P. Stoica, *Space-Time Block Coding for Wireless Communications*. Cambridge: Cambridge University Press, 2003.

[15] J. G. Proakis, *Digital Communications*, 4th edition. New York: McGraw-Hill, Inc, 2001.

INITIAL DISTRIBUTION LIST

1. Defense Technical Information Center
   Ft. Belvoir, Virginia

2. Dudley Knox Library
   Naval Postgraduate School
   Monterey, California

3. Chairman
   Department of Electrical and Computer Engineering
   Naval Postgraduate School
   Monterey, California

4. Professor Tri Ha
   Department of Electrical and Computer Engineering
   Naval Postgraduate School
   Monterey, California

5. Professor Ric Romero
   Department of Electrical and Computer Engineering
   Naval Postgraduate School
   Monterey, California

6. Embassy of Greece
   Office of Naval Attaché
   Washington, District of Columbia

7. LTJG Mintzias Efstathios
   Hellenic Navy General Staff
   Athens, Hellas (Greece)

DEPARTMENT OF THE NAVY
NAVAL POSTGRADUATE SCHOOL
DUDLEY KNOX LIBRARY
411 DYER ROAD, ROOM 110
MONTEREY, CALIFORNIA 93943-5101

T900
NPS (130)
14 May 14

From: University Librarian, Naval Postgraduate School
To: Defense Technical Information Center (DTIC-OQ)

Subj: CHANGE IN DISTRIBUTION STATEMENT FOR ADB372258

1. Request a distribution statement change for:

ADB372258: Mintzias, Efstathios. Performance of Complex Spreading MIMO Systems With Interference. Monterey, CA: Naval Postgraduate School, Department of Electrical and Computer Engineering, June 2011. UNCLASSIFIED [Further dissemination only as directed by Naval Postgraduate School June 2011 or higher DoD authority.]

2. Upon consultation with NPS faculty, the School has determined that, effective May 13, 2014, the distribution limitations on this report have been removed and distribution has been broadened to public release.

3. POC for this request is George Goncalves, Librarian, Restricted Resources and Services, 831-656-2061, DSN 756-2061 (gmgoncal@nps.edu).

ELEANOR S. UHLINGER
University Librarian